CENTRO DE INVESTIGACIÓN Y DE ESTUDIOS AVANZADOS DEL INSTITUTO POLITÉCNICO

UNIDAD ZACATENCO

DEPARTAMENTO DE BIOMEDICINA MOLECULAR

“El papel de la proteína inhibidora del complejo Arp2/3 arpin en la regulación de las funciones de la barrera endotelial”

TESIS

Que presenta

Armando Montoya García

Para obtener el grado de

DOCTOR EN CIENCIAS

EN LA ESPECIALIDAD DE

BIOMEDICINA MOLECULAR

Director de Tesis:

Dr. Michael Schnoor

Ciudad de México **Agosto 2023**

THE CENTER FOR RESEARCH AND ADVANCED STUDIES OF THE NATIONAL POLYTECHNIC INSTITUTE

ZACATENCO UNIT

DEPARTMENT FOR MOLECUAR BIOMEDICINE

"The role of the Arp2/3 inhibitory protein arpin in the regulation of endothelial barrier functions"

THESIS

Presented by

Armando Montoya García

To obtain the degree

PhD in science

IN THE SPECIALITY

MOLECULAR BIOMEDICINE

Thesis Director:

Dr. Michael Schnoor

Mexico City **August 2023**

DEDICATORIA

Para Maggy y Pato
que impulsaron mi sueño de
convertirme en científico

AGRADECIMIENTOS

A mis padres, que desde pequeño me alentaron a cumplir mi sueño de terminar un doctorado para convertirme en científico. La disciplina, perseverancia y responsabilidad que sembraron en mí fue culminante para ser el profesional que soy el día de hoy.

Al Dr. Michael Schnoor, quien ha confiado en mí, desde la maestría, para descubrir las funciones de arpin en la barrera endotelial y ha sido un excelente mentor en estos cuatro años de trabajo experimental.

A mis asesores que se tomaron el tiempo para aconsejarme, evaluarme y leer la presente tesis.

A la Dra. Hilda Vargas, que sacrificó tiempo de su trabajo para ayudarme en los experimentos necesarios para la caracterización del ratón KO de arpin

A la futura Dr. Karina Jiménez, quien ha sido mi mejor amiga desde que inicié mi formación en el CINVESTAV y siempre ha estado para mí, incluso en los momentos más difíciles.

A la Dr. Sandra Chánez que me capacitó cuando llegué al laboratorio y me trasmitió todo lo que ella sabía. Sus consejos fueron la mejor de las enseñanzas.

A mi amiga la Dra. Idaira Guerrero que me enseñó todo el análisis por inmunofluorescencia y los experimentos con el músculo de cremaster.

A las M. en C. Karina Belén e Iliana, por su apoyo técnico en la caracterización del ratón KO de arpin.

A mis alumnos Nelson y Jirehl que empezaron aprendiendo, pero fueron de mucho apoyo técnico al final de su estancia.

A todos mis amigos y familiares que han estado al pendiente de mí y han entendido que he sacrificado tiempo con ellos por terminar mis estudios de doctorado.

Finalmente quiero agradecer también al CONACyT y al CINVESTAV por el todo apoyo económico durante el doctorado y para asistir a congresos, importantes para mi formación académica.

INDEX

ABSTRACT

The endothelium is a semi-permeable barrier covering the vasculature that separates blood from underlying tissues and that gets activated during inflammation leading to increased endothelial permeability and adhesion of leukocytes. Such alterations of endothelial integrity depend on endothelial actin dynamics and actin-binding proteins (ABP) that control actin remodeling, including the Arp2/3 complex, which induces the formation of branched actin networks. The activity of the Arp2/3 complex is tightly regulated by nuclear promoting factors (NPFs) that are locally antagonized by the inhibitory proteins PICK1, gadkin and arpin. Arpin was recently discovered and competitively binds Arp2/3 to prevent NPF binding. Arpin colocalizes with the NPF WAVE2 at the lamellipodial edge in fibroblasts, where it is thought to finetune Arp2/3 activity and cell migration. However, expression and functions of arpin in the endothelium have not yet been described. Here, we show that arpin mRNA and protein are expressed in different endothelial cells (EC) and downregulated by the pro-inflammatory cytokines TNFα and IL-1β. Loss of arpin in human umbilical vein endothelial cells (HUVEC) increases the formation of contractile actin stress fibers leading to increased permeability in an Arp2/3-independent manner. Instead, inhibition of ROCK1 and ZIPK, kinases involved in the generation of actomyosin stress fibers, rescues the loss-of-arpin effects on actin filaments and permeability. Moreover, for the first time, we describe arpin-deficient mice, which are viable but show a characteristic vascular phenotype in the lung including edema, microhemorrhage and vascular congestion, increased F-actin levels, and vascular permeability. The new data from this thesis reveal that, apart from being an Arp2/3 inhibitor, arpin is also a regulator of actomyosin contractility and endothelial barrier integrity. Restoring arpin levels might be a new treatment strategy to improve the outcomes of inflammatory diseases and cancers that are characterized by loss of arpin.

.

RESUMEN

El endotelio es una barrera semipermeable que recubre los vasos sanguíneos, separa la sangre de los tejidos adyacentes y se activa durante la inflamación dirigiendo al incremento en la permeabilidad y la adhesión de leucocitos. Dichas alteraciones en la integridad endotelial dependen de la dinámica de la actina endotelial y de proteínas de unión a actina, como el complejo Arp2/3 que induce la formación de redes de actina ramificada. La actividad del complejo Arp2/3 se encuentra regulada por los factores promotores de la nucleación (NPFs) que están localmente antagonizados por las proteínas inhibidoras PICK1, gadkin y arpin. Arpin fue recientemente descubierta y competitivamente se une al complejo Arp2/3 impidiendo la unión de los NPFs. Arpin co-localiza con el NPF WAVE2 en los lamelipodios de fibroblastos, donde regula el complejo Arp2/3 y la migración celular. Sin embargo, la expresión y funciones de arpin en el endotelio no han sido aún descritas. En este trabajo, se demostró que arpin se expresa a niveles de RNA mensajero y proteína en diferentes células endoteliales y que se disminuye por las citocinas proinflamatorias TNFα e IL-1β. La deficiencia de arpin en células HUVEC incrementa la formación de fibras de estrés que dirigen al incremento en la permeabilidad en un mecanismo independente al complejo Arp2/3. En cambio, la inhibición de ROCK1 y ZIPK, cinasas involucradas en la generación de fibras de estrés, rescata los efectos de la pérdida de arpin en los filamentos de actina y la permeabilidad. Además, por primera vez, se describe el ratón deficiente de arpin, el cual es viable, pero muestra un fenotipo vascular en el pulmón que incluye edema, microhemorragia, congestión vascular, e incrementos en los niveles de actina filamentosa y la permeabilidad vascular. Los resultados de esta tesis revelan que, además de inhibir al complejo Arp2/3, arpin también regula la formación de fibras de estrés y la integridad de la barrera endotelial. Restaurar los niveles de arpin podría resultar en una nueva estrategia de tratamiento para mejorar las consecuencias de las enfermedades inflamatorias y cánceres que están caracterizados por la falta de arpin.

1. INTRODUCTION

1.1 THE ENDOTHELIUM

The endothelium is a monolayer of endothelial cells (ECs) that constitutes the inner cellular lining of all blood vessels including arteries, veins, and capillaries. Therefore, it is in direct contact with the blood and circulating cells. ECs are anchored to the basal lamina, which is an important scaffold of every blood vessel. The inside of this scaffold is lined with endothelial cells, while the outside is covered with smooth muscle cells or pericytes. The shape of ECs varies across the vascular tree, but they are generally thin and slightly elongated, being roughly 50–70 μm long, 10–30 μm wide and 0.1–10 μm thick [1].

ECs form a semi-permeable barrier that separates the blood from underlying tissues, and controls the passage of fluids, ions, macromolecules, and cells across blood vessel walls. This barrier is mediated by cell-cell adhesive structures, including tight junctions (TJs), adherens junctions (AJs) and other adhesion proteins such as PECAM-1, which are connected to the actin cytoskeleton via several adaptor molecules [2] (Figure 1.1).

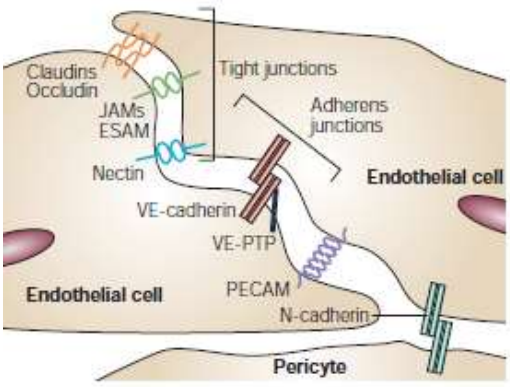

Figure 1.1. The main transmembrane proteins in endothelial cell-cell contacts. Tight junctions are constituted by claudins, occludin, members of the junctional adhesion molecule (JAM) family and endothelial cell selective adhesion molecule (ESAM). At adherens junctions, adhesion is mostly promoted by vascular endothelial cadherin (VE-cadherin), which is associated with vascular endothelial protein tyrosine phosphatase (VE-PTP). Nectins participate in the organization of both TJs and AJs. Platelet endothelial cell adhesion molecule (PECAM) contributes to endothelial cell–cell adhesion but is not restricted to any type of junction. N-cadherin promotes adhesion of ECs to smooth muscle cells and pericytes [3].

Endothelial TJs are frequently intermingled with AJs along the cleft and regulate the diffusion of solutes and thus vascular permeability [2, 3]. TJs are formed by the homophilic interaction of cell-cell adhesion molecules such as members of the claudin family (claudins 1, 5 and 12), occludin, junctional adhesion molecules (JAMs) A, B and C and the endothelial cell selective adhesion molecule (ESAM) (Figure 1.1). Claudins are the principal barrier-forming proteins, with claudin-5 being restricted to ECs and thus critical for the regulation of vascular permeability, especially in the blood-brain barrier [4]. JAMs mediate endothelial cell-cell interactions and regulate leukocyte transendothelial migration (TEM). Occludin and claudins are linked to the intracellular linker proteins zona occludens (ZO)-1, ZO-2, ZO-3, cingulin, afadin, and calcium/calmodulin-dependent serine protein kinase (CASK), which together mediate the interaction between the adhesion molecules and actin filaments [2, 3, 5].

On the other hand, VE-Cadherin is the key transmembrane component of endothelial AJs (Figure 1.1) and is expressed only in ECs [2]. The cytosolic domains of VE-cadherin are connected to p120-catenin and β-catenin, which bind to α-catenin that can join directly or indirectly (through vinculin, α-actinin and eplin) to the actin cytoskeleton. VE-cadherin together with PECAM-1 initiates and maintains endothelial cell-cell contacts, holding the ECs together to give mechanical support to the endothelium and to enable complete junction formation [2, 3, 6]. Moreover, PECAM-1 can modulate cell adhesion and migration probably through interaction with integrins, and it also participates in vascular angiogenesis and serves as a receptor for leukocytes during transendothelial migration (TEM) [7, 8]

The nectin-afadin complex (Figure 1.1) has been described in both AJs and TJs. In this complex, ponsin binds to afadin, vinculin and α-catenin and thereby helps to anchor the complex to actin. Nectins and afadin colocalize with cadherins and reciprocally interact with α-catenin. However, afadin was also

found to be associated with JAM-A; and nectins with ZO-1 depending on the type of ECs [3, 5].

1.2 FUNCTIONS OF THE VASCULAR ENDOTHELIUM DURING INFLAMMATION.

The precise regulation of expression, distribution and function cell adhesion molecules is essential to control the regulation of vascular permeability to allow selective and specific passage of ions, macromolecules, and cells from the blood to underlying tissues. Opening and resealing of the junctional barrier must occur during normal physiological processes, but also during inflammatory responses [9]. In response to injury or infection, controlled opening or loosening of endothelial junctions plays a critical role in supporting an effective inflammatory response. This leads to increased vascular permeability to macromolecules such as immunoregulatory and pro- and anti-inflammatory proteins [10].

Vascular permeability is dynamically controlled by a number of inflammatory mediators and extracellular stimuli (Figure 1.2) such as vascular endothelial growth factor (VEGF), histamine, thrombin, several cytokines (TNF-α, IL-1β), the gram-negative bacterial endotoxin, lipopolysaccharide (LPS) and oxidized low-density lipoprotein (oxLDL) [11]. All these molecules can regulate endothelial junctions by affecting expression, localization and stability of junctional proteins [9, 10, 12]. For example, histamine significantly reduces ZO-1 expression in retinal ECs [13] and VEGF increases permeability by affecting occludin and ZO-1 localization at TJ and decreasing levels of occludin expression [14]. Several inflammatory mediators such as VEGF, TNFα and histamine also change AJ composition by inducing phosphorylation of the VE-cadherin cytoplasmic tail and of its associated catenins causing VE-cadherin/catenin dissociation and VE-cadherin internalization [15]. JAM-C is also localized at the junctions in response to VEGF, histamine [16] and thrombin [17] causing increased paracellular flux. Moreover, stimulation with

TNFα and IFNγ causes a reduction and redistribution of PECAM-1 away from junctions and a twofold increase in paracellular permeability [18]. In all these contexts, ECs regulate the endothelial barrier through internalization, storage, and recycling of the junction molecules.

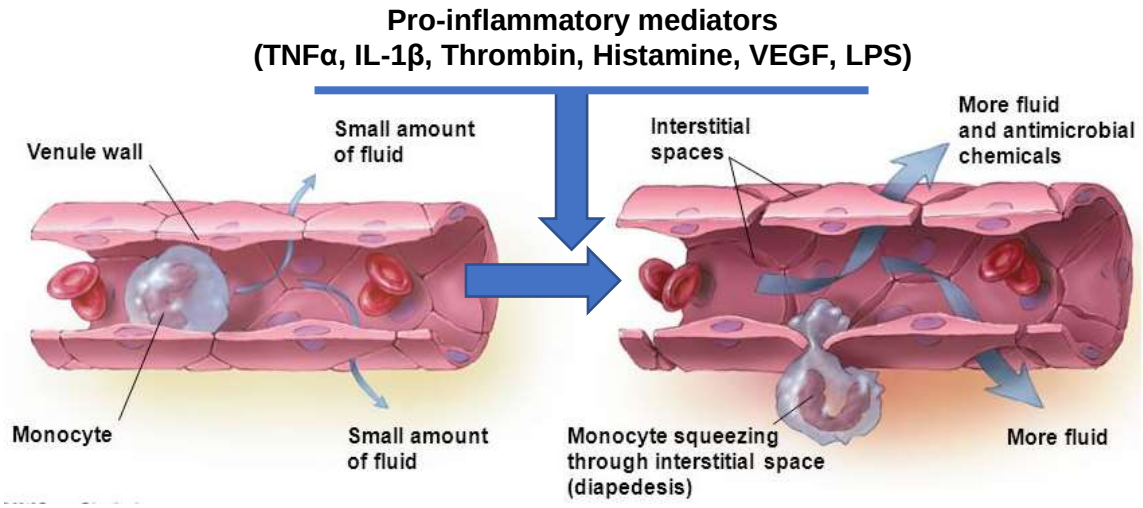

Figure 1.2. Dynamic regulation of vascular permeability. Endothelial permeability is dynamically controlled during inflammation by several mediators that decrease endothelial barrier function. In basal conditions, endothelial cells preserve low basal vascular permeability, but when inflammation occurs, vascular permeability increases, and leukocytes and plasma proteins can cross the vessel wall.

Additionally ECs actively contribute to the transmigration of leukocytes at sites of inflammation, where a cascade of different events is triggered to allow circulating leukocytes to bind to the vascular endothelium and to interact with the blood vessel wall through a series of steps including tethering, rolling, arrest, crawling and, finally, transendothelial migration (TEM or diapedesis), which can occur para- or trans-cellularly (Figure 1.3) [19-21]. All these steps are mediated by several adhesion molecules expressed on the apical ECs surface in response to different proinflammatory mediators such as TNFα, IL-1β and LPS. The endothelial selectins, E-selectin and P-selectin mediate the capture of leukocytes from the rapidly flowing blood. This transient interaction, in combination with the blood flow, results in the rolling of leukocytes on the apical endothelial cell surface [20]. The rolling of leukocytes facilitates their contact with chemokines presented on the apical endothelial surface to induce activation of leukocyte integrins [21] that can then bind to intercellular adhesion

molecule 1 (ICAM-1) and vascular cell adhesion molecule 1 (VCAM-1) on ECs. These interactions mediate firm adhesion and spreading of leukocytes on the ECs surface subsequently leading to leukocyte crawling on the luminal surface of blood vessels, which depends on ICAM-1 and -2 in ECs and their ligand MAC-1 in leukocytes [20]. Before leukocytes can transmigrate, ECs extend membrane structures at their apical surface termed docking structures [22] or transmigratory cups [23]. They are enriched in clustered ICAM-1, VCAM-1, the actin cytoskeleton and actin-biding proteins (ABPs) [24]. These structures are thought to strengthen leukocyte-endothelial interactions and guide leukocytes to suitable exit sites [19, 20].

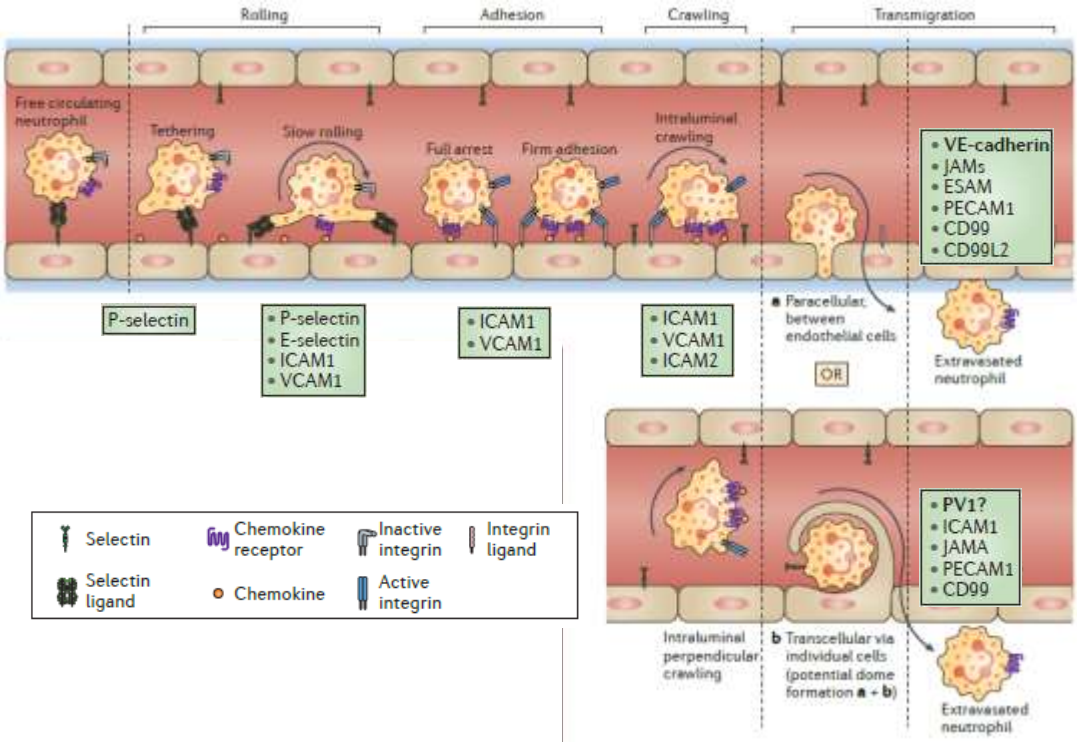

Figure 1.3. The neutrophil extravasation cascade. Sequential steps of leukocyte recruitment form the inflamed vasculature to the tissue. Two possible ways of transmigration are known: a) paracellular (between ECs) and b) transcellular (through ECs). Green squares indicate the adhesion molecules present in endothelial tissue needed for each transmigration step. Modified form Kolaczkowska and Kubes [21].

Finally, leukocytes need to cross the vascular endothelium to leave the vasculature through two different ways of transmigration: paracellular, between ECs and transcellular, through ECs. This final step requires ICAM-1, ICAM-2,

VCAM-1, as well as different junctional proteins, including PECAM-1, ESAM, CD99 and JAMs. All these molecules support transmigration of leukocytes because their absence reduces transmigration. Of note, the paracellular route requires homophilic adhesive interactions of JAM-A, PECAM-1 and CD99 in this sequential order [19-21]. By contrast, VE-cadherin [25] and occludin [26] need to be internalized as they inhibit transmigration. Leukocytes usually extravasate via the paracellular way (~90%), but they preferentially use the transcellular pathway to cross endothelia with strong junctions such as the blood-brain barrier [21].

1.3 THE ACTIN CYTOSKELETON IN ENDOTHELIAL CELLS

For the regulation of vascular permeability and leukocyte migration, the endothelial barrier needs to be flexible, and this flexibility is provided by controlled actin cytoskeletal dynamics [6, 19, 27]. In ECs, actin constitutes approximately 5–15% of the total protein content [28] and globular(G) β- and γ-actin subunits alternatively polymerize in a helical fashion to form a double-stranded filamentous structure known as filamentous (F)-actin [6], with a well-balanced amount of G-actin and F-actin [29]. The actin cytoskeleton is a highly dynamic structure that polymerizes and depolymerizes according to cellular demands.

Actin polymerization happens through two processes, nucleation and elongation [30]. Nucleation occurs after the formation of small actin oligomers (dimers, trimers, or tetramers). However, actin nucleation is rate limiting due to the instability of the actin oligomers and the activity of actin monomer-binding proteins that suppress spontaneous actin nucleation [31, 32]. For these reasons, cells express different ABPs known as actin-nucleation proteins that stabilize the formation of actin oligomers, which are described below. Once there is a stable oligomer of actin monomers, the elongation process starts, where ATP-bound G-actin molecules bind constantly and quickly to form F-

actin at the barbed (or +) end of the filament. F-actin can also depolymerize due to hydrolysis of bound ATP into ADP at the pointed (or -) end of the filament [31, 32]. Elongation and depolymerization are controlled by ABP that stabilize these processes such as profilin and cofilin, respectively [6, 33].

The best-known intermediaries that control ABP activity and actin dynamics in ECs are the Rho-family GTPases (Rho, Rac and Cdc42) that are activated in response to several pro-inflammatory mediators [6, 27, 34]. ABPs help to coordinate actin remodeling [19, 27, 35] by directly binding actin or serving as scaffold molecules to connect actin filaments directly to other cellular structures or proteins including TJ and AJ to control endothelial barrier functions [27].

Depending on the cellular needs, actin filaments can be newly assembled, elongated, branched, or disassembled. Proteins that assemble actin filaments *de novo* or that produce actin branches on exiting filaments are called actin nucleators [27, 36, 37]. There are three types of proteins classified as actin nucleators: spires, formins and the actin-related protein-2/3 (Arp2/3) complex [36]. The spire proteins are conserved among metazoan species and studies using *Drosophila melanoganster* spire indicate that the four tandem G-actin-binding Wiskott-Aldrich syndrome protein (WASP)-homology-2 (WH2) domains scaffold four G-actin subunits to induce polymerization of a new actin filament [38]. Formins are conserved actin polymerization machines in most eukaryotes, and form dimers with their formin-homology-2 (FH2) domains to stabilize G-actin dimers or trimers to facilitate the nucleation event [39], additionally formins process movement on growing barbed ends of actin filaments while protect them from capping protein and accelerate actin filament elongation depending on profilin [40]. The Arp2/3 complex serves as a template for the initiation of new actin filament branches on existing filaments. Arp2/3 requires nucleation promoting factors (NPFs) to become fully activated [36]; and recently, also inhibitory proteins have been identified that guarantee fine-tuning of Arp2/3 activity as described below.

In ECs, F-actin composes supramolecular organized cytoskeletal structures. For example, junction-associated actin filaments (JAAFs) [41] exist as contractile actin bundles that localize to and stabilize mature EC junctions, or as cytoplasmic stress fibers that span from focal adhesions to AJs [6]. RhoA promotes the formation of contractile actomyosin stress fibers and focal adhesions [42]. Actin stress fibers contain myosin-II and α-actinin to enable contractile force development, a characteristic that contributes to shear stress resistance, decreases endothelial barrier stability, and induces cell migration [6]. Additionally, stress fibers contribute to the formation of docking structures that surround and guide the neutrophils to transmigrate through the endothelium [19].

Classical lamellipodia (cLP) and junction-associated intermittent lamellipodia (JAIL) are other types of organized actin cytoskeletal structures in ECs that are composed of branched actin networks [41, 43]. cLP are formed to promote endothelial cell migration [43], while JAIL generate new VE-cadherin-based adhesion sites [44]. Branched actin structures that form both cLP and JAIL are formed by the Arp2/3 complex and its NPF WAVE [41, 44] (described below).

1.4 THE ARP2/3 COMPLEX

The only nucleator for branched actin network formation is the heptameric Arp2/3 complex that is conserved in almost all eukaryotes. *In vitro* studies have revealed that the Arp2/3 complex binds existing actin mother filaments and initiates the formation of daughter filaments that branch off the mother filaments at a ~70° angle [36, 45].

The Arp2/3 complex is a ~250 kDa stable multiprotein complex of seven subunits (Figure 1.4) [46]. Two of these subunits are the actin-related proteins, Arp2 and Arp3, giving the complex its name. In the inactive conformation of Arp2/3 the subunits Arp2 and Arp3 are separated from each other. The other subunits of the Arp2/3 complex are ArpC1 (which is present in two isoforms in

Humans ArpC1A and ArpC1B), ArpC2, ArpC3, ArpC4, and ArpC5 that work as scaffold for the complex [36, 45, 47].

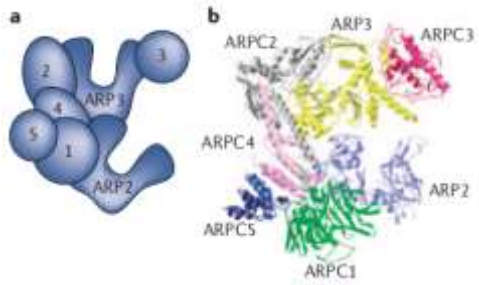

Figure 1.4. Structure of the Arp2/3 complex. a) Cartoon of the subunit organization in the Arp2/3 complex. b) Ribbon diagram of the crystal structure of the bovine Arp2/3 complex with subunits labelled in different colors. Taken from Goley and colleagues [36] based on the model published by Robinson and colleagues[48].

The active conformation of the Arp2/3 complex enables the subunits Arp2 and Arp3 to adopt the conformation of actin molecules within an actin filament thus initiating the elongation of a lateral branch (Figure 1.5). However, the interaction with NPFs is required to fully activate the Arp2/3 complex [36]. Although the structure and biochemistry of the Arp2/3 complex have been well studied *in vitro*, the *in vivo* functions have mostly been inferred from its localization patters (Figure 1.6) due to lethality of the genetic deletion of any of the Arp2/3 subunits in model organisms ranging from yeast [49] to mice [50-52].

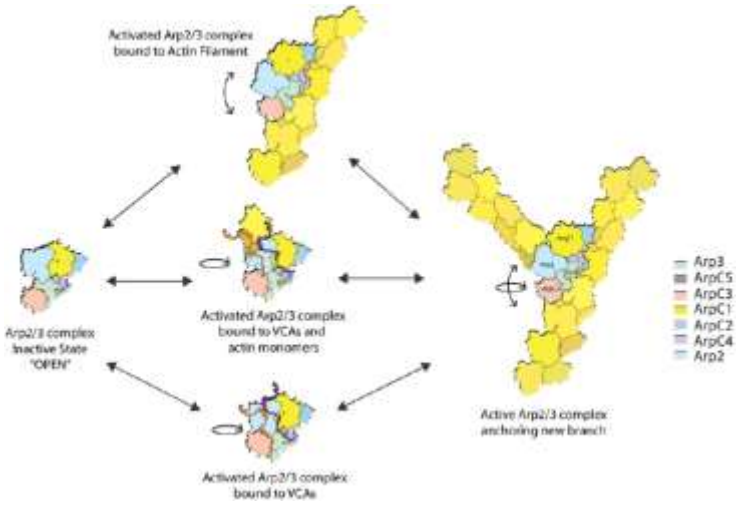

Figure 1.5. Model of conformational changes associated with Arp2/3 complex activation. The inactive conformation of the Arp2/3 complex maintains Arp2 and Arp3 separated (open state). Binding of the VCA domain of NPFs promotes a rotational movement that brings Arp2 and Arp3 into proximity and favors binding to a mother actin filament. Upon binding to a mother filament, the Arp2/3 complex experiences an additional conformational change. These two movements can occur independently or in combination to fully activate the Arp2/3 complex and start the polymerization of a new actin branch. Taken from Espinoza-Sanchez and colleagues [53].

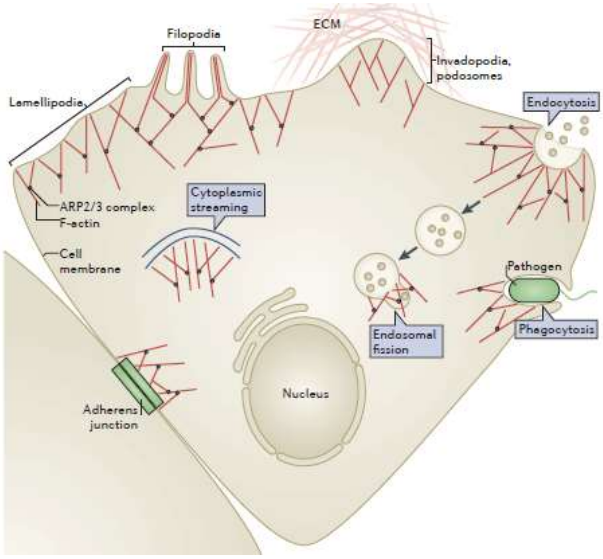

Figure 1.6. Cellular functions of actin filaments and the Arp2/3 Complex. Actin branches nucleated by the Arp2/3 complex are located at the leading edge of migrating cells, cell junctions, phagosomes, and endosomes of vesicular trafficking. Actin branches in the cytoplasm contribute to cytoplasmic streaming (blue lines). Arp2/3-generated branched actin at the leading edge provides the protrusive force that is required to generate and extend the broad sheet-like protrusions known as lamellipodia. The leading edge of migrating cells also hosts distinct thin protrusions known as filopodia, which are characterized by bundled parallel arrays of elongated and unbranched F-actin; however, some bundled actin filaments found in filopodia are thought to be nucleated from Arp2/3-branched networks. The Arp2/3 complex also localizes in invadopodia and podosomes, which are specialized protease-rich structures implicated in cell invasion and matrix degradation. ECM: extracellular matrix. Taken from Rotty and collaborators [45].

In ECs, the Arp2/3 complex controls JAIL that are small lamellipodia-like structures (1-5 μm) at established endothelial junctions that form to support and re-establish cell contacts at sites where VE-cadherin is temporarily lacking. An interdependent regulation of VE-cadherin-mediated cell adhesion and Arp2/3-mediated, actin-driven JAIL formation was proposed to control VE-cadherin dynamics at endothelial AJ to guarantee cell contact stability and junction remodeling [44, 54]. Additionally, Arp2/3 is involved in the endocytosis of occludin to allow for transendothelial migration of monocytes across the blood-brain barrier during inflammation [26]. These data highlight the importance of Arp2/3-mediated endothelial barrier regulation and leukocyte extravasation. However, Arp2/3 alone is a weak activator of actin branching. Thus, several proteins exist that activate this complex depending on the subcellular location [47] as described below.

1.5 THE NUCLEATION-PROMOTING FACTORS (NPFs)

NPFs are activators of the Arp2/3 complex that can be divided into two classes (Figure 1.7). Type I NPFs are characterized by their COOH-terminal domain that contains three short peptide motifs, the verprolin-homology domain or WH2 (W or V), the cofilin-homology domain or central domain (C), and the acidic end (A) characterized by a tryptophan residue at the antepenultimate position in an acidic domain. This characteristic COOH-terminus is referred to as the WCA or VCA domain. The CA domain binds to the Arp2/3 complex and induces its conformational activation. The WH2 motif binds to one globular actin molecule and delivers it to activated Arp2/3. These two events are required to initiate an actin branch [55]. On the other hand, the NH_2-terminus varies considerably between NPF. The WCA is blocked under resting conditions and maintains NPF in an inactive conformation. Binding of small GTPases releases the masked WCA domain and activates an NPF.

The domains present in the NH_2-terminus define the different families of type I NPFs [47]. Type I NPFs include Wiskott-Aldrich syndrome protein

(WASP), neural WASP (N-WASP), three WASP family verprolin-homologous proteins (WAVE1, 2 and 3), WASP and SCAR homologues (WASH) and WASP homolog associated with actin, membranes and microtubules (WHAMM) [46, 47]. The WASP family is composed of the ubiquitous N-WASP and the hematopoietic WASP. (N)-WASP and WASP mainly work at the plasma membrane after its activation by Cdc42. In the WAVE family, WAVE2 is ubiquitously expressed, while the other two are enriched in the brain and are moderately expressed in some hematopoietic lineages. Basically, WAVE localizes at the edge of lamellipodia, where G-actin molecules incorporate into branched actin networks [56]. The WASH family involves 15 to 20 different genes depending on the species because the gene coding for WASH is located in a subtelomeric region sensitive to recombination [57]. WASH is activated after the interaction with the phospholipid PI4P and can activate the Arp2/3 complex at the surface of endosomes [58]. WHAMM is preferentially expressed in epithelial tissues, where it is localized at the Golgi and cis-Golgi to regulate anterograde transport [46, 47].

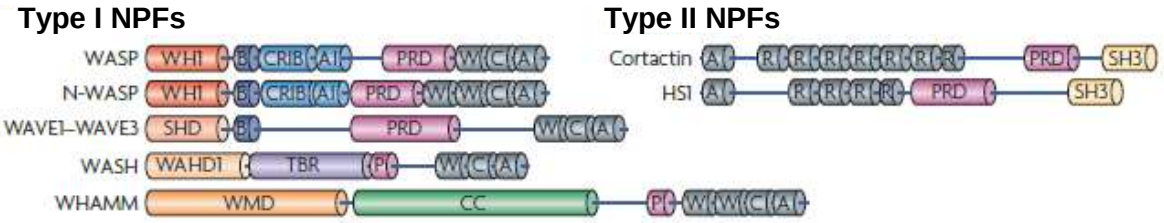

Figure 1.7. Schematic representation of the domain structures of mammalian NPFs. Type I nucleation-promoting factors (NPFs) contain carboxy-terminal WCA domains, that bind G-actin and the Arp2/3 complex. Type II NPFs contain an acidic domain at the NH_2 terminus that binds Arp2/3, central F-actin-binding repeats, and regulatory COOH-terminal domains. CRIB, Cdc42–Rac interactive binding; P, polyproline; PRD, Pro-rich domain; SHD, SCAR homology domain; TBR, tubulin-binding region; WH1, WASP homology 1 domain; WAHD1, WASH homology domain 1. Taken from Campellone and Welch **[46].**

In endothelial monolayers, the class I NPF WAVE2 is important for maintaining the endothelial barrier because it promotes VE-cadherin localization at AJ and the maturation of cell-cell junctions. WAVE2 is also required for the formation of the docking structures that guide lymphocytes across the transcellular route during diapedesis [59]. On the other hand, N-

WASP is essential for endothelial cell migration and PECAM-1 localization [60] and N-WASP depletion in human dermal microvascular endothelial cells enhances endothelial barrier integrity due to a VE-Cadherin increase at cell-cell junctions [61].

Type II NPFs such as cortactin and its homologue HS1 have acidic domains at their amino terminus that bind the Arp2/3 complex and tandem repeat domains that bind F-actin [45], but lack the complete VCA domain. Thus, they cannot deliver G-actin and are only weak NPF. Instead, cortactin has been shown to stabilize newly generated filament branches [55]. Cortactin stabilizes the endothelial barrier through the regulation of actomyosin stress fibers mediated by ROCK1 [27]. Loss of cortactin leads to defective RhoG activation and ICAM-1 clustering leading to less neutrophil adhesion and transmigration [24]. Additionally, cortactin and E-selectin interaction regulate PMN transendothelial migration via Arp2/3 that allows the formation of branched actin at lamellipodia protrusions and reticular junctions between ECs [62].

1.6 ARP2/3 INHIBITORY PROTEINS

The function of the Arp2/3 complex is to induce actin polymerization and to generate actin branches in response to different stimuli. Because actin filaments are substrates and products of the branching reaction, the autocatalytic process generates an exponential increase in actin filaments [47]. To this end, the Arp2/3 complex needs to be strictly regulated to avoid excessive actin polymerization and branching. The regulation of Arp2/3 complex activity is achieved by endogenous inhibitory proteins through direct binding to the Arp2/3 complex and competing with NPF. These proteins including PICK1, gadkin and arpin, were more recently discovered [47, 63]. The general idea is that an inhibitory protein is diffusely located throughout the cytoplasm to maintain the Arp2/3 complex silent until activated. However, a theory has been postulated that these three inhibitory proteins are specifically localized at different cellular locations, similar to the activators, suggesting that

they compete with specific NFP to control Arp2/3 activity only at specific cellular substructures (Figure 1.8) [47, 63]. In this compartmentalization theory, WAVE and arpin regulate Arp2/3 at lamellipodia, (N)-WASP and PICK1 at clathrin-coated pits, and WASH and Gadkin at endosomes.

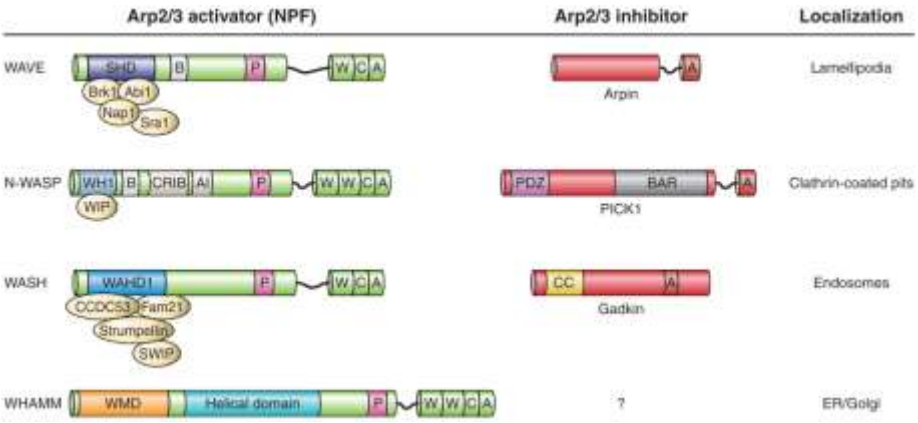

Figure 1.8. Organization of activating and inhibiting proteins of the Arp2/3 complex according to their subcellular location. All activators contain a NH2-terminal WCA domain, which binds and activates the Arp2/3 complex. All inhibitors contain an acidic motif (A), which binds also to the Arp2/3 complex to compete with NPF in the indicated sub-cellular locations. SHD, Scar/WAVE homology domain; B, basic domain; P, proline-rich region; WH1, WASP homology 1; CRIB, Cdc42 and Rac1 interactive binding region; AI, autoinhibition domain; WAHD1, WASH homology domain 1; WMD, WHAMM membrane-interacting domain; CC, coiled coiled; PDZ, PSD95-Dlg1-ZO1 domain; BAR, bin-amphiphysin-rvs domain. NOTE: An inhibitory protein antagonizing WHAMM remains to be identified.[47].

1.7 GADKIN

Gadkin interacts with the Arp2/3 complex through an acidic motif. This interaction enables gadkin to sequester Arp2/3 at motile endosomal vesicles thus inhibiting Arp2/3 activation. In different gadkin knockout cells, including B16F1, Cos7, HeLa and MEF, spreading was more efficiently and migration velocity was also increased due to an overactivation and a partial redistribution of Arp2/3 to the plasma membrane [64]. It is tempting to speculate that gadkin could antagonize the WASH complex at the surface of endosomes due to its localization [47], but this has not been experimentally proven yet.

1.8 PICK1

PICK1 is a protein containing a PDZ and a BAR domain. The PDZ domain connects PICK1 to numerous membrane receptors and transporters, such as AMPA receptor of the glutamate neurotransmitter. The BAR domain dimerizes and induces curved membranes through its banana-shaped membrane binding interface [65] and enables PICK1 to bind to F-actin [66].In the COOH-terminus, PICK1 contains an acidic motif with a tryptophan residue in the antepenultimate position that binds and inhibits the Arp2/3 complex. This inhibition is required for appropriate neuronal morphology in developing neurons. Inhibitory functions of PICK1 are regulated by the GTPase Arf1. PICK1 regulates AMPA receptor trafficking, and in particular clathrin-dependent endocytosis. Thus, it is thought that PICK1 antagonizes N-WASP at clathrin-coated pits [66, 67].

1.9 ARPIN

Arpin is the most recently identified protein that can inhibit Arp2/3. It was identified in a bioinformatic analysis that contains a typical COOH-terminal acidic motif (A) with a tryptophan residue in the antepenultimate position that binds to Arp2/3 (Figure 1.9a) but lacked the required V and C motifs for Arp2/3 activation. *In vitro*, arpin binds to the Arp2/3 complex (Figure 1.9b and 1.9c) [68]. Two possible arpin-binding sites in Arp2/3 have been identified: one located near the interface of the Arp3 and ArpC2 subunits; and the other near the interface of the Arp2 and Arp3 subunits with both binding sites possibly corresponding to the two WCA-binding sites [69] thus allowing for competition with NPFs.

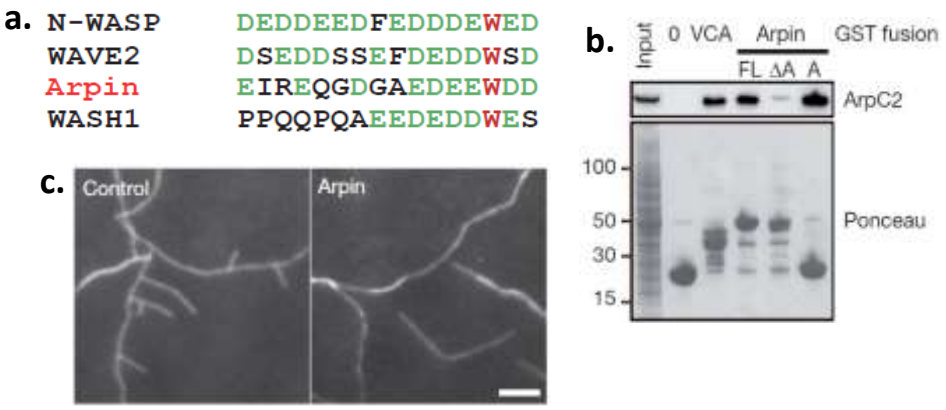

Figure 1.9. Arpin inhibits Arp2/3 activation *in vitro*. a) Alignment of the acidic motives of three NFP and arpin (in red the characteristic tryptophan of the domain). **b)** Arpin binds to the Arp2/3 complex through its acidic C-terminal region. Glutathione S-transferase (GST) pulldown with full-length arpin (FL), its last 16 amino-acids (A), ArpinΔA or the VCA domain of N-WASP as a positive control. ArpC2 is a subunit of the Arp2/3 complex. **c)** Assembly of branched actin networks monitored by TIRF microscopy using rhodamine-labelled actin in the presence or absence of arpin. Scale bar, 5 mm. Taken from Dang and collaborators (2013) [68].

Arpin is enriched at the lamellipodial tip in mouse embryonic fibroblasts (MEFs), where it colocalizes with Brk1, a subunit of the WAVE complex (Figure 1.10) [68]. This co-localization suggests that arpin can antagonize the activity of WAVE and inhibit the Arp2/3 complex in this subcellular location to regulate random migration by controlling migration speed and directional persistence [68]. However, later studies revealed that arpin is not essential for chemotaxis [70].

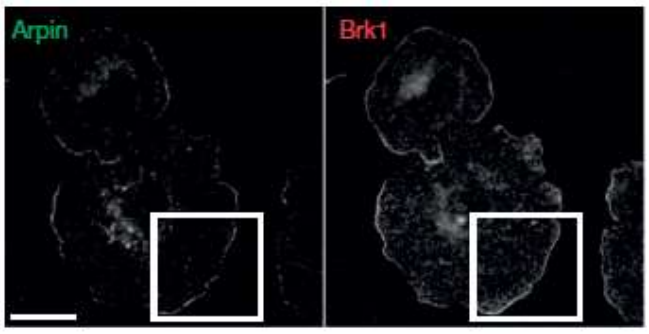

Figure 1.10. Arpin colocalizes with Brk1, a subunit of the WAVE complex, at the lamellipodial tip in MEFs. Scale bar, 20 um. Taken from Dang and collaborators (2013) [68].

Given that WAVE2 contributes to endothelial barrier integrity, arpin may also compete with WAVE2 in endothelial cells to regulate barrier functions. Previous research from our group demonstrated that arpin was expressed in colon epithelial cells and that ulcerative colitis patients had lower arpin levels in acutely inflamed tissue areas. Arpin is associated with junctional epithelial proteins and stabilized epithelial barrier integrity under basal and inflammatory conditions in an Arp2/3-dependent fashion [71]. However, nothing is known about the expression and functions of arpin in endothelial barrier regulation during inflammation. Given the functional similarity of epithelium and endothelium, we hypothesized that arpin is also expressed in ECs to control vascular barrier functions.

2. JUSTIFICATION

It is well-known that the endothelial actin cytoskeleton changes to modify junction architecture during inflammation leading to increased endothelial permeability and the recruitment of leukocytes. One critical regulator of actin cytoskeleton dynamics and endothelial barrier functions is the Arp2/3 complex. Arp2/3 activity is controlled by several proteins such as the newly identified arpin that locally antagonizes the Arp2/3 activator WAVE. Arpin has been shown to regulate junction architecture and permeability in colon epithelial cells. However, the role of arpin in regulating endothelial barrier functions during inflammation is unknown.

3. HYPOTHESIS

The Arp2/3 complex inhibitor arpin regulates endothelial permeability and leukocyte transmigration during inflammation.

4. GENERAL OBJECTIVE

To analyze the role of arpin in the regulation of endothelial permeability and leukocyte transendothelial migration.

5. PARTICULAR OBJECTIVES

1. To analyze arpin expression and localization in endothelial cells under basal and inflammatory conditions.
2. To generate and characterize arpin-depleted HUVEC.
3. To determine the role of arpin in the regulation of endothelial permeability *in vitro*.
4. To analyze the role of arpin in the regulation of actin dynamics.
5. To unravel the functions of arpin in the regulation of leukocyte transendothelial migration *in vitro*.
6. To characterize arpin$^{-/-}$ mice and analyze vascular permeability and leukocyte extravasation in comparison to WT mice.

6. MATERIALS AND METHODS

Table 6.1. Buffers and Solutions. All buffers were prepared in deionized water purified using a Mili-Q-system (Millipore).

Buffer	Recipe
Bacteria Lysis Buffer, pH 8.0	50 mM NaH_2PO_4 300 mM NaCl 10 mM Imidazole
Wash Buffer, pH 8.0	50 mM NaH_2PO_4 300 mM NaCl 20 mM Imidazole
Elution Buffer, pH 8.0	50 mM NaH_2PO_4 300 mM NaCl 250 mM Imidazole
SDS lysis buffer	10mM Tris-HCl 2mM EDTA 25mM HEPES 1% SDS
RIPA lysis buffer	20 mM Tric-HCl pH 7.5 150 mM NaCl 1 mM Na_2EDTA 1 mM EGTA 1% NP-40 1% sodium deoxycholate
SDS-PAGE Running Buffer, pH 8.3	20 mM Tris-HCl pH 6.8 192 mM glycine 0.1% SDS
Transfer Buffer, pH 8.3	20 mM Tris-HCl pH 6.8 192 mM glycine 0.1% SDS 20% methanol

5X SDS Loading sample buffer	250 mM Tris-HCl pH 6.8 10% SDS 30% glycerol 5% β-mercaptoethanol 0.02% bromophenol blue
TBS-T, pH 8.0	150 mM NaCl 10 mM Tris-Base 0.1% Tween-20
Blocking solution for Western blot	5% milk powder or 5% BSA TBS-T
TAE electrophoresis buffer, pH 8.0	40 mM Tris 20 mM acetic acid 1 mM EDTA
PBS	138 mM NaCl 3 mM KCl 8.1 mM Na_2HPO_4 1.5 mM KH_2PO_4
PBS-T	PBS 0.05% Tween-20
OPD (o-phenylenediamine dihydrochloride) solution, pH 5.0	0.4 mg/mL OPD 0.4 mg/mL H_SO_s 0.05 M H_2PO_4 0.05 M $Na_3C_6H_5O_7$
Hypotonic solution, pH 7.4	0.2% NaCl 1% BSA 20 mM Hepes
Hypertonic solution, pH 7.4	1.6% NaCl 1% BSA 20 mM HEPES

Table 6.2. Antibodies

Supplier	Antibody	Catalogue Number
Santa Cruz (California)	Anti-VE-Cadherin (clone F-8)	sc-9989
	Anti-ICAM-1 (clone 15.2)	sc-107
	Anti-β-catenin (clone E-5)	sc-6963
	m-IgG$_1$ BP-HRP	sc-525408
	Mouse anti-rabbit IgG-HRP	sc-2357
Thermo Fisher Scientific (Waltham, MA).	Anti-ZO-1	61-7300
	Anti-claudin-5 (clone 4C3C2)	35-2500
	Anti-γ-Tubulin (GTU-00)	T6557
	Anti- Coronin1B	PA5-21799
	Alexa Fluor-488 goat anti-mouse IgG	A11001
	Alexa Fluor-568 rabbit anti-mouse IgG	A11061
	Alexa Flour-647 goat anti-mouse IgG	A21236
	Alexa Fluor-647 goat anti-rabbit IgG	A21245
	Alexa Flour-568 donkey anti-rabbit IgG	A10042
Cell Signaling Technology (Danvers, MA).	Anti-WASP	4860
	Anti-WAVE2 (clone DSC8)	3659
	Anti-p-Cofilin (S3) (clone 77G2)	3313
	Anti-Cofilin	3312
	Anti-pMLC (Ser19)	3671
	Anti-MLC	3672
	Anti-pMYPT1 (Thr696)	5163
	Anti-pMYPT1 (Thr853)	4563
	Anti-MYPT1	2634
	Anti-ROCK1 (clone C8F7)	4035
	Anti-DAPK3/ZIPK	2928
Sigma Aldrich (St. Louis, MO)	Anti-vinculin	V4139

BD Bioscience (Franklin Lakes, NJ)	Anti-mDia	610848
US Biological Life Science (Salem, MA)	Anti-MRP14 (Clone 2B10)	376767
Biolegend (San Diego, CA)	APC Anti-ICAM-1 (Clone HCD54) PE Anti-VCAM-1 (Clone STA) PerCP/Cyanine5.5 Anti-P-selectin (Clone AK4) PE/Cyanine7 Anti-E-selectin (Clone HAE-1f) Anti-PECAM-1 (clone MEC 13.3)	322712 305806 30924 336016 102502
Donated[1]	Anti-cortactin (clone 289H10) Anti-arpC5 (Clone 323H3)	NA
Donated[2]	Anti-Actin	NA

[1]Cortactin monoclonal (clone 289H10) and arpC5 monoclonal (clone 323H3) antibodies were kindly provided by Dr. Klemens Rottner and Dr. Theresia Stradal (Helmholtz Centre for Infection Research, Braunschweig, Germany).

[2]Actin monoclonal antibody was kindly provided by Dr. José Manuel Hernández (Department of Cell Biology, Cinvestav-IPN, Mexico City, Mexico).

Table 6.3. Reagents

Supplier	Reagent	Catalogue Number
Peprotech	Recombinant human TNFα Recombinant human IL-1β Recombinant human IL-8	300-01A 200-01B 200-08M
Sigma-Aldrich	CK-666 Y27632 Puromycin dihydrochloride	SML0006 Y0503 P8833
ROCHE	Complete PhosSTOP	11697498001 04906837001

Tocris Bioscience (Bristol, UK)	HS38	5768/5
Thermo Fisher Scientific	Alexa Flour 488 phalloidin	A12379
Biolegend	Flash Phalloidin Red 594	424203

6.1 EXPRESSION AND PURIFICATION OF RECOMBINANT ARPIN

The full length human arpin sequence was cloned into the pET-32a(+) expression vector generated by GenScript (Piscataway, NJ). Arpin sequence was clones between the restriction sites BamH1 and XhoI. The Arpin-pET-32a(+) construct was used to transform Rosetta (DE3) *E. coli*. Overexpression of the fusion protein was induced by adding 1 mM isopropyl-D-thiogalactopyranoside (IPTG; Sigma Aldrich, St. Louis, MO) to the transformed cell culture for 18 hours at 20°C. The fusion protein was extracted from the bacteria using Bacteria Lysis Buffer and by sonicating them five times at 60% amplitude for 30 seconds, the lysate was centrifuged at 10 min at 15,000 g to remove all the cellular debris. The fusion protein contains two His-tags that makes it easily to purify using Ni-NTA agarose affinity chromatography (Qiagen; Hilden, Germany). Then, the supernatant was transferred into a column that contains 2 mL of Ni-NTA resin, the flow through fraction was collected and it contained any protein which did not bound to the resin. The resin was washed twice with 20 mL Wash Buffer and the protein was eluted twice with 10 mL Elution Buffer, in each step a sample of 100 µL was taken to analyzed by 12% SDS-PAGE. Protein concentration was determined by DC Assay as it is described below (Bio-Rad, Hercules, CA) and purity was analyzed by 12% SDS-PAGE.

6.2 PRODUCTION OF POLYCLONAL ANTIBODIES AGAINST ARPIN.

500 µg of purified recombinant arpin were used to immunize one rabbit by subcutaneous injection of an emulsified 1:1 mixture of protein and TiterMax Gold (Sigma Aldrich; St. Louis, MO). At 14, 21 and 35 days after the first immunization, the rabbit was re-immunized with subcutaneous injections of 140 µg of recombinant arpin each. Pre-immune and immune sera were analyzed by ELISA and Western blot as described below. All sera were used for western blots and immunofluorescence stainings.

6.3 ELISA

96-well plate was sensibilized with 5 µg of recombinant arpin in 100 µL carbonate coating buffer (Thermo Fisher Scientific, Waltham, MA), overnight at 4°C. Then, the plate was washed 5 times with PBS-T and blocked with 5% skim-milk. Next, incubation with pre-immune and immune sera at different dilutions was performed overnight at 4°C, followed by 5 washing steps with PBS-T and an incubation of anti-rabbit secondary antibody conjugated with HRP at RT for 2 hours. Then, the plate was washed again 5 times with PBS-T and 100 µL OPD solution was used to reveal the ELISA, the reaction was stopped with 100 µL 2 N sulfonic acid. Absorbances were quantified using a spectrophotometer at 450 nm.

6.4 CELL CULTURES

Human umbilical vein endothelial cells (HUVEC) were isolated from donated discarded umbilical cords. Under sterile conditions, the umbilical cords were washed with sterile water to remove excess blood. In the upper end of the cord vein, a cannula with a syringe containing PBS and Streptomycin/Penicillin was inserted and the inside content of the cord removed. Then, both cord ends were sealed with hemostatic clamps and, subsequently, 0.25% trypsin-EDTA (Sigma) was instilled using a 25 mL syringe until the vein was filled and then incubated at 37°C for 10 min in a water bath.

Every 2 minutes, the umbilical cord was gently massaged to facilitate the digestive process. Next, the clamp of the lower end was removed, and the content recovered and centrifuged at 1500 rpm for 5 minutes. The cell pellet was resuspended in Endothelial Cell Media (ECM, ScienCell™ Research Laboratories, Carlsbad, CA) supplemented with 10% Fetal Bovine Serum (FBS) plated into growth-enhanced treated T25 flask (TPP, Trasadingen, Switzerland) and kept at 37°C in a humid atmosphere containing 5% CO_2. Cells from passage 1 to 7 were used for functional experiments. For inflammatory conditions, HUVEC monolayers with 80% confluency were treated with 15 ng/mL TNFα (PeproTech, Mexico City, Mexico) or 15 ng/mL IL-1β (PeproTech) for 18 hours.

HEK-293T cells were cultivated in DMEM medium (Sigma-Aldrich) supplemented with, 1X pyruvate, 1X non-essential amino acids, 1X sodium pyruvate and 10% FBS and kept at 37°C in a humid atmosphere containing 5% CO_2.

Human microvascular endothelial cells (HMEC-1) were cultured in MCDB-131 medium (Sigma-Aldrich) supplemented, 1 µg/mL hydrocortisone, 20 µg/mL endothelial cell growth supplement, 10 mM L-glutamine, and 10% FBS and kept 37°C in a humid atmosphere containing 5% CO_2.

The mouse brain endothelial cell line bEnd.3 was cultured in DMEM medium (Sigma-Aldrich) supplemented with 10% FBS and kept at 37°C in a humid atmosphere containing 5% CO_2.

Murine lung endothelial cells (MLEC) were isolated and cultured as described [27].

6.5 RNA EXTRACTION

Cell monolayers growing in a 6-well plate were added 0.3 mL of TRIzol Reagent (Thermo Fisher Scientific, Waltham, MA) directly to lyse the cells, incubated for 5 min to allow the complete dissociation of the nucleproteins complex and transferred into a 1.5 mL microtube. Then 60 µL of chloroform (Sigma Aldrich, St. Louis, MO) were added and incubated for 3 min. The

mixture was centrifugated for 15 min at 12,000 g at 4°C. The aqueous phase containing the RNA was transferred into a new 1.5 mL microtube. Next, 150 µL of isopropanol (Sigma Aldrich) were added to the aqueous phase and incubated for 10 min at 4 °C to allow the precipitation of RNA. Then, the sample was centrifuged for 10 min at 12,000 g for 4 °C and the supernatant was discarded. The RNA pellet was washed with 0.3 mL of 75% ethanol (Sigma Aldrich) and vortexed for 10 sec. The sample was centrifuged for 5 min at 7,500 g at 4°C and the supernatant was discarded. The RNA was dried at RT for 10 min and resuspended in 20 µL or RNase-free water. Finally, the RNA in suspension was incubated in heat block at 60°C for 10 min. The RNA was quantified using a nanodrop 2000 (Thermo Fisher Scientific) the ratio 260/280 ~2, indicates pure RNA.

6.6 DNase I TREATMENT

To remove genomic DNA from the RNA preparations, DNase I treatment was carried out in a total volume of 20 µL: 10 µg RNA, 2 µL 10X reaction buffer with $MgCl_2$ and 2 µL DNase I, RNase-free (Thermo Fisher Scientific). The mixture was incubated at 37°C for 30 min. To finish the reaction, the sample was added 2 µL 50 mM EDTA and incubated at 65°C for 10 min. The RNA was prepared as a template for reverse transcriptase.

6.7 cDNA SYNTHESIS

The RevertAid First Strand cDNA Synthesis Kit was used to synthesize cDNA from RNA template DNA-free. The reaction was carried out in a total volume of 20 µL: 2.5 µg of RNA, 1 µL of Oligo $(dT)_{18}$, 4 µL 5X Reaction buffer, 1 µL of 20U/ µL RiboLock RNase Inhibitor, 2 µL 10 mM dNTP mix and 1 µL 200U/ µL RevertAid M-MuLV RT. The mixture was incubated at 42°C for 60 min. To terminate the reaction, the sample was incubated at 70°C for 5 min. The cDNA was used for End-Point and Quantitative (q) PCR.

6.8 END-POINT PCR

End-point PCR was carried out in a total volume of 10 µL: 9 µL Platinum® PCR SuperMix 1.1X, 0.15 µM forward primer, 0.15 µM reverse primer, and 125ng/µL cDNA. PCR conditions were as follows: 95 °C for 3 min, followed by 35 cycles of 95 °C for 30 sec, 60 °C for 30 sec and 72 °C for 30 sec and a final extension at 72 °C for 10 min The PCR products were separated by electrophoresis on 2% agarose gels.

6.9 qRT-PCR

qRT-PCR was carried out in a total volume of 10 µL containing 5.0 µL Power SYBR Green PCR Master Mix 2X (Qiagen, Hilden, Germany), 125 ng cDNA, and 0.15 µM of each primer in a 195 StepOne Real-Time PCR System (Applied Biosystems, Foster City, CA). Conditions were set as follows: activation at 95°C for 10 min, 40 cycles including denaturation at 95 °C for 15 s, and data acquisition during annealing/extension at 60 °C for 60 s. Following the last cycle, melting curves were recorded by heating from 60 to 95°C in increments of 0.5°C/s. 7SL was used as house-keeping gene. 7SL scRNA is a nonprotein-coding RNA (npcRNA) suitable for qPCR data normalization in the human transcriptome given its stable expression [72]. Relative expression was quantified using the $2^{-\Delta\Delta CT}$ method [73]. Primers that were used are listed in Table 6.4.

Table 6.4. Primer sequences used in qRT-PCR

Gene	Forward 5'- 3'	Reverse 5'- 3'
h7SL scRNA	5'-ATCGGGTGTCCGCACTAAGTT -3'	5'-CAGCACGGGAGTTTTGACCT -3'
hArpin	5'-AAACCAGCCTGATCAACACA-3'	5'-AAATTCTCATGCCTCAGCCT-3'
hPICK1	5'-ATGATTCAGGAGGTGAAGGG-3'	5'-CGGTGCTTGACTTTCTTCAA-3'
hGadkin	5'-GAAATGACGACAGCACATCC-3'	5'-TAAGTGCTGCCCGTAGAATG-3'

6.10 PROTEIN EXTRACTION AND QUANTIFICATION

HUVEC and HMEC-1 monolayers were washed once with cold PBS. Then, cells were lysed using SDS lysis buffer, Complete protease inhibitor cocktail (Roche, Basel, Switzerland) and PhosSTOP phosphatase inhibitor

cocktail (Roche) and sonicated three times at 40% amplitude for 10 seconds. Next, the extracted protein was quantified using the DC Protein Assay (Bio-Rad). A calibration curve was measured with a series of Bovine Gamma Globulin (BGG) dilutions ranging in concentration from 1 to 7 µg/µL. A sample of 1 µL of the lysates was mixed with 10 µL of the reagent A' (20 µL of reagent S in 1 mL of reagent A) and 80 µL of the reagent B. All samples were incubated at room temperature under gentle agitation for 15 minutes. Finally, samples were measured at 750 nm using a Tecan® Infinite M200 Plate Reader. To determine the protein concentration, the absorbance value of the unknown samples was compared to the calibration curve using linear regression.

6.11 WESTERN-BLOT

40 µg of total protein were separated by 8%, 10% or 12% SDS-PAGE (110 V, 120 minutes). Then, the separated extracts were transferred onto a nitrocellulose membrane (0.45 µm, Bio-Rad, Hercules, CA) at 350 mA for 90 minutes. Subsequently, the membrane was blocked in blocking solution (5% BSA or 5% Svelty-milk in TBS-T) for 1 h. Afterwards, the primary antibody of interest in blocking solution was added to the membrane and incubated overnight at 4°C. Then, the primary antibody was removed, and the membrane was washed three times with TBS-T for 10 min. Next, the species-specific secondary antibody coupled to HRP was added to the membrane and incubated for at least 1 h at room temperature. The secondary antibody was removed, and the membrane was washed three times with TBS-T for 10 min. Finally, the bands were revealed using Super west *Femto* maximum sensitivity substrate (Thermo Fisher Scientific) using a ChemiDoc device (Bio-Rad).

6.12 CELL IMMUNOFLUORESCENCE

HUVEC were seeded on glass coverslips (pretreated with 0.8% gelatin at 37°C for 30 minutes) in a 24-well plate. The confluent cells were fixed using 4% PFA at room temperature for 10 min. The fixed cells were washed with PBS three times and permeabilized with 0.1% Triton X-100 for 10 minutes at 4°C.

Samples were blocked in PBS containing 3% BSA. Subsequently, cells were incubated with primary antibodies diluted in blocking solution at 4°C overnight. After washing the samples three times with PBS for 5 min, cells were incubated with species-specific fluorescently labeled secondary antibodies and rhodamine or Alexa Fluor 488 labeled phalloidin for 1 h at room temperature in the dark. Finally, samples were washed three timed with PBS in the dark and the cover slips were mounted on glass slides using Vecta Shield containing DAPI to stain nuclei.

6.13 GENERATION OF VIRAL PARTICLES

For the generation of arpin-depleted HUVEC, shRNA (short harpin RNA) against arpin (shRNA arpin: 5'-GGAGAACTGATCGATGTATCT-3', REF) and a control scrambled sequence (shRNA scrambled: 5'-CGGAGAAGTGGAGAAGCATAC-3') which has no specific mRNA targets were cloned into the expression vector pLKO.1.

Lentiviral particles were generated using the TransLenti Viral Packaging Mix (Thermo Scientific). This kit contains the plasmids pTLA1-Pak, pTLA1-Enz, pTLA1 Env, pTLA1-Rev and pTLA1-TOFF, which encode for the proteins necessary to form the viral particles. The viral packaging plasmids and the lentiviral vector pLKO.1 containing either arpin-specific shRNA or a scrambled control shRNA were mixed as follows: 6 µg pTLA1-Pak, 4 µg pTLA1-Enz, 6 µg pTLA1 Env, 4 µg pTLA1-Rev, 8 µg pTLA1-TOFF and 9 µg pLKO1-shRNA Ctrl/Arpin. The plasmid mixture in 2.4 mL DMEM medium without serum containing 0.14 mL poliethylenimine (PEI) at 1 mg/mL were incubated at room temperature for 15 minutes. Then, the mixtures were added to a culture of HEK-293T cells at 80% confluence in a 10 cm culture dish and incubated at 37°C with 5% CO_2 for 4 h. Afterwards, the medium was exchanged with fresh medium. After 48 h, the medium was collected and stored at 4°C. Fresh medium was added and collected again 24 h later. Recovered media at 48 h and 72 h was filtered using 0.45 µm filters to remove cell debris. The collected

supernatants were centrifuged at 13,000 rpm, 4°C for 2 hours and the viral pellet used as described below.

6.14 GENERATION OF ARPIN-DEPLETED HUVEC

The viral pellet was resuspended in 3 mL HUVEC medium together with 1 µg/mL polybrene. This mixture was added to monolayers of sub-confluent HUVEC in growth-enhaced treated 6-well plates (TPP, Trasadingen, Switzerland); and the plates were centrifuged at 3000 rpm for 1 h to facilitate lentiviral contact with the cells. HUVEC were then incubated at 37°C for 24 h, followed by exchange with fresh medium containing 1.5 µg/mL puromycin (Sigma-Aldrich) to select the infected cells. A survival curve using different puromycin concentrations revealed that 1.5 µg/mL is the minimum concentration killing 100% of non-transfected HUVEC after 48 h. The medium containing puromycin was changed every three days until infected cells grew to confluence (~4-7 days). After reaching confluency, cells were trypsinized and seeded into T25 flasks for expansion. Knock-down efficiency was tested by Western-blot.

6.15 FITC-DEXTRAN PERMEABILITY ASSAY

60,000 HUVEC were seeded on 6.5-mm-diameter transwell filters (CORNING, Life Science) with 0.4-µm pore size coated with 0.8% gelatin and cultivated for 48 h. Then, 0.25 mg/mL 150 kDa FITC-dextran was added to the upper chamber and the medium of the lower chamber was changed. After 60 minutes, a sample of 100 µl medium was taken from the lower chamber and used to quantify the FITC-dextran that crossed the endothelial monolayer using a spectrofluorometer with excitation of 480 nm and emission of 520 nm. For analyzing permeability during inflammatory conditions, before adding FITC dextran, HUVEC monolayers were treated with 15 ng/mL TNFα (PeproTech) for 18 h.

6.16 CALCIUM-SWITCH ASSAY

HUVEC were seeded on coverslips coated with 0.8% gelatin in ECM medium that contains several sources of calcium. To generate a calcium-free environment the cells were cultivated for 2 h in ECM medium no FBS in the presence of EGTA (2.5 mM) to chelate free calcium. Then the media containing EGTA was washed off and exchanged with normal ECM medium containing 10% of FBS. Cells were cultivated for 0, 30 min, 1, 2, 4, 6 and 24 h, then fixed using 4% PFA and stained for VE-Cadherin as described above.

6.17 ISOLATION OF HUMAN POLYMORPHONUCLEAR (PMN) CELLS.

6 mL blood were collected from a consenting healthy donor in blood collection tubes. 3 mL of Histopaque 1119 and 3 ml of Histopaque 1077 (Sigma-Aldrich) were layered in a 15 mL conical centrifuge tube, and the collected blood was carefully added on top of the Histopaque 1077 layer. The tube was centrifuged at 2750 rpm at 4°C for 30 minutes without brakes. The PMN were collected from the interface of the Histopaque 1119 and Histopaque 1077 layers. The PMN suspension was washed twice with 10 mL PBS at 4°C; then cells were centrifuged at 1500 rpm at 4°C for 5 min, and 10 mL of hypotonic solution (0.2% NaCl, 1% BSA, 20mM HEPES) was added to the PMNs for one minute on ice to lyse erythrocytes followed by addition of 10 mL hypertonic solution (1.6% NaCl, 1% BSA, 20mM HEPES) at 4°C. Subsequently, PMN cells were centrifuged at 1500 rpm and resuspended in RPMI 1640 medium supplemented with 10% FBS at 4°C. Cells were counted using a Neubauer chamber and stored on ice until used in transmigration assays.

6.18 TRANSENDOTHELIAL MIGRATION (TEM) ASSAY

60,000 HUVEC were seeded on 6.5-mm-diameter transwell filters (CORNING, Life Science) with 5.0-µm pore size coated with 0.8% gelatin and grown to confluence. Then, cells were activated with 15 ng/mL TNFα for 18 hours. The monolayers on filters were washed twice with ECM medium. Then,

the upper reservoirs were filled with 100 µL RPMI 1640 medium (Sigma Aldrich) containing $5x10^5$ neutrophils. The lower reservoirs were filled with 600 µL of medium containing 80 ng/mL IL-8 (Peprotech, Mexico City, Mexico) as chemoattractant. After 45 min at 37°C the numbers of transmigrated neutrophils in the lower reservoir were counted using a Neubauer chamber.

6.19 FLOW CYTOMETRY

HUVEC seeded in 6-well plates with 80% of confluency, activated or not with 15 ng/mL TNFα for 18 hours were incubated with APC anti-human ICAM-1, PE anti-human VCAM-1, PE/Cy7 anti-human E-selectin and PerCP/Cy5.5 anti-human P-selectin (Biolegend, San Diego, CA) for 30 min. Subsequently, HUVEC were washed with PBS and detached using TrypLE™ Express Enzyme (Gibco) at 37°C for 5 min. Then, cells were washed with PBS and fixed using 4% PFA for 30 min. Finally, cells were washed once and resuspended with Perm Wash (10% FBS, 0.1% Saponin, 2.5mM EDTA in PBS). Cells were analyzed using a CytoFLEX flow cytometer and FlowJo v10.0 software.

6.20 GENERATION OF ARPIN$^{-/-}$ MICE

Arpin$^{-/-}$ mice on a C57Bl/6 genetic background were generated by CYAGEN (Santa Clara, CA) using the CRISPR/Cas9 methodology with two gRNA sequences (gRNA(3): 5'-CTATGCAGCAGGGTAGCGCCAGG-3' and gRNA(4): 5'-CGCACAGTGATAGTCGGAGCCGG-3') that target the exon 3 of the arpin mouse gene (Figure 6.1). Cas9 mRNA and gRNA sequences were co-injected into fertilized mouse eggs to generate targeted knockout offspring. F0 founder animals were identified by genotyping and sequencing. Positive founders were bred with C57Bl/6 WT mice to test germline transmission. Positive F1 animals were shipped and used to establish a colony at the animal facility of Cinvestav-IPN. All mouse experiments have been approved by the animal care and use committee of Cinvestav-IPN.

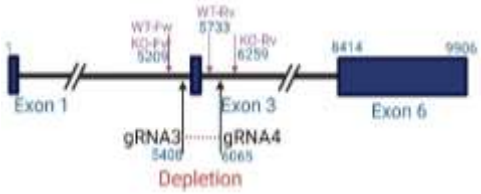

Figure 6.1. Arpin mouse gene showing exon 3, which was depleted using two gRNA sequences and CRISP/Cas9 technology to generate a complete arpin KO (arpin$^{-/-}$) mouse model.

6.21 GENOTYPING

Genomic DNA was prepared from mouse tail samples dissolved in 12 mM NaOH and 0.2 mM EDTA and incubated at 98°C for 1 h, followed by addition of 40 mM Tris-HCl pH 5.5. Then, the samples were centrifuged at 15,000 rpm for 5 min and the supernatant used for PCR. Genotyping of the WT and arpin-targeted alleles were performed in two PCR setups using the following primers: forward 5'-GCTGGCAACTTCAATCCTGCCT-3'; and reverse 5'-GAGACAAACAAGTCAGTCTAACAGCCTC-3', producing a PCR fragment of 552 bp derived from the WT allele only; and forward 5'-GCTGGCAACTTCAATCCTGCCT-3'; and reverse 5'-CAGTGTTCCCAGGGCTTGTCTGA-3', producing PCR fragments with a size of 1073 bp (WT allele) and ~420 bp (mutant allele) PCR was carried out in a total volume of 10 µL and PCR conditions were as follows: 94 °C for 5 min, followed by 35 cycles of 94 °C for 30 sec, 60 °C for 30 sec and 72 °C for 60 sec, a final extension at 72 °C for 5 min and 4 °C ∞. The PCR products were separated by electrophoresis on 2% agarose gels.

6.22 HISTOLOGY

For mouse lung hematoxylin and eosin staining, mice were anesthetized and sacrificed. Then, the thoracic cavity was opened, and lungs were collected and submerged in 4% PFA for 48-72 h. Next, lung tissues were dehydrated with alcohol solutions for 1h each, 70% ethanol, 96% ethanol, absolute ethanol, alcohol-Xylol and 100% Xylol. Then, lungs were embedded in Paraffin I for 2 h and Paraffin II for 2 h. Tissues blocks were placed intro paraffin molds and left them at RT to solidify. Afterwards, samples were cut into 8 µm sections,

mounted on glass slides and deparaffinized with the same alcohol solutions as paraffin embedding in the inverted order. Next, samples were washed with tap water twice, Harris hematoxylin was added to the tissues, incubated at RT for 7 min and washed twice with tap water. Acidic alcohol was added for 10 sec and washed twice with tap water. Lithium carbonate solution was added and incubated for 10 sec and washed with tap water twice. Samples were incubated for 1 min with 80% ethanol and incubated for 15 sec with eosin. Finally, samples were washed with ethanol and xylol solutions as was previously described and mounting resin was added to the samples.

The histological analyses and score calculations were done by a pathologist in a blinded fashion. The histological score considers the presence or absence of edema, microhemorrhage, congestion, presence of immune cells in the tissue and the extent of all these parameters across the tissue. A score of 0 indicates no inflammation; 1 low inflammation; 2 moderate inflammation; 3 high inflammation [74, 75].

6.23 LUNG IMMUNOFLUORESCENCE

For mouse lung tissue staining, mice were anesthetized and sacrificed. Then a 1:1 dilution of Tissue-Tek (Fisher Health Care, Waltham, MA) and PBS was injected via the trachea into the lungs, and the trachea was ligated to avoid leakage. The lungs were collected and embedded in Tissue-Tek. Then, the samples were frozen, cut into 8 µm sections using a cryostat (Leica, Wetzlar, Germany) onto glass slides. Subsequently, tissue sections were fixed in absolute ethanol at -20 °C for 30 min and incubated with 0.2% $NaHB_4$ for 5 minutes at RT to reduce autofluorescence. Samples were blocked using a PBS solution containing 6% BSA and 0.01% Tween. Subsequently, samples were incubated with primary antibodies diluted in 6% BSA in PBS at 4°C overnight. Tissue samples were washed three times with PBS for 5 min and then incubated with rhodamine-labeled phalloidin (Thermo Fisher Scientific) and species-specific fluorescently labeled secondary antibodies in the dark for 1 h at room temperature. The samples were then incubated in 0.1% Sudan Black

B diluted in 70% ethanol for 5 min at room temperature to further reduce autofluorescence. Finally, preparations were washed with water and mounted in vecta-shield containing DAPI to stain nuclei.

6.24 CREMASTER TISSUE IMMUNOFLUORESCENCE

For cremaster muscle staining, mice were anesthetized, sacrificed, and the cremasters collected and fixed in 4% PFA for 45 min at 4°C. Next, the tissues were blocked and permeabilized with a solution of PBS containing 25% FBS and 0.5% Triton X-100 for 4 h at room temperature. Then, cremaster muscles were incubated with primary antibodies diluted in a solution of PBS with 10% FBS at 4°C overnight. Tissues were washed three times with PBS for 10 min and incubated with species-specific fluorescently labeled secondary antibodies in the dark for 2 h at room temperature. Finally, cremaster muscles were washed three times with PBS for 30 min in the dark and mounted on glass slides.

All samples were examined using a laser confocal microscope (Leica TCS SP8) and analyzed using ImageJ software (NIH, Bethesda, MD) or Imaris Software (Oxford instruments, Abingdon, UK).

6.25 VASCULAR PERMEABILITY ASSAY

For permeability assays in the lungs, arpin$^{+/+}$ and arpin$^{-/-}$ male mice, between 8 to 12 weeks old, were anesthetized with 125 mg/kg ketamine hydrochloride and 12.5 mg/kg xylazine and injected with 50 mg of 150 kDa FITC-dextran (Sigma-Aldrich) per 1 kg of body weight via the cannulated carotid artery. After 30 min, the mice were perfused with 30 mL of PBS to remove all the blood from the circulation. Then, lungs were collected, weighted, and homogenized in 1 mL of PBS. A sample of 100 µL was used to measure the fluorescence in the tissue using a fluorometer with excitation of 480 nm and emission of 520 nm and the mean fluorescence intensity (MFI) was normalized to tissue weight.

Modified Miles assay in the skin were performed using female 8-12-week-old arpin$^{+/+}$ and arpin$^{-/-}$ mice as was described [24]. Mice were injected

intraperitoneally with 4 mL of 1.5% Evans Blue in PBS per kg of weight. After 2 hours, mice were anesthetized with an intraperitoneal injection of 125 mg/kg ketamine hydrochloride and 12.5 mg/kg xylazine. Subsequently, 50 µL of PBS containing 450 ng Histamine or PBS only were intradermally injected into the shaved back skin. After 30 min, the mice were sacrificed, and the skin around the injection sites was cut (circles of approx. 1 cm in diameter) and weighted. The skin circles were immersed separately in 1 ml of formamide for 24 h to extract the blue dye and then read spectrophotometrically at 620 nm. Permeability values were expressed at OD per gram tissue.

6.26 INTRAVITAL MICROSCOPY

2 h before cremaster muscle exteriorization, arpin$^{+/+}$ and arpin$^{-/-}$ male 6-8-week-old mice were injected intrascrotally with 300 ng TNFα in 0.3 mL 0.9% saline solution. Mice were anesthetized with an intraperitoneal injection of 125 mg/kg ketamine hydrochloride and 12.5 mg/kg xylazine and cremaster muscles were exteriorized and fixed prepared intravital microscopy as described [76]. The muscle was extended to clearly visualize the blood vessels. Postcapillary venules with a diameter of 20 to 40 µm were recorded using an intravital upright microscope using a 40x water immersion objective. DIC images taken with 10x objective were used to analyze extravasated cells into the tissue. Rolling and arrested leukocytes in the venules were quantified by transillumination intravital microscopy. Leukocyte rolling velocity was obtained with recorded videos and analyzed with ImageJ (NIH Bethesda, MD), calculating the distance that a leukocyte migrated in the vessel in 5 sec.

6.27 STATISTICS

Statistical analyses were performed using Prism 8.0 software (GraphPad). Two-tailed Student's t-test or two-tailed Student's t-test with Welch's correction was assessed for two group comparison. Two-way ANOVA was assessed for multiple group comparisons. χ^2 tests were performed to test the probability of the deviation between the observed and the expected values in mating statistics.

7. RESULTS

7.1 RECOMBINANT ARPIN PURIFICATION AND PRODUCTION OF A POLYCLONAL ANTI-ARPIN ANTIBODY.

As there is no available commercial anti-arpin antibody, a rabbit polyclonal anti-arpin antibody was generated. To this end, first, the recombinant human full-length arpin protein was expressed in Rosetta (DE3) *E. coli*. Overexpression of the recombinant tagged protein (Figure 7.1A) was induced using IPTG and purification of the protein from bacterial lysates was performed using Ni-NTA agarose affinity chromatography, exploiting the two His-tags of the recombinant protein that have with high affinity for nickel (Figure 7.1B).

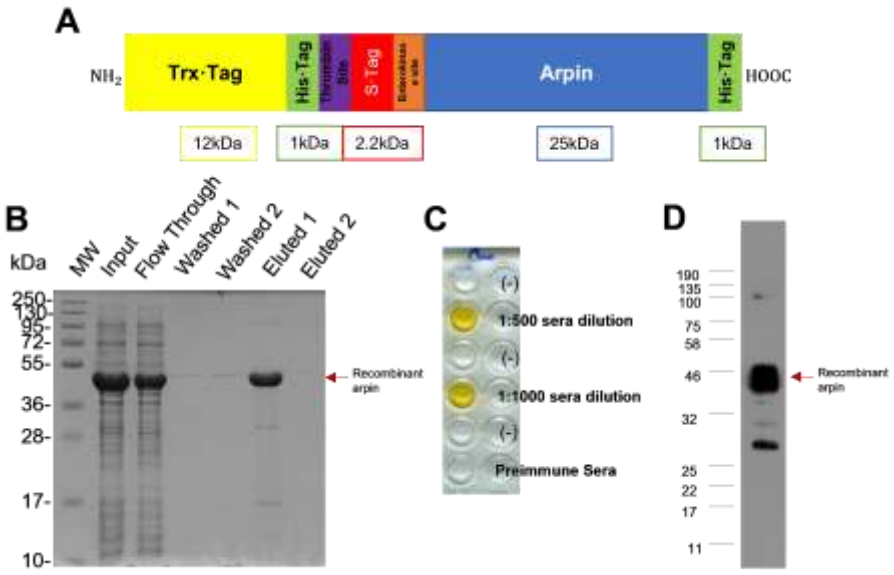

Figure 7.1. Purification of recombinant arpin and polyclonal anti-arpin antibody test. (A) Schematic representation of the recombinant arpin protein (~46 kDa) used to produce the polyclonal arpin-antibody in a rabbit. The molecular weight of the tags and protein that compose the entire recombinant protein are shown. **(B)** Representative Coomassie blue staining after SDS-PAGE following purification of the recombinant arpin using Ni-NTA agarose affinity chromatography. The different lanes represent all steps of the purification process. Eluted 1 fraction was enriched for recombinant arpin and thus used for the immunization of the rabbit. MW= molecular weight bands. **(C)** ELISA experiment using two dilutions of the serum derived from the immunized rabbit to test reactivity against the recombinant arpin protein. **(D)** Representative Western-blot using the immune serum at 1:4000 dilution to test the recognition of the recombinant arpin protein

Eluted 1 fraction was highly enriched for the recombinant arpin at the predicted molecular weight of 46 kDa, and therefore used for immunizations. After three immunizations of the same rabbit, sera were pooled and used to test for reactivity against the recombinant arpin protein by ELISA and Western blot. As shown in figures 7.1 C and D, the pooled serum contains polyclonal anti-arpin antibodies and recognized the recombinant protein at the expected molecular weight.

7.2 ARPIN IS PRESENT IN ENDOTHELIAL CELLS WITH A CYTOSOLIC LOCALIZATION.

Arpin was first discovered and described in fibroblast [68]. Later, arpin expression was discovered in other cells including epithelial [71]. However, arpin expression in endothelial cells had not been studied. In this project, it was discovered that arpin mRNA is expressed in different the human endothelial cells HMEC-1 and HUVEC (Figure 7.2A)., and as the mouse endothelial cells bEnd.3 and MLEC (Figure 7.2B). Western blot of arpin confirmed that the protein was also present at similar levels in the human endothelial cells HUVEC and HMEC-1with the predicted molecular weight of ~25 kDa (Figure 7.3A).

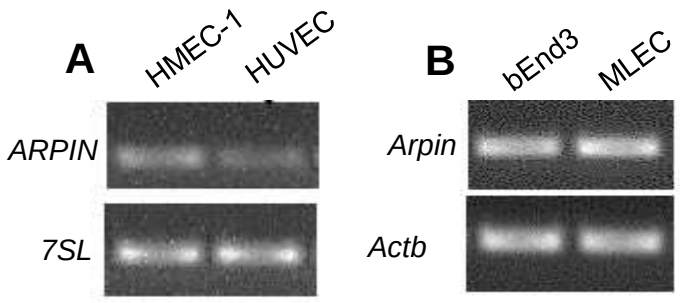

Figure 7.2. Arpin mRNA is expressed in endothelial cells. (A) End-Point RT-PCR for *ARPIN* and *7SL* as house-keeping gene using cDNA derived from the human microvascular endothelial cell line (HMEC-1) and primary human umbilical vein endothelial cells (HUVEC). **(B)** End-Point RT-PCR for A*rpin* and *Actb* as house-keeping gene using cDNA derived from the mouse brain endothelial cell line bEnd.3 and primary murine lung endothelial cells (MLEC). (n=3)

In confluent HUVEC monolayers, arpin was localized throughout the cytoplasm. However, line scan analysis revealed that arpin was enriched close to vascular endothelial cadherin (VE-cadherin) at mature and immature cell-

cell junctions (Figure 7.3B). Exploring the localization of arpin in postcapillary venules of the cremaster muscle using PECAM-1 to identify vein endothelial cell-cell junctions, it was observed that arpin localizes throughout the cytosol with an enrichment near to and at cell-cell junctions (Figure 7.4), similar to what it was observed in HUVEC. This junctional localization of arpin in both HUVEC monolayers and mouse cremaster venules suggests that arpin could participate in the regulation of the endothelial barrier that gets compromised during inflammation.

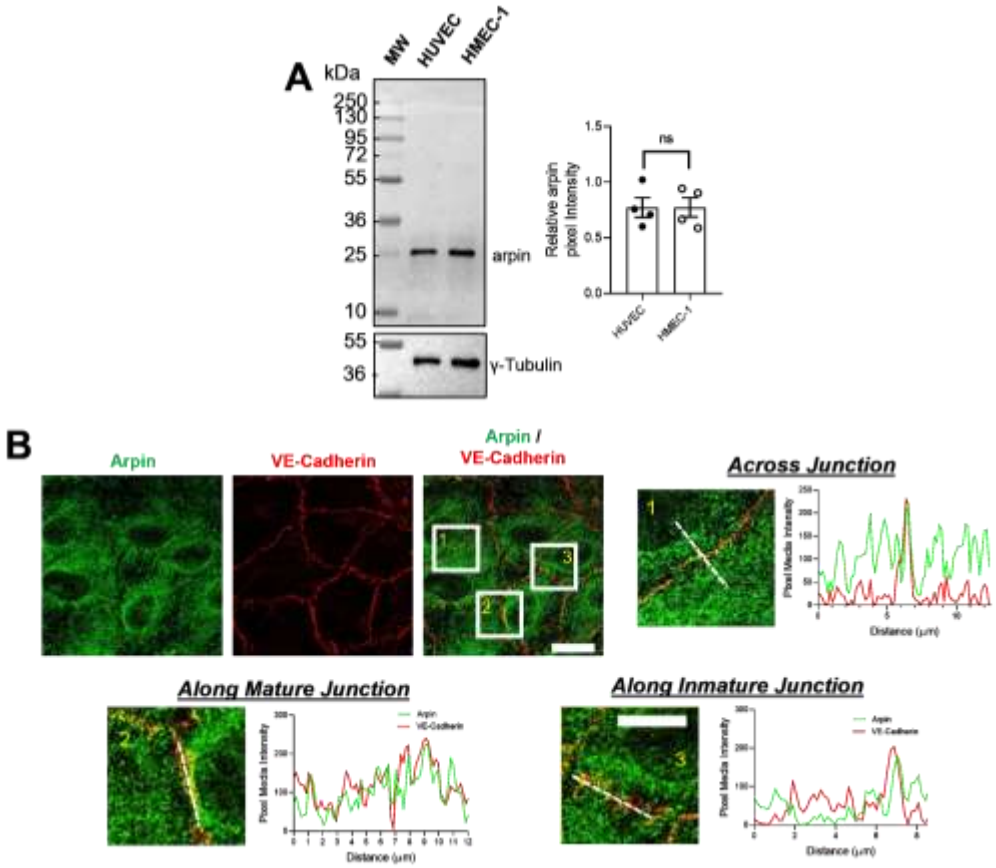

Figure 7.3. Arpin localizes in the cytosol with an enrichment at cell-cell junctions. (A) Representative Western blot for arpin in human umbilical vein endothelial cells (HUVEC) and human microvascular endothelial cells (HMEC-1). The graph on the right shows the densitometry analysis of the arpin band normalized to γ-tubulin as a loading control (n=4). MW= molecular weight bands. **(B)** Representative immunofluorescence of arpin (green) and VE-Cadherin (red) in HUVEC show arpin enrichment at cell-cell contacts (40x objective; scale bar = 20 µm). Magnified views of boxed regions are shown (4.3x digital zoom; scale bar = 5 µm). The graphs indicate the line scans performed with ImageJ software along the dashed lines in the magnified images. Profiles of pixel intensity means of arpin and VE-Cadherin across junctions (1), along mature junctions (2) and along immature junctions (3) are represented. 25 images each were analyzed from three independent experiments. Data are represented as mean ± standard error of the mean (SEM); ns: non-significant.

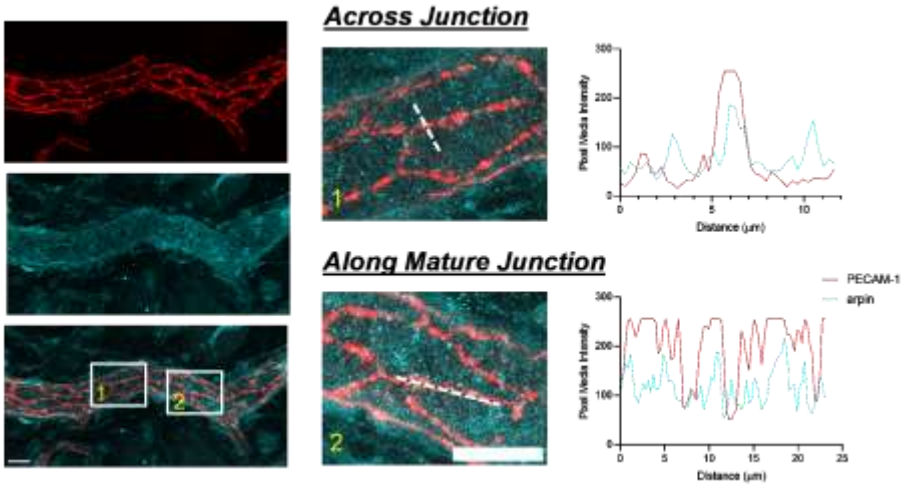

Figure 7.4. Arpin localizes in the cytosol with an enrichment at cell-cell contacts in postcapillary venules of the cremaster muscle. Representative immunofluorescence of arpin (blue) and PECAM-1 (red) in post-capillary venules of the cremaster muscle to analyze arpin localization at cell-cell contacts *in vivo* (40x objective; scale bar = 20 µm). Magnified views of boxed regions are shown (3.3 digital zoom; scale bar = 10 µm). The graphs indicate the line scans performed with ImageJ software along the dashed lines in the magnified images. Profiles of the pixel intensity means of arpin and PECAM-1 across junctions (1), and along mature junctions (2) are shown. 15 images each were analyzed from four mice.

7.3 ARPIN IS DOWNREGULATED DURING INFLAMMATION.

Endothelial cells are activated by pro-inflammatory cytokines such as TNFα and IL-1β leading to decreased endothelial barrier integrity [77, 78]. To investigate arpin regulation during inflammation, it was analyzed *ARPIN* gene expression by qRT-PCR in HUVEC monolayers after stimulation with TNFα for 4 and 18 h. Interestingly, arpin expression was reduced around 50% after TNFα stimulation for 4 and 18 h, but expression of other Arp2/3 inhibitors that also contain an acidic motif, namely *AP1AR* and *PICK1*, was not significantly changed (Figure 7.5A). Western blot and densitometry analysis corroborated arpin downregulation at the protein level after TNFα treatment (Figure 7.5B). Increased protein levels of Intercellular Adhesion Molecule 1 (ICAM-1) were used here as positive control for the inflammatory response.

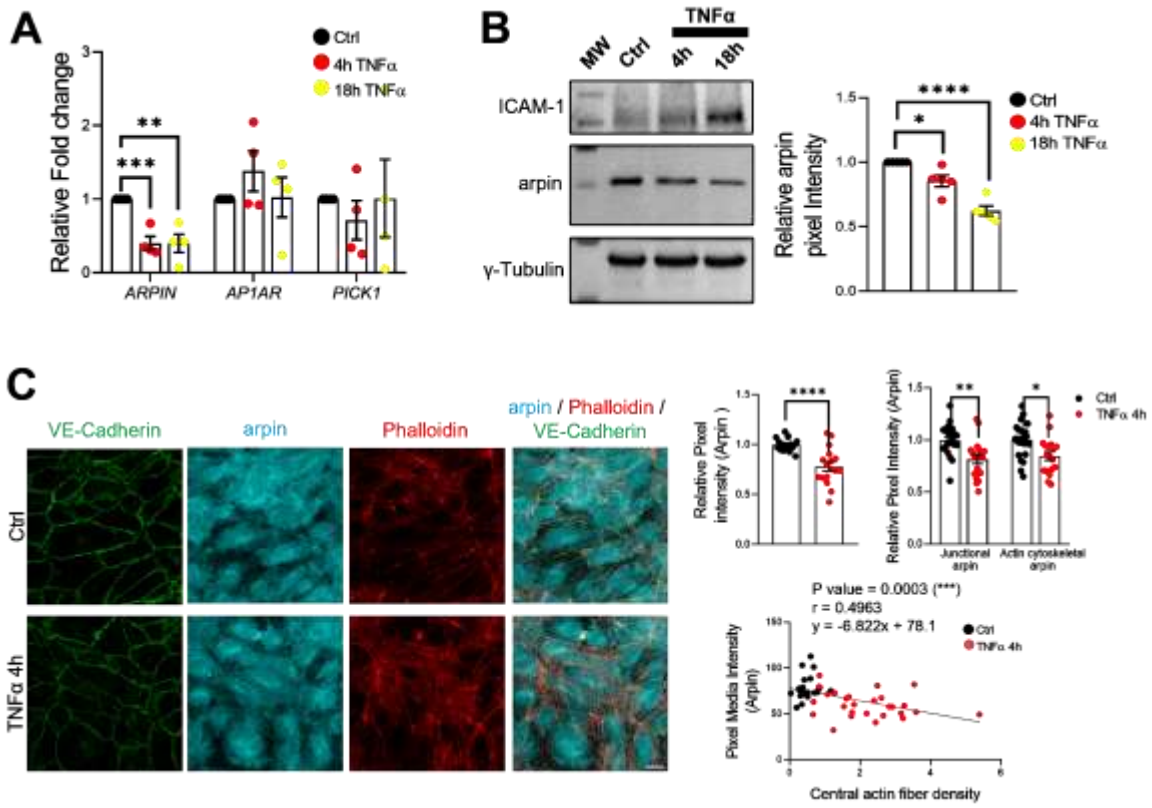

Figure 7.5. Arpin is downregulated by TNFα. (A) qRT-PCR for *ARPIN*, *AP1AR* and *PICK1,* inhibitors of the Arp2/3 complex using cDNA from HUVEC treated or not with TNFα for the indicated times (n=4). Data are shown as foldchange expression normalized to the control condition and the housekeeping gene *7SL.* **(B)** Representative Western blot for arpin in HUVEC treated or not with TNFα for the indicated times (n=5). ICAM-1 overexpression was used as a positive control of the induction of inflammation. MW= molecular weight bands. The graph shows the densitometry analysis of arpin bands normalized to the control condition and to γ-tubulin as loading control (set to 1). **(C**) Representative immunofluorescence of arpin (blue) and VE-Cadherin (green) together with F-actin staining using phalloidin (red) in HUVEC treated or not with TNFα for 4 h (40x objective, scale bar = 20 μm). The graphs show arpin pixel intensity quantification after treatment normalized to the average of ctrl HUVECs: top-left, total arpin was analyzed in 17 images from four independent experiments; top-right, junctional and actin cytoskeletal arpin in 19 images each were analyzed from three independent experiments; and bottom graph, Pearson's correlation analysis shows that arpin is inversely correlated to central actin fiber density (Pearson's correlation coefficient, r; 49 cells were analyzed from three independent experiments). All data are represented as mean ± SEM; *p<0.05; **p<0.01; ***p<0.0001; ****p<0.0001.

Immunostaining of arpin in HUVEC treated or not with TNFα confirmed the decrease of arpin protein levels (Figure 7.5C). This downregulation was not only observed for total arpin, but arpin was also reduced at cell-cell contacts and actin filaments (Figure 7.5C). Remarkably, arpin downregulation significantly correlated with the increase of actin stress fibers induced by TNFα

(Figure 7.5C). Similar results of arpin downregulation were also observed after IL-1β stimulation in HUVEC monolayers after 4 and 18 hours (Figure 7.6A), again with a decrease of total arpin, and arpin localized at junctions and at actin filaments (Figure 7.6B). Also here, arpin reduction significantly correlated with an increase of actin stress fibers (Figure 7.6B).

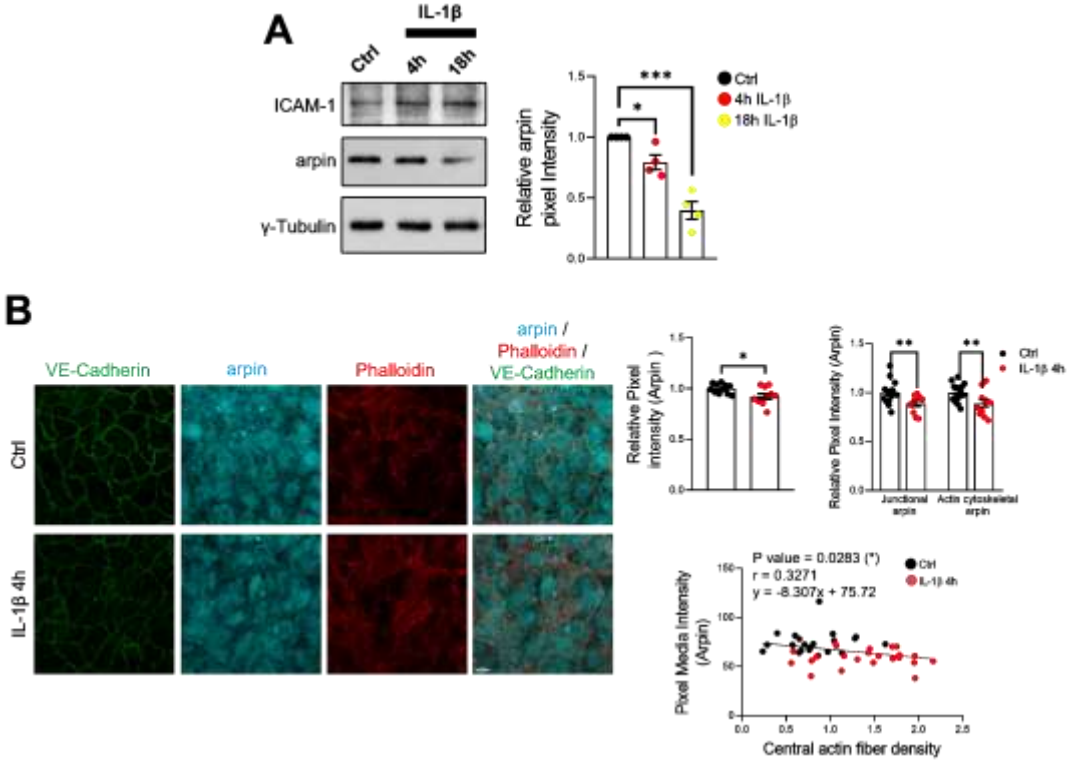

Figure 7.6. Arpin is reduced by IL-1β. (A) Representative Western blot for arpin in HUVEC treated or not with IL-1β for the indicated times (n=4). ICAM-1 overexpression was used as a positive control of the induction of inflammation. The graph shows the densitometry analysis of arpin bands normalized to the untreated control and γ-tubulin (set to 1). **(B)** Representative immunofluorescence of VE-Cadherin (green) and arpin (blue) with F-actin staining using phalloidin (red) in HUVEC treated or not with IL-1β (40x objective, scale bar = 20μm). The graphs show arpin pixel intensity quantification after treatment normalized to the average of ctrl HUVECs: top-left, total arpin was analyzed in 11 images from three independent experiments; top-right, junctional and actin cytoskeletal arpin in at least 11 images each were analyzed from three independent experiments; and bottom graph, Pearson's correlation analysis shows that arpin is inversely correlated to central actin fiber density (Pearson's correlation coefficient, r; 45 cells were analyzed from three independent experiments). All data are represented as mean ± SEM; *p<0.05; **p<0.01; ***p<0.0001.

To confirm this finding in vivo, we stained post-capillary venules of the cremaster muscle inflamed with TNFα for 2 and 4 h and found that the arpin immunofluorescence signal was also decreased by around 50%, which again

occurred at the same levels for both junctional and non-junctional arpin (Figure 7.7A). Strong recruitment of neutrophils confirmed the correct induction of inflammation in this model. Taken together, arpin is downregulated in EC in response to pro-inflammatory cytokines *in vitro* and *in vivo* suggesting that arpin participates in the regulation of endothelial barrier barrier functions during an inflammatory process.

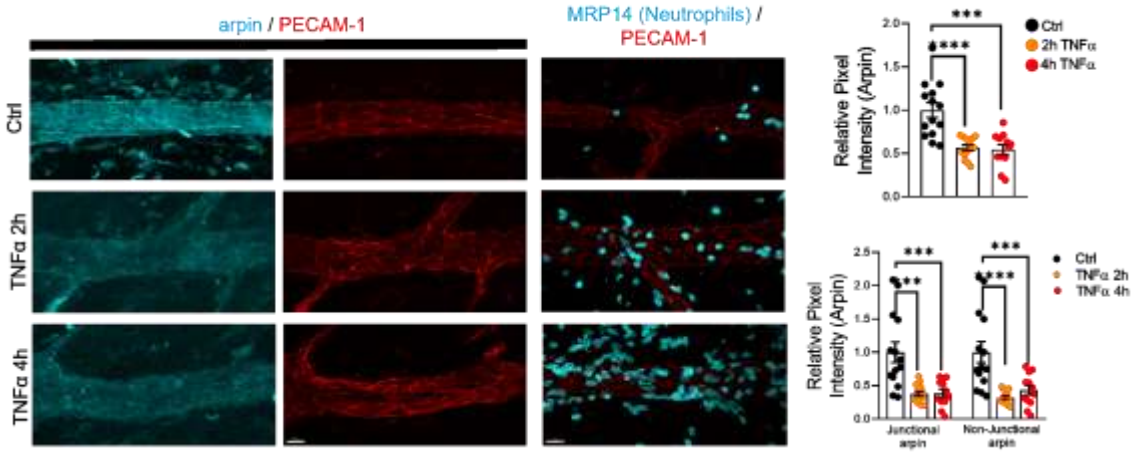

Figure 7.7. Arpin is downregulated by TNFα in mouse post-capillary veins. Representative immunofluorescence for arpin (blue) and PECAM-1 (red) in postcapillary venules of the cremaster muscle treated or not with TNFα at the indicated times. PECAM-1 (red) and MRP14 (blue; neutrophils) stainings on the right are shown as positive control for the induction of inflammation (40x objective, scale bar = 20 μm). The top graph shows total arpin pixel intensity quantification in the venules after TNFα treatment normalized to the average of control conditions (12-14 venules were analyzed from four mice in each group). The bottom graph shows junctional and non-junctional arpin quantification after TNFα treatment normalized to the average of control conditions (12-14 venules were analyzed from four mice in each group). All data are represented as mean ± SEM; **p<0.01; ***p<0.001; ****p<0.0001.

7.4 ARPIN DEPLETION CAUSES HYPERPERMEABILITY AND MODIFIES JUNCTION ARCHITECTURE.

To study the role of arpin in the regulation of the endothelial barrier, we generated stable arpin-depleted HUVEC using lentiviral particles that express either a shRNA sequence against arpin (shArpin) or a control sequence (shCtrl) that has no targets. Stable clones were selected using puromycin. Arpin protein levels were reduced by more than 80% in shArpin-transduced cells (Figure

7.8A). Of note, arpin expression did not modify the protein levels of the NPFs WAVE2 and WASP, and neither the level of arpC5, a subunit of the Arp2/3 complex, suggesting that the Arp2/3 complex remains intact without arpin (Figure 7.8A).

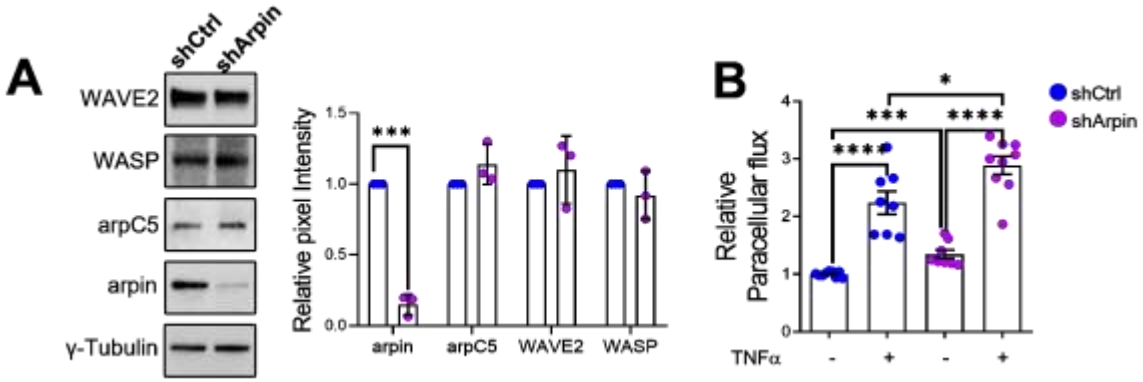

Figure 7.8. Arpin-depletion induces endothelial hyperpermeability. (A) Representative Western blots for WAVE2, WASP, the Arp2/3 subunit ArpC5 and arpin in lysates of control (shCtrl) and arpin-depleted (shArpin) HUVEC. The graph shows the densitometry analysis of protein bands normalized to the respective control bands (set to 1) and γ-tubulin as a loading control (n=3)**. (B)** Paracellular flux of 150 kDa FITC-dextran across confluent control and arpin-depleted HUVEC monolayers seeded on 0.4 µm pore size transwell filters treated or not with TNFα for 18 h. Data are represented as relative permeability normalized to control HUVEC (set to 1; n=9 in three independent experiments).

In vitro filter-based permeability assay, using control and arpin-depleted HUVEC revealed that although arpin-depleted HUVEC formed monolayers, the paracellular flux of 150 kDa FITC-dextran across these untreated cells increased 34.5% (±3.7%) compared to control HUVEC (Figure 7.8B). Additionally, stimulation with TNFα significantly increased permeability in control HUVEC as expected, and the permeability in arpin-depleted HUVEC was even higher than in control cells (Figure 7.8B), suggesting that arpin-depletion and TNFα induce endothelial hyperpermeability by different mechanisms.

To determine whether the increase in permeability in the absence of arpin is due to changes in the protein levels of cell-cell junction proteins, Western blots were performed and revealed that the total levels of the AJ proteins VE-Cadherin, β-catenin and vinculin were not altered by the lack of arpin (Figure 7.9A), which was also true for the TJ proteins ZO-1 and Claudin-

5 (Figure 7.9B). However, immunostainings of VE-Cadherin and β-catenin showed that arpin-depletion led to the formation of junction gaps, and discontinuous and perpendicular junctional pattern that indicate immature junctions, which was not observed in control HUVEC (Figure 7.9C). In the absence of arpin, VE-Cadherin and β-catenin got internalized with stronger signals in the cytoplasm (Figure 7.9C).

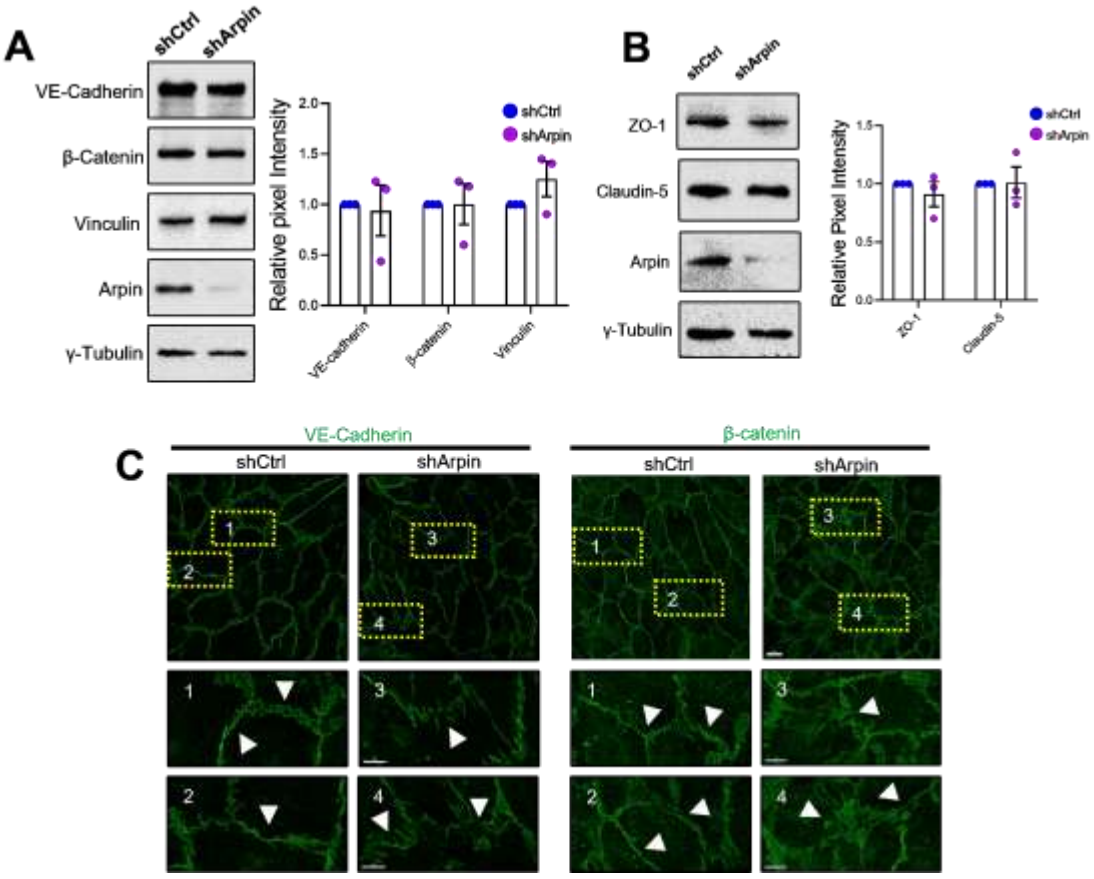

Figure 7.9. Arpin depletion induces changes in the junction achitecture. (A) Representative Western blots for VE-Cadherin, β-catenin, vinculin, and arpin in lysates of control (shCtrl) and arpin-depleted (shArpin) HUVEC. The graph shows the densitometry analysis of the protein bands normalized to the respective control bands (set to 1) and γ-tubulin as loading control (n=3)**. (B)** Representative Western blots for ZO-1, claudin-5 and arpin in lysates of control and arpin-depleted HUVEC. The graph shows the densitometry analysis of ZO-1 and claudin-5 bands normalized to shCtrl HUVEC (set to 1) and γ-tubulin as loading control (n=3). **(C)** Immunofluorescence of VE-Cadherin and β-catenin in control and arpin-depleted HUVEC (40x objective, scale bar = 20 μm; dashed boxes indicate magnified areas that emphasize changes in cell-cell junctions; 3.3x digital zoom, scale bars = 5 μm). Arrows mark linear and mature junctions in control HUVEC and interrupted junctions with gaps showing junction protein internalization in arpin-depleted HUEC. Representative images of four independent experiments are shown. All data are represented as mean ± SEM.

To further investigate the role of arpin in the formation of cell-cell junctions, control and arpin-depleted HUVEC were subjected to calcium-switch assays, in which both AJ and TJ are lost when Ca^{+2} is removed, and they re-assembled when Ca^{+2} is added back. This experiment demonstrated that control and arpin-depleted HUVEC formed new junctions at similar rates. After depletion, both cell types started forming junctions 2 hours after calcium addition, and 24 hours later both cell types showed mature cell-cell junctions again (Figure 7.10A and 7.10B). These results suggest that arpin is not required for junction assembly, but rather for stabilizing existing junctions.

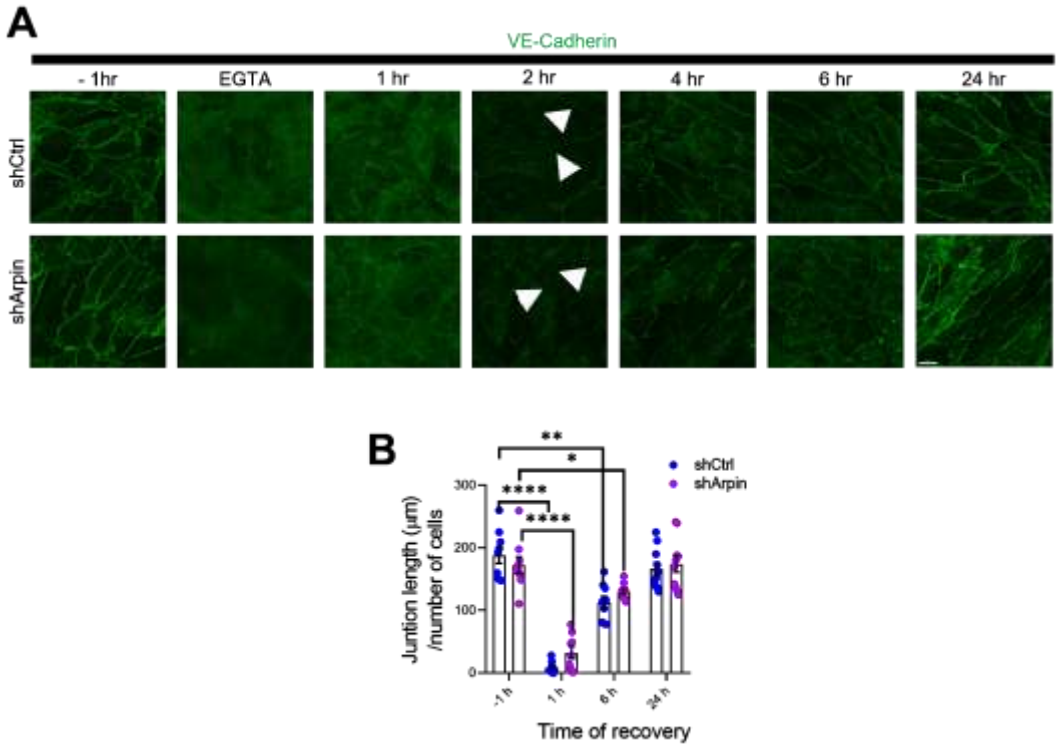

Figure 7.10. Arpin is not essential for junction assembly. (A) Representative immunofluorescence of VE-Cadherin in control (shCtrl) and arpin-depleted (shArpin) HUVEC in calcium-switch assays over time (63x objective; scale Bar = 20 µm). **(B)** The graph shows the quantification of junctional length per number of cells, calculated using ImageJ software. Representative images of three independent experiments are shown. Data are represented as mean ± SEM; *p<0.05; **p<0.01; ****p<0.0001.

7.5 ARPIN DEPLETION INDUCES ACTIN FILAMENT FORMATION.

It is well studied that the endothelial actin cytoskeleton affects barrier homeostasis, with increased formation of actin stress fibers usually leading to increased endothelial permeability [79, 80]. To analyze whether the actin cytoskeleton changes after arpin-depletion, F-actin was stained in control and arpin-depleted HUVEC using phalloidin. Quantifying the total signal of phalloidin in both cells revealed that arpin-depleted HUVEC statistically significantly increased the levels of F-actin compared with control HUVEC (Figure 7.11A). Additionally, the central actin filaments that cross the cell body were quantified showing that arpin depletion leads to an increase in these filaments (Figure 7.11B). Western blot analysis of total actin levels showed no significant differences between control and arpin-depleted HUVEC (Figure 7.11C), suggesting that G-actin levels are reduced in arpin-depleted HUVEC in parallel to increased formation of F-actin.

Then, we analyzed whether other proteins involved in actin cytoskeleton dynamics are altered after loss of arpin. However, protein levels of cortactin, coronin1B, p-cofilin (deactivated form of cofilin) and total cofilin did not show any significant changes in response to arpin depletion (Figure 7.11D).

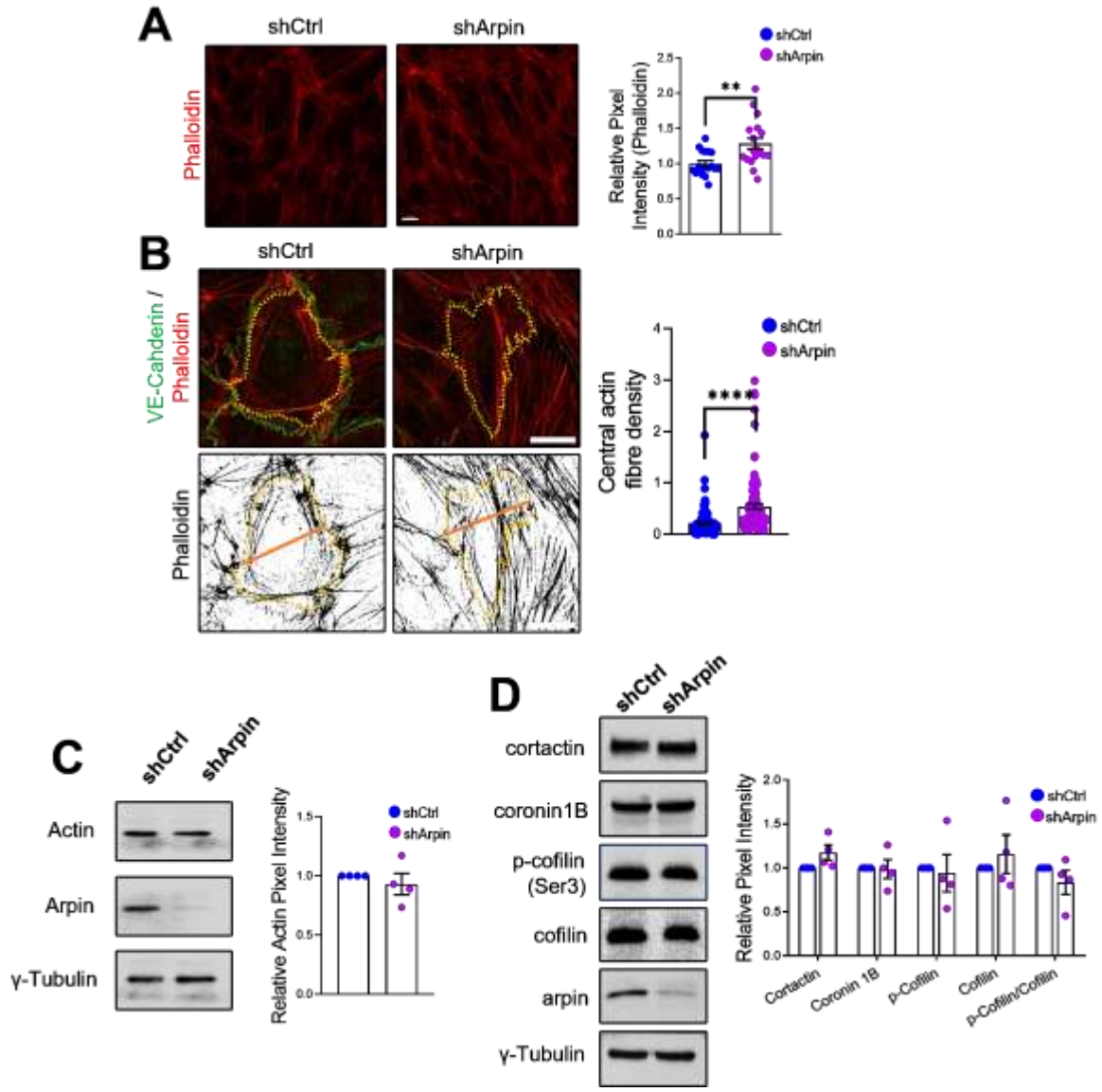

Figure 7.11. Actin filament formation is induced after arpin-depletion. (A) Representative F-actin staining using phalloidin in control (shCtrl) and arpin-depleted (shArpin) HUVEC (40x objective, scale bar = 20µm). The graph shows phalloidin pixel intensity quantification normalized to the average of control HUVEC. 18 images were analyzed in each group from four independent experiments. **(B)** Top panel: representative immunofluorescence of VE-Cadherin with F-actin staining using phalloidin in control and arpin-depleted HUVEC. Bottom panel: the method of central actin fiber quantification using the phalloidin signal as reported before [79] is shown (63x objective, scale bar = 5 µm). Individual cells are delineated with yellow dashed lines. The graph shows quantification of the mean central actin fiber density along the orange lines. 109 cells were analyzed in each group from 3 independent experiments. **(C)** Representative Western blot for total actin in lysates of control and arpin-depleted HUVEC. The graph shows the densitometry analysis of the actin bands normalized to control HUVEC and γ-tubulin as a loading control (n=4). **(D)** Representative Western blots for cortactin, coronin1B, p-cofilin, cofilin and arpin in lysates of control and arpin-depleted HUVEC. The graph shows the densitometry analysis of the protein bands normalized to the respective control bands (set to 1) and γ-tubulin as a loading control (n=4). All data are represented as mean ± SEM; **p<0.01; ****p<0.0001.

7.6 ARP2/3 COMPLEX INHIBITION DOES NEITHER RESCUE F-ACTIN FORMATION NOR HYPERPERMEABILITY IN ARPIN-DEPLETED HUVEC.

The first function of arpin described was that it inhibits the Arp2/3 complex in fibroblasts [68]. Thus, to analyze whether the observed phenotype in arpin-depleted HUVEC, i.e. hyperpermeability and alterations in actin cytoskeleton, are due to an increase in Arp2/3 complex activity, arpin-depleted HUVEC were treated with the pharmacological Arp2/3 inhibitor CK666. Unexpectedly, quantification of total F-actin staining with phalloidin revealed no changes in the pixel media intensity between arpin-depleted HUVEC that were treated or not with CK666 (Figure 7.12A and 7.12B). Besides, the central actin fiber density was also not significantly different after treatment with CK666 in arpin-depleted or control HUVEC (Figure 7.12C). In both cases arpin-depleted HUVEC had more actin filaments than control HUVEC. Interestingly, filter-based permeability assays revealed an increase in the paracellular flux in both, control and arpin-depleted HUVEC, after Arp2/3 inhibition (Figure 7.12D). These surprising results suggest that arpin regulates actin filament formation and permeability in HUVEC through a mechanism independent of Arp2/3 complex inhibition.

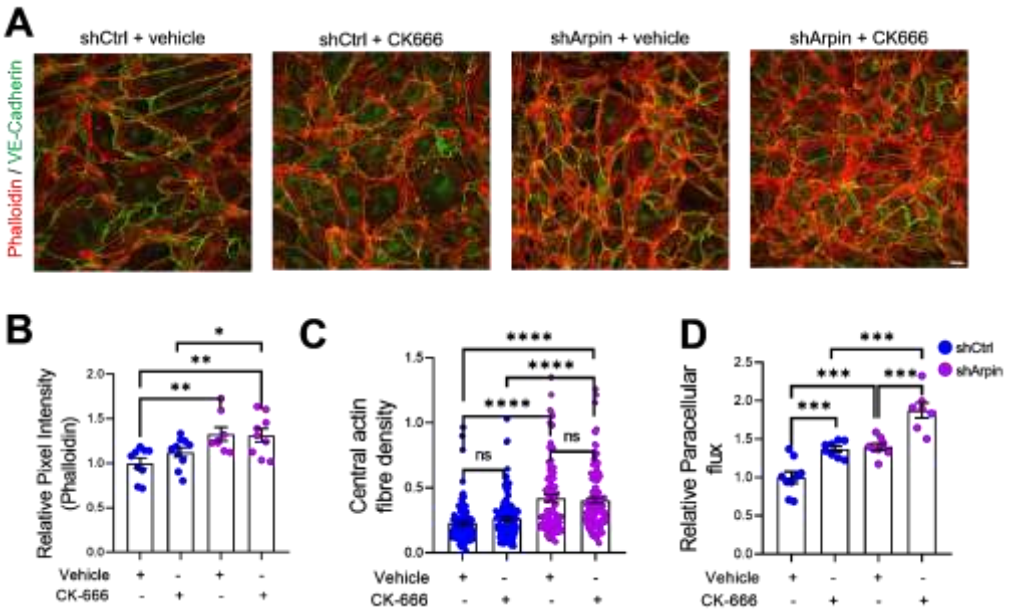

Figure 7.12. Actin cytoskeleton alterations and hyperpermeability are not rescued after inhibition of the Arp2/3 complex in arpin-depleted HUVEC. (A) Immunofluorescence of VE-Cadherin with F-actin staining using phalloidin in control (shCtrl) and arpin-depleted (shArpin) HUVEC treated with 100 µM of the Arp2/3 inhibitor CK-666 or vehicle (40x objective, scale bar = 20 µm). Representative images of three independent experiments are shown. **(B)** Total phalloidin pixel intensity quantification normalized to the average of shCtrl HUVEC. Nine images were analyzed in each group from three independent experiments. **(C)** Central actin fiber density quantification done as described in figure 7.11B. 100 cells were analyzed in each group from three independent experiments. (**D)** Paracellular flux assays using confluent control and arpin-depleted HUVEC monolayers on 0.4 µm pore transwell filters treated with CK-666 or vehicle (n=7-9 from three independent experiments). Data are normalized to control HUVEC treated with vehicle (set to 1). All data are represented as mean ± SEM; *p<0.05; **p<0.01; ***p<0.001; ****p<0.0001.

7.7 LOSS OF ARPIN LEADS TO INCREASED FORMATION OF ACTIN STRESS FIBERS.

Given that arpin acts in an Arp2/3-independent manner in HUVEC and that central actin filaments crossing the cell body observed in arpin-depleted HUVEC showed stress fiber morphology, it was investigated whether these actin structures are contractile actomyosin stress fibers, that are known to destabilize the endothelial cell-cell contacts by mechanical forces and thus destabilize endothelial barrier integrity [42]. Therefore, Western blot analysis revealed an increase in the phosphorylation of myosin light chain (MLC) at serin-19 in arpin-depleted HUVEC (Figure 7.13A). Additionally, it was found an increase in the phosphorylation at Theonin-696 and Threonin-853 of the

Myosin Phosphatase Target Subunit 1 (MYPT1), a phosphatase known to dephosphorylate MLC (Figure 7.13B); and these phosphorylations are known to inhibit MYPT1 activity [81]. Moreover, the total protein levels of ROCK1 and ZIPK1, kinases involved in the phosphorylation of MLC and MYPT1, were increased in arpin-depleted HUVEC (Figure 7.13C). Together, these results suggest that the increased central actin filaments in arpin-depleted HUVEC are contractile actomyosin stress fibers that can destabilize cell-cell junctions and thus induce hyperpermeability.

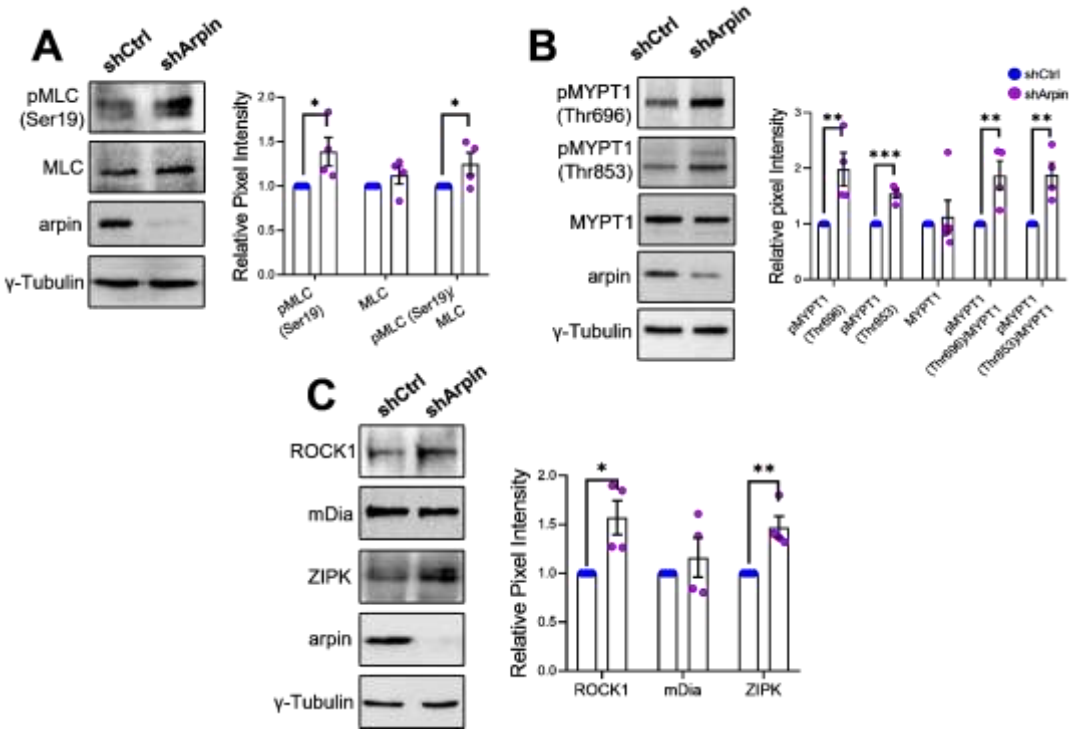

Figure 7.13. Actin stress fiber formation is increased after arpin depletion. (A) Representative Western blots for pMLC (Ser19), MLC and arpin in lysates of control (shCtrl) and arpin-depleted (shArpin) HUVEC. The graph shows the densitometry analysis of the protein bands (n=4). **(B)** Representative Western blots for pMYPT1 (Thr696), pMYPT1 (Thr853), MYPT1, and arpin in lysates of control and arpin-depleted HUVEC. The graph shows the densitometry analysis of the protein bands (n=4). **(C)** Representative Western blots for ROCK1, mDia, ZIPK, and arpin in lysates of control and arpin-depleted HUVEC. The graph shows the densitometry analysis of the protein bands (n=4). All protein bands were normalized to the respective control band (set to 1) and γ-tubulin as loading control. All data are represented as mean ± SEM; *p<0.05; **p<0.01; ***p<0.001.

7.8 PHARMACOLOGICAL INHIBITION OF ROCK1/2 AND ZIPK RESCUES THE OBSERVED PHENOTYPE IN ARPIN-DEPLETED HUVEC.

Given the increased levels in the phosphorylation of MLC and MYPT1, and total protein levels of ROCK1 and ZIPK, we hypothesized that inhibition of ROCK1/2 by Y27632 and ZIPK by HS38 might normalize stress fiber formation and hyperpermeability in arpin-deficient HUVEC. Indeed, phalloidin staining and quantification of the total phalloidin signal and the central actin fiber density showed a significant reduction in arpin-depleted HUVEC treated with Y27632 compared with untreated arpin-depleted HUVEC. However, the phalloidin signal was not decreased to the levels observed in Y27632-treated control HUVEC (Figure 7.14 A-C). Concomitantly, filter-based permeability assays revealed that Y27632-treated arpin-depleted HUVEC had reduced permeability, but still higher than control HUVEC treated with the ROCK1/2 inhibitor (Figure 7.14D). Overall, all these results that arpin can participate in the regulation of the endothelial barrier through ROCK1/2-induced actomyosin stress fibers.

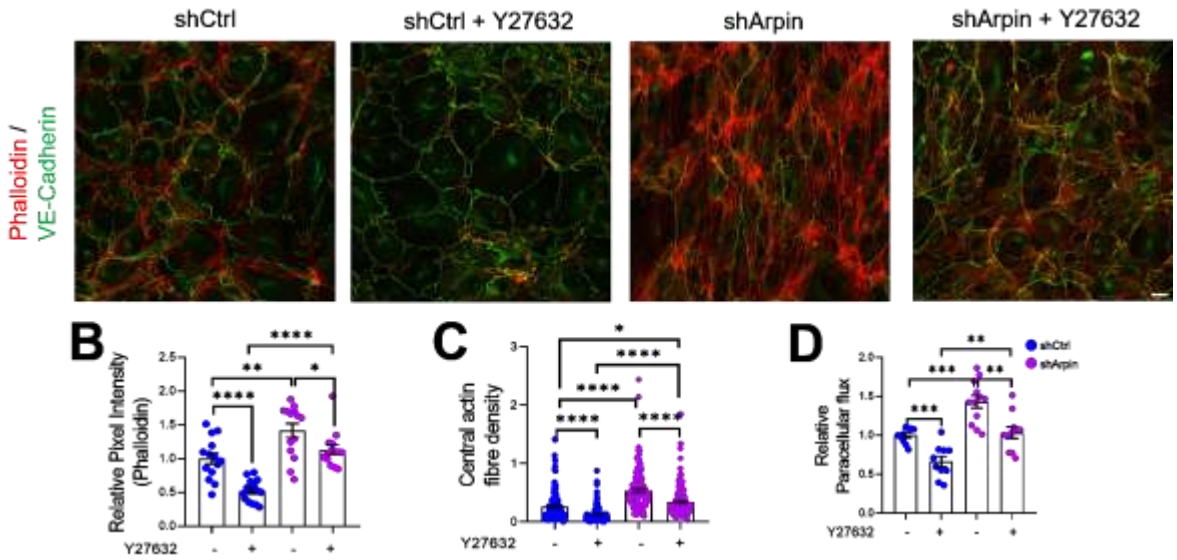

Figure 7.14. ROCK1/2 inhibition partially rescues stress fiber formation and hyperpermeability in arpin-depleted HUVEC. (A) Representative immunofluorescence of VE-Cadherin with F-actin staining using phalloidin in control (shCtrl) and arpin-depleted (shArpin) HUVEC treated or not with 10 μM of the ROCK1/2 inhibitor Y27632 (40x objective, scale bar = 20μm). Representative images of three independent experiments are shown. **(B)** Phalloidin pixel intensity quantification normalized to the average of control HUVEC. 14 images were analyzed in each group from three independent experiments. **(C)** Central actin fiber density quantification done as described in figure 7.11B. At least 140 cells in each group from three independent experiments were analyzed. **(D)** Paracellular flux assays with 150 kDa FITC-dextran using confluent control and arpin-depleted HUVEC monolayers on 0.4 μm pore transwell filters treated or not with Y27632 (n=10-12 from four independent experiments). All data are represented as mean ± SEM; *p<0.05; **p<0.01; ***p<0.001; ****p<0.0001.

Next, inhibition of ZIPK by HS38 in arpin-depleted HUVEC demonstrated a reduction in the total signal of phalloidin and central actin fiber density to the levels observed in HS38-treated and untreated control HUVEC (Figure 7.15 A-C). Interestingly, and different from Y27638, HS38 was not able to decrease actin filament formation in control HUVEC. Filter-based permeability assays confirmed these results and showed a complete rescue of the actin changes in arpin-depleted HUVEC after treatment with HS38. Moreover, HS38 treatment in TNFα-treated arpin-depleted HUVEC reduced the higher permeability but not to the basal levels, suggesting that inhibition of ZIPK rescues the hyperpermeability caused by the lack of arpin but not the one caused by the effects of TNFα treatment (Figure 7.15D and E). These results also suggest that the mechanisms that increase permeability after TNFα treatment are different from the ones caused by arpin depletion.

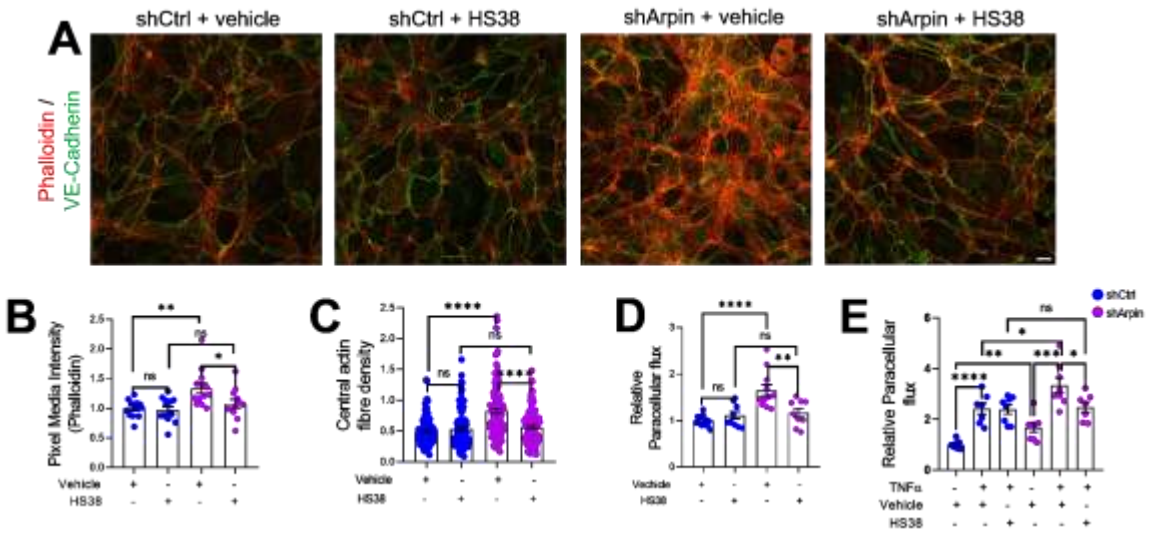

Figure 7.15. ZIPK inhibition rescues stress fiber formation and hyperpermeability in arpin-depleted HUVEC. (A) Representative immunofluorescence of VE-Cadherin with F-actin staining using phalloidin in control (shCtrl) and arpin-depleted (shArpin) HUVEC treated with 10 μM of the ZIPK inhibitor HS38 or vehicle (40x objective; scale bar = 20μm). Representative images of three independent experiments are shown. **(B)** Phalloidin pixel intensity quantification normalized to the average of control HUVEC treated with the vehicle. 13 images were analyzed in each group from three independent experiments. **(C)** Central actin fiber density quantification done as described in figure 11B. At least 125 cells in each group from three independent experiments were analyzed. **(D-E)** Paracellular flux assays with 150 kDa FITC-dextran using confluent control and arpin-depleted HUVEC monolayers on 0.4 μm pore transwell filters treated with **(D)** 10 μM HS38 or vehicle (n=9-12 in four independent experiments), or **(E)** treated or not with 15 ng/mL TNFα and with 10 μM HS38 or vehicle (7-8 in three independent experiments). All data are represented as mean ± SEM; *p<0.05; **p<0.01; ***p<0.001; ****p<0.0001.

7.9 LOSS OF ENDOTHELIAL ARPIN INCREASES NEUTROPHIL TRANSMIGRATION.

During inflammation, the endothelium not only regulates vascular permeability but it also controls leukocyte recruitment and transendothelial migration [24, 82]. To discover whether arpin also regulates the transmigration of neutrophils, filter-based neutrophil transendothelial migration assays were performed using control and arpin-depleted HUVEC monolayers. Remarkably, the number of neutrophils that transmigrated across the arpin-depleted HUVEC monolayer were significantly higher compared with neutrophils that transmigrated across the control HUVEC monolayer (Figure 7.16A). However, the surface levels of the endothelial adhesion molecules P- and E-selectin, ICAM-1 and VCAM-1, implicated in the regulation of neutrophil adhesion to the

apical side of the endothelium, were not affected by the absence of arpin (Figure 7.16 B-E).

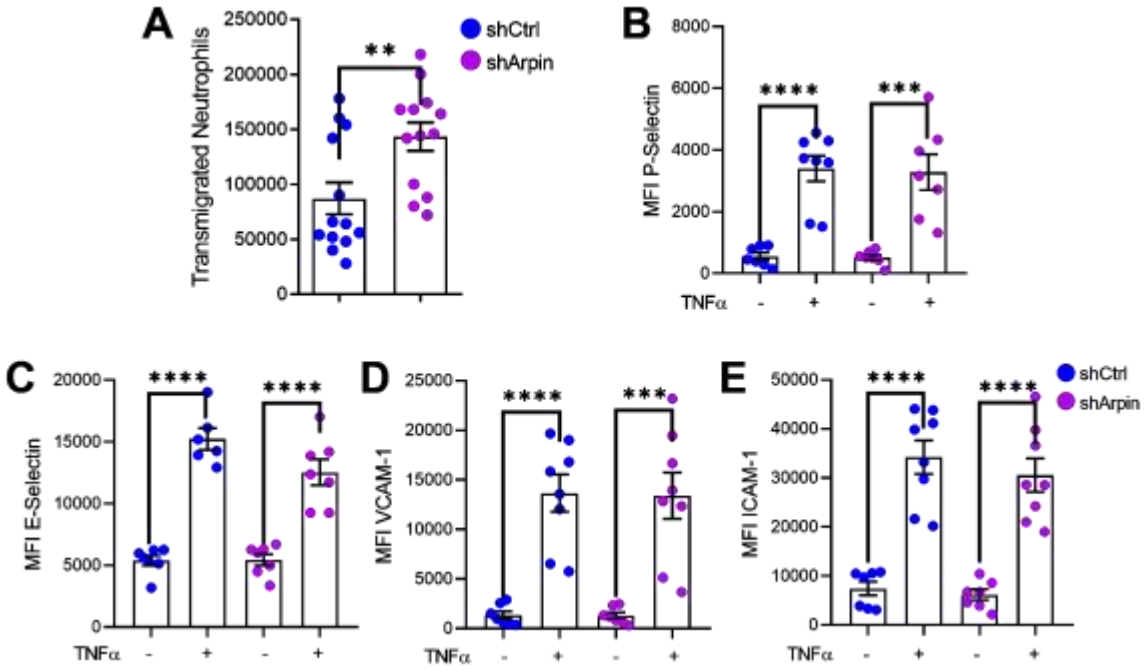

Figure 7.16. Arpin depletion increases neutrophil transmigration. (A) Isolated human primary neutrophils were allowed to transmigrate across confluent monolayers of control (shCtrl) and arpin-depleted (shArpin) HUVEC activated with TNFα on 5 µm pore transwell filters (n=13 in three independent experiments). **(B-E)** Surface levels of adhesion molecules: **(B)** P-selectin, **(C)** E-selectin, **(D)** VCAM-1 and **(E)** ICAM-1 in control and arpin-depleted HUVEC activated or not with TNFα, as measured by flow cytometry (n=9 in three independent experiments). All data are represented as mean ± SEM; **p<0.01; ***p<0.001; ****p<0.0001.

7.10 ARPIN DEFICIENT MICE ARE VIABLE AND BREED TO MENDELIAN RULES.

To discover the functions of arpin in vivo, we generated a total arpin knockout mouse on the C57BL/6 genetic background using the CRISPR/Cas method to eliminate the exon 3 of the *Arpin* gene with two specific gRNA sequences (see materials and methods). PCR using tail-extracted genomic DNA samples clearly distinguished the 3 genotypes, arpin$^{+/+}$ (WT), arpin$^{+/-}$ (heterozygous) and arpin$^{-/-}$ (KO; Figure 7.17). As expected, Western blot of arpin in different organs confirmed its absence in the knock-out lysates (Figure 7.18A). Arpin$^{-/-}$ mice were viable and did not demonstrate any different phenotype compared to arpin$^{+/+}$ mice by simple visual inspection. We did not

observe alterations in development, weight (Figure 7.18B), appearance or susceptibility to any diseases compared to arpin$^{+/+}$ mice under pathogen-free conditions. Moreover, offspring was born according to Mendelian ratios when breeding female and male arpin$^{+/-}$ mice (Table 7.1).

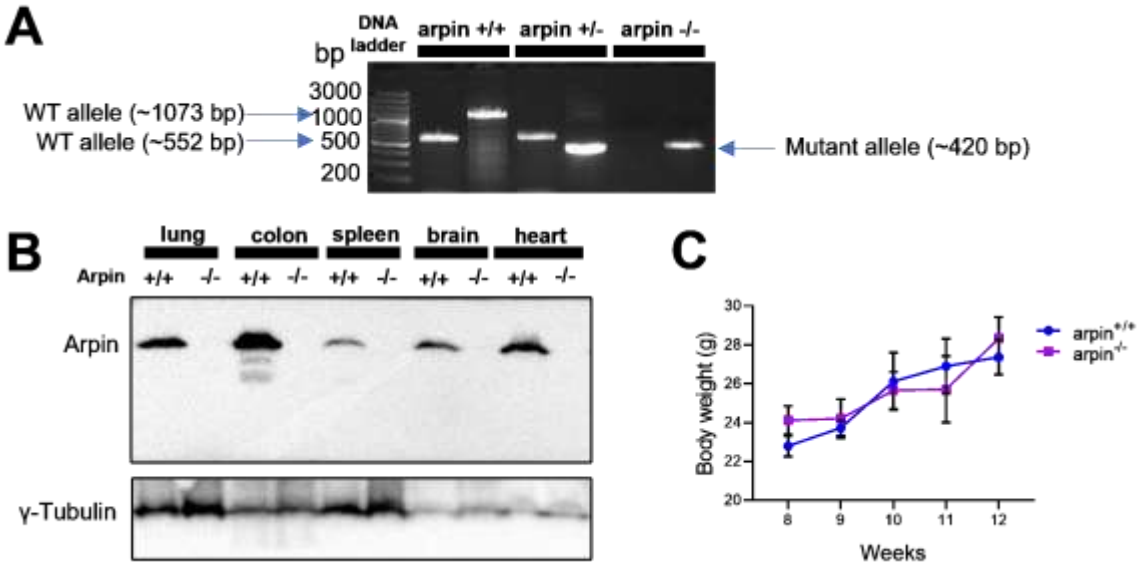

Figure 7.17. Arpin-deficient mice are viable. (A) Representative genotyping PCR using genomic DNA from mice carrying WT (arpin$^{+/+}$), heterozygous (arpin$^{+/-}$), and deleted (KO, arpin $^{-/-}$) alleles. The different WT alleles and the mutant (KO) alleles are shown. **(B)** Representative Western blot for arpin in lysates of the designated organ tissues from arpin$^{+/+}$ and arpin$^{-/-}$ mice (n=3). **(C)** The graph shows the average weight of arpin$^{+/+}$ and arpin $^{-/-}$ mice over time (at least 3 arpin$^{+/+}$ and arpin$^{-/-}$ mice were weighted at each time point).

Table 7.1. Mating statistics of arpin$^{+/-}$ mice. Genotyping of 126 littermates from breedings of heterozygous (arpin$^{+/-}$) male and female mice are shown. $\chi 2$ test probability is shown. Deviations from Mendelian rules (expected) are non-significant.

	Expected	Observed	Probability (χ^2)	Degrees of freedom	P value
Male	63	66	0.286	1	0.5930
Female	63	60			
arpin$^{+/+}$	31.5	31	0.540	2	0.7635
arpin$^{+/-}$	63	60			
arpin$^{-/-}$	31.5	35			

7.11 ARPIN-DEFICIENT MICE HAVE INCREASED VASCULAR PERMEABILITY.

The lung is a highly vascularized organ [83], and showed high protein levels of arpin (Figure 7.18A). For this reason, this organ was chosen to unravel whether arpin also regulates endothelial barrier functions *in vivo*. Permeability assays in the lung tissues revealed that arpin$^{-/-}$ mice have tow-fold higher permeability than arpin$^{+/+}$ mice without any permeability-inducing stimulus (7.18C). To further investigate if this is increase in permeability is specific for the lung, modified Miles assays in the back skin were also performed. The basal vascular permeability in the skin of the arpin$^{-/-}$ mice was also higher compared with arpin$^{+/+}$ mice. Using histamine as permeability-inducing stimulus, permeability increased in both arpin$^{+/+}$ and arpin$^{-/-}$ mice, but it was higher in arpin$^{-/-}$ mice (Figure 7.18D). This finding is in agreement to with the observation in control and arpin-depleted HUVEC treated or not with TNFα. In fact, Western blot of the junctional proteins VE-Cadherin, β-catenin, vinculin, claudin-1 and -5 of lung tissue lysates showed no differences in the total levels of all these proteins between arpin$^{+/+}$ and arpin$^{-/-}$ mice, again similar to what was observed in vitro, suggesting that the hyperpermeability is not due to changes in junction molecule expression.

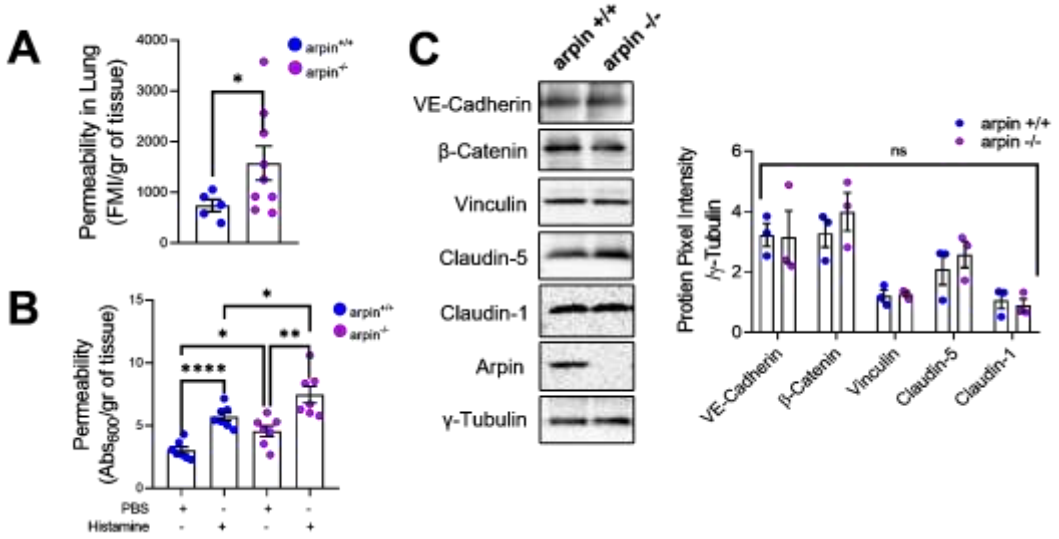

Figure 7.18. Arpin-deficient mice exhibit increased vascular permeability. (A) Permeability assay in the lung in arpin$^{+/+}$ and arpin$^{-/-}$ mice. 150 kDa FITC-dextran was injected via the cannulated carotid artery into mice. Animals were sacrificed, perfused, then lungs collected, weighted, and homogenized in PBS. The homogenized tissue containing the leaked FITC-dextran was quantified using a fluorometer. (5 arpin$^{+/+}$ and 8 arpin$^{-/-}$ mice were analyzed). **(B)** Modified Miles assays to determine vascular permeability in the back skin of arpin$^{+/+}$ and arpin$^{-/-}$ mice under basal and inflammatory conditions. Extracted Evan's blue dye from skin tissues was measured in a spectrophotometer at 620 nm and presented as Optical Density (OD) per gram tissue (7 mice were analyzed in each group). **(C)** Representative Western blots for the indicated junctional proteins in lysates of lung tissue from arpin$^{+/+}$ and arpin$^{-/-}$ mice. The graph shows the densitometry analysis of the protein bands normalized to γ-tubulin as loading control (n=3). All data are represented as mean ± SEM; ns: non-significant; *p<0.05; **p<0.01; ****p<0.0001.

Histological analysis by hematoxylin and eosin staining of lung tissue from arpin$^{+/+}$ and arpin$^{-/-}$ mice showed normal architecture and morphology in arpin$^{+/+}$ mice as expected (Figure 7.19A, images 1 and 2). However, various irregularities were seen in the arpin$^{-/-}$ lungs that correspond to a vascular phenotype. These abnormalities include reduction of the alveolar space volume (Figure 7.19A, images 3, asterisk), indications of hemorrhage and microhemorrhage (Figure 7.19A, images 4 and 5, arrowheads), and presence of interalveolar edema (Figure 7.19A, images 6, asterisks). Consequently, arpin$^{-/-}$ mice had a significantly higher histological score than arpin$^{+/+}$ mice (Figure 7.19B).

We also performed an immunofluorescence of PECAM-1 to identify blood vessels in the lung, together with phalloidin staining to recognize F-actin

(Figure 7.19C). Quantifying the total levels of F-actin specifically in the lung endothelium using PECAM-1 as template, we detected significantly increased actin filaments in arpin$^{-/-}$ mice (Figure 7.19D), similar to what was observed in arpin-depleted HUVEC suggesting that the increased permeability in the lungs was also due to an increase in the formation of actin stress fibers.

Additionally, endothelial cell-cell junctions in post-capillary veins of the cremaster muscle were also analyzed by immunofluorescence staining under basal conditions (Figure 7.20). In venules of arpin$^{-/-}$ mice, internalization of VE-cadherin, as indicated by zipper-like structures, was observed (Figure 7.20A, arrowheads), again similar to what was seen in arpin-depleted HUVEC. Moreover, ZO-1 staining displayed a discontinuous pattern in arpin$^{-/-}$ mice, while it was continuous in arpin$^{+/+}$ mice (Figure 7.20B, arrowheads). Overall, these results confirm the potential role of arpin in regulating endothelial barrier integrity also *in vivo.*

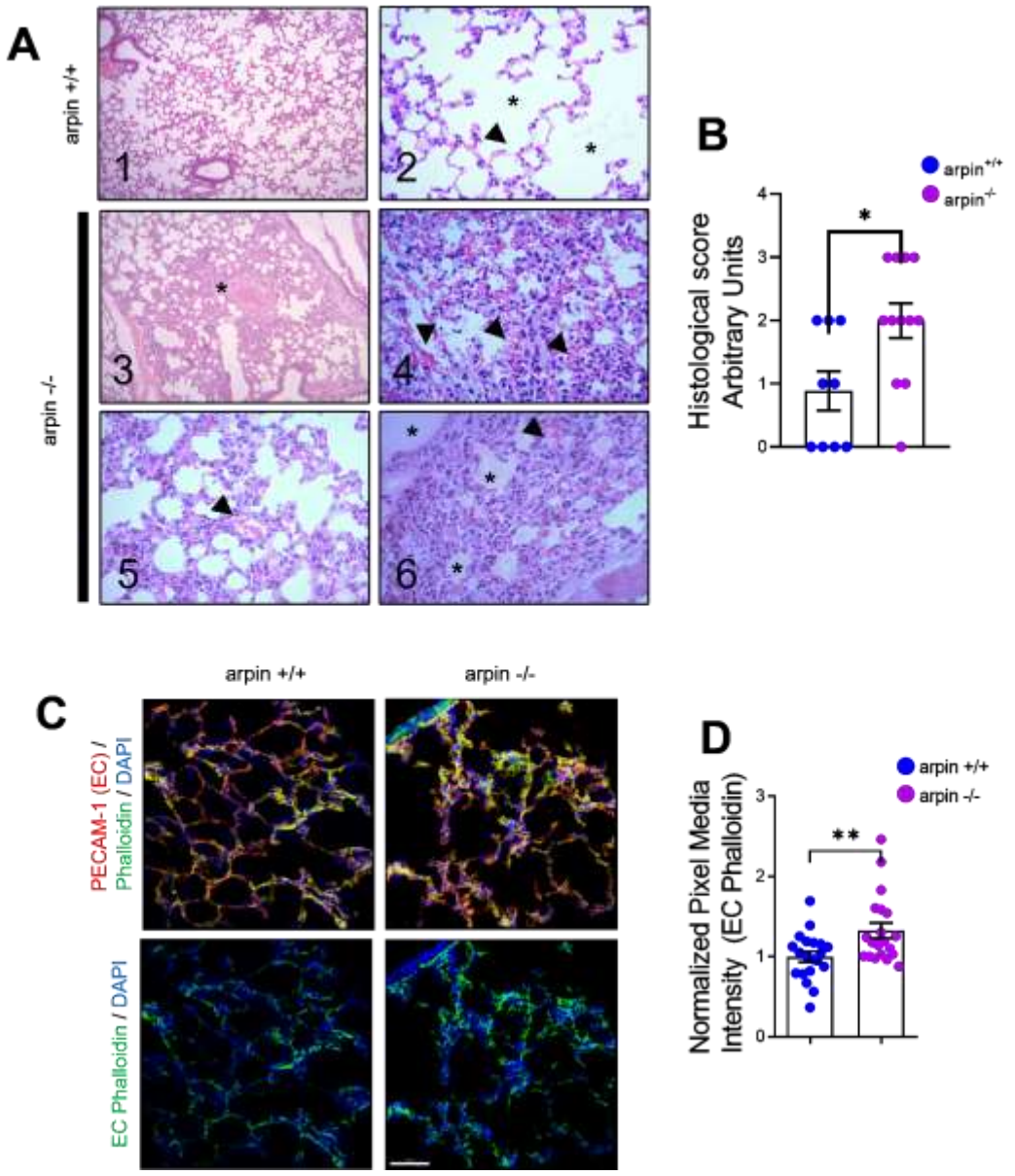

Figure 7.19. Arpin-deficient lungs show altered lung structure and increased F-actin formation. (A) Representative images of hematoxylin and eosin staining of lung tissues of arpin$^{+/+}$ (images 1 and 2) and arpin$^{-/-}$ (images 3-6) mice. Image 1 shows normal histology (10x objective). Image 2 indicates normal structure of alveoli (*) and the blood vessels (arrowheads) without any pathology (40x objective). Image 3 shows some areas with reduced alveolar volume (*) in arpin$^{-/-}$ mice (10x objective). Image 4 shows isolated interalveolar hemorrhages (arrowheads). Image 5 indicates congestion and dilatation of the capillaries (arrowheads). Image 6 reveals interalveolar edema (*) and microhemorrhage (arrowhead; 40x objective in images 4-6). **(B)** The graph shows the histological score of the lung tissue (9 images from arpin$^{+/+}$ and 12 images from arpin$^{-/-}$ mice were analyzed). **(C)** Representative immunofluorescence for PECAM-1 with F-actin staining using phalloidin in cryosections from arpin$^{+/+}$ and arpin$^{-/-}$ mice lungs. Images in the bottom show endothelial cell (EC) F-actin extracted using PECAM-1 as a template of ECs (40x objective, scale bar = 50µm). **(D)** The graph shows F-actin pixel intensity quantification in EC from arpin$^{-/-}$ lungs normalized to the average of images from arpin$^{+/+}$ lungs (20 images were analyzed from three mice in each group). All data are represented as mean ± SEM; *p<0.05; **p<0.01.

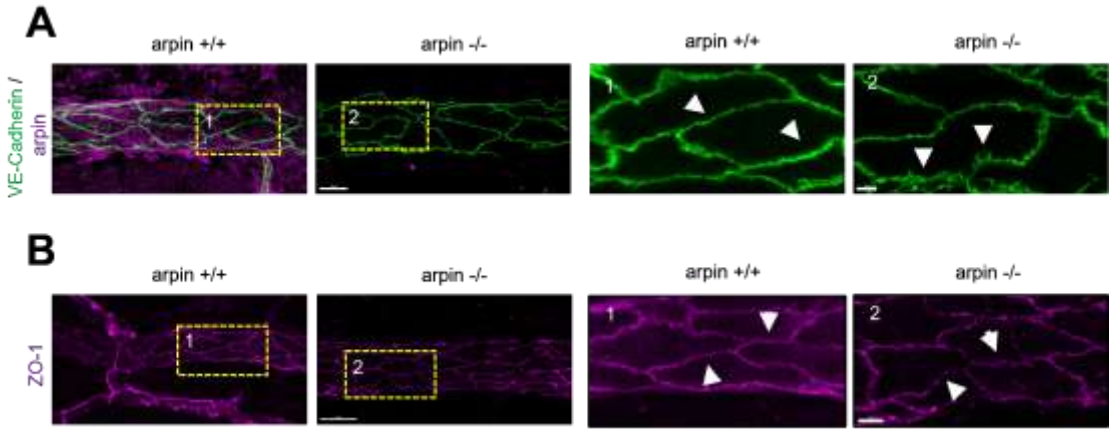

Figure 7.20. Arpin deficiency changes venular junction architecture in cremaster muscles. Representative immunofluorescence for (A) arpin and VE-Cadherin, and (B) ZO-1 in postcapillary venules of arpin$^{+/+}$ and arpin$^{-/-}$ cremaster muscles. (n=3; dashed boxes indicate magnified areas, 40x objective; scale Bar = 20 µm). Arrows in the magnifications to the right show the altered junction architecture in the absence of arpin (4x digital zoom; scale Bar = 5 µm).

7.12. ARPIN DEFICIENCY INCREASES NEUTROPHIL TRANSMIGRATION *IN VIVO*.

Finally, it was analyzed whether arpin-depletion alters the extravasation of neutrophils *in vivo*. Analyzing TNF-inflamed cremaster muscles stained for VE-cadherin and MRP-14 by confocal microscopy, it was found more extravased neutrophils in arpin-deficient mice compared to WT mice (Figure 7.21A), which is similar to what was observed with arpin-depleted and control HUVEC monolayers and primary WT neutrophils. Analyzing neutrophil rolling and firm adhesion by intravital microscopy, we did not detect any changes in rolling velocity (Figure 7.21B), but a 33% (±8.91%) increase in the number of neutrophils that firmly adhered to the endothelium in arpin$^{-/-}$ mice compared with arpin$^{+/+}$ mice (Figure 7.21C). Moreover, differential interfering contrast (DIC) images confirmed increased neutrophil transmigration in inflamed cremaster muscles of arpin$^{-/-}$ mice (Figure 7.21D). Hemograms revealed that the numbers of leukocytes, including neutrophils in peripheral blood were not significantly changed in arpin$^{-/-}$ mice compared with arpin$^{+/+}$ mice (Table 7.2), suggesting that the increase in neutrophil extravasation cannot be explained

by an increase in neutrophil numbers. All together, these results suggest the potential role of arpin in regulating neutrophil transmigration *in vivo*.

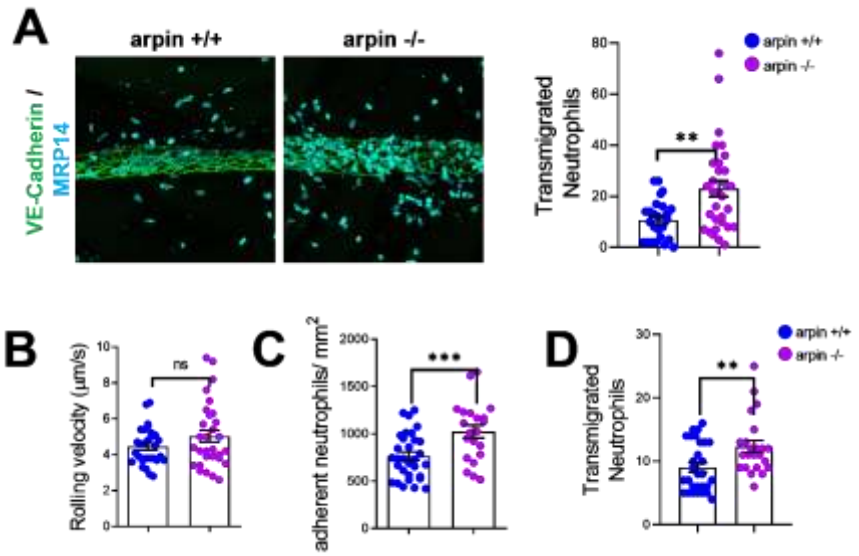

Figure 7.21. Arpin deficiency increases neutrophil adhesion and transmigration *in vivo*. **(A)** Representative immunofluorescence of VE-Cadherin (green) to visualize the veins and MRP14 (blue) to visualize neutrophils in post-capillary venules of the cremaster muscled of arpin$^{+/+}$ and arpin$^{-/-}$ mice inflamed with 300 ng TNFα for 2 h. The graph on the right shows quantification of transmigrated neutrophils. (n=4 mice in each group were analyzed). Intravital video microcopy in the inflamed cremaster muscle of arpin$^{+/+}$ an arpin$^{-/-}$ mice was used to investigate **(B)** the rolling velocity and **(C)** the number of firmly adherent cells and (D) the number of neutrophils that transmigrated as counted from DIC images taken after video microscopy. To induce inflammation, 300 ng TNFα were injected intrascrotally 2 h before the analysis. (n=4 mice in each group were analyzed). All data are represented as mean ± SEM; ns: non-significant; **p<0.01; ***p<0.001.

Table 7.2. Hemograms of arpin$^{+/+}$ and arpin$^{-/-}$ mice.

Parameter	arpin$^{+/+}$ (n=8)		arpin$^{-/-}$ (n=11)		P value
	mean	SD	mean	SD	
Leukocytes (x10^9 cells/L)	3.16	1.195	2.56	1.07	0.2599
Neutrophils (x10^9 cells/L)	0.79	0.79	0.53	0.35	0.3425
Lymphocytes (x10^9 cells/L)	2.35	1.14	1.96	0.90	0.4085
Monocytes (x10^9 cells/L)	0.02	0.05	0.05	0.05	0.3897
Erythrocytes (x10^{12} cells/L)	7.53	0.72	7.83	0.58	0.3344
Platelets (x10^9 cells/L)	852.0	200.3	738.1	357.3	0.4520
Hemoglobin (g/L)	110.9	7.6	113.4	6.9	0.5015
Hematocrit (L/L)	0.25	0.03	0.24	0.021	0.7500

8. DISCUSSION

In this project, the role of arpin in the regulation of the endothelial barrier was studied. To this end, we first generated a polyclonal rabbit anti-arpin antibody that allowed the discovery of novel and remarkable arpin functions. Here, we unequivocally demonstrate that arpin is expressed in EC with a mainly cytosolic localization, but it is also enriched at the cell-cell junctions. Importantly, arpin is downregulated under inflammatory conditions and consequently participates in the regulation of endothelial permeability, junction architecture, actin remodeling, and neutrophil transmigration. Most unexpectedly, arpin controls endothelial barrier functions in an Arp2/3-independent fashion by controlling the formation of contractile actomyosin stress fibers in a ROCK/ZIPK-dependent mechanism. Finally, we generated and characterized here the first arpin knock-out mice, which are viable and develop as WT mice, but exhibit a vascular phenotype in the lung with increased vascular permeability, edema formation and hemorrhages. Also, leukocyte extravasation was increased in arpin KO mice. Thus, we provide experimental evidence that arpin controls the endothelial barrier both *in vitro* and *in vivo*.

Arpin is expressed in endothelium, *in vivo* and *in vitro*, and it is localized throughout the cytoplasm but with junction enrichment. This localization at cell-cell contacts has been also described for other actin-regulators in ECs. For example, WAVE2 [59] and Arp2/3 complex [44] localize close to junctions to maintain the integrity of the endothelial barrier through actin cytoskeleton remodeling. N-WASP normally localizes throughout the cytosol, but it is re-localized to cell-cell junctions in colocalization to F-actin during inflammation to assist in junction remodeling [61]. These similarities indeed suggest an important role for arpin in the regulation of actin cytoskeleton dynamics. However, arpin was discovered first to be enriched at the lamellipodial tip in fibroblasts to regulate random migration, speed, and directionality[68]. Here, we only analyzed arpin localization in confluent HUVEC monolayers and not in

migrating HUVEC, thus we do not exclude that arpin may also localize at lamellipodia tip during endothelial cell movement, similar to coronin1B that localizes at cell-cell junctions in confluent HUVEC monolayers, but is also detected at classical lamellipodia (cLP) and JAIL in subconfluent HUVEC monolayers, where it contributes to actin-dependent cell-cell junction formation [84]. Future studies will reveal whether arpin also localizes at cLP and JAIL in EC to regulate endothelial cell movement or junction formation under specific conditions such as neo-angiogenesis or vascular wound healing.

Importantly, arpin is downregulated after activation of EC by pro-inflammatory cytokines suggesting that the loss of arpin contributes to EC changes that occur during inflammation such as remodeling of the actin cytoskeleton and junction weakening that allow for the passage of pro- and anti-inflammatory proteins, and leukocyte recruitment, essential processes for combating invading pathogens and resolving inflammatory responses. In this respect, arpin downregulation was also observed during epithelial inflammation. Arpin levels were not only reduced in colon epithelial cells after stimulation with pro-inflammatory cytokines, but also in the colon tissue of mice with DSS-induced colitis and in patients with active ulcerative colitis [71]. Remarkably, in all these models arpin downregulation correlated with disruption of the epithelial barrier, suggesting that loss of arpin, in epithelium, is associated with pathogenic events such as Chron's disease, ulcerative colitis, celiac disease, irritable bowel syndrome, enterocolitis and enteric infections [71]. By contrast, arpin downregulation at the endothelial barrier seems to be required for correct induction of the inflammatory response including opening of endothelial junctions to facilitate leukocyte extravasation. Other ABP and NPF have been implicated in maintaining the endothelial barrier under basal and inflammatory conditions such as adducin [85], cortactin [24, 79], N-WASP [61], WAVE2 [59],. This is the first study showing that a protein relating with the actin cytoskeleton dynamics is downregulated during inflammation in endothelium. However, it remains to be investigated how and when arpin expression is recovered after the acute inflammatory response and

whether arpin recovery then plays a role during inflammation resolution. Therefore, it will be important to study how arpin levels are regulated after the inflammatory cue has been removed and during vascular diseases. Such research will complete the entire panorama of arpin regulation at the endothelial barrier during inflammation.

Otherwise, arpin was also reduced in human rhinovirus-infected macrophages leading to impaired phagocytosis due to a failure in the progression and completion of the phagocytic cup [86]. Additionally, low arpin expression in breast cancer cells was correlated with high Akt activation and high cell migratory capacity and proliferation [87]. Therefore, arpin downregulation in proinflammatory environments and cancer seems to be critical in different cells to control different cellular functions in different pathological contexts. Our qRT-PCR results suggest that arpin downregulation happens at the transcriptional level. However, nothing is yet known about the arpin promoter region or how arpin mRNA is regulated at the post-transcriptional level. Thus, characterization of arpin expression regulation is needed to know how to restore arpin expression to fulfill its functions in different cells.

In EC, the Arp2/3 complex has been implicated in several cellular processes including barrier formation through the formation of new VE-cadherin adhesion sites [44], and recovery of the pulmonary endothelial barrier through F-actin polymerization to induce lamellipodia [88]. Thus, it was tempting to speculate that arpin could inhibit Arp2/3 complex activity to regulate endothelial barrier integrity. This hypothesis was further supported by findings in epithelium, where arpin participates in regulating epithelial barrier integrity in an Arp2/3-dependet manner by preventing the internalization of junction proteins and thus epithelial barrier disruption [71]. Unexpectedly, in this project, we found that arpin regulates the endothelial barrier through mechanisms independent of Arp2/3 inhibition. Instead, we discovered here that arpin regulates the endothelial barrier through the formation of actomyosin stress

fibers in a ROCK1/ZIPK-dependent fashion. In EC, both ROCK1 and ZIPK, are activated downstream of pro-inflammatory mediators such as TNFα, due to the activation of RhoA [89, 90], leading to the phosphorylation of MYPT1 and MLC to support the generation of actomyosin stress fibers, reduction of the barrier-stabilizing cortical actin ring, disruption of cell-cell junction architecture, and increased permeability [91, 92]. Therefore, the increased permeability observed in the arpin-depleted HUVEC may well be secondary to the enhanced actomyosin stress fibers, similar to what was observed in cortactin-depleted HUVEC that also showed an increase of actomyosin contractility and loss of barrier functions [27]. Remarkably, cortactin was first described as NPF of Arp2/3, but in EC it also regulated RhoA/ROCK1-dependent stress fiber formation [93]. It remains unknown how these two findings are related, but it is clear now that arpin acts independently of Arp2/3 to regulate the endothelial barrier. In EC, TNFα stimulation not only activates ZIPK but also increases its protein levels in an unknown mechanism [90]. Phosphorylation of MLC and stress fibers formation is also lower after ZIPK depletion [94], which agrees with what we observed in arpin-depleted HUVEC that showed more levels of ZIPK and MLC phosphorylation, and more actomyosin contractility. Besides, pharmacological inhibition of ZIPK in arpin-depleted HUVEC restored actin filament formation and permeability under basal conditions and during TNFα-induced inflammation. Overall, these data suggest a mechanistic association of arpin and ZIPK in the regulation of endothelial barrier integrity. However, more research is needed to discover the exact link between these proteins. For example, protein interactome studies of arpin binding partners will reveal whether the nature of this link is direct or indirect. Arpin has not been described as an ABP, however, a recently published actin interactome showed that actin can interact transiently with arpin [95]. Thus, the possibility exists that arpin can directly regulate actin cytoskeleton dynamics. Future research will reveal if arpin can interact with G-actin, F-actin or both; and how this direct association contributes to actin cytoskeleton remodeling, junction architecture dynamics, and endothelial barrier regulation. Moreover, it was found very recently that

dactylopodia, lamellipodia-like membrane protrusions implicated in angiogenesis of invasive EC, are regulated by a spatiotemporal interaction of the Arp2/3 complex with non-muscle myosin IIA (NMIIA) [96]. In this mechanism, VEGF induces filopodia formation and actomyosin contractility via Cdc42 and NMIIA. Next, new filopodia adhere to extravascular matrices leading to the activation of Arp2/3 via Rac1-dependent integrin signaling and the formation of dactylopodia. However, it remains unknown how these processes induced by NMIIA and Arp2/3 leading to dactylopodia formation are connected. Possible scenarios may involve arpin given that it can do both inhibit Arp2/3 complex activity and control the formation of actomyosin contractility. Future research will answer if arpin is present in these actin-related structures to generate endothelial cell invasion and if and how arpin connects the two different actin dynamics mechanisms, i.e. actin branching and actomyosin contractility, and how both are implicated in the spatiotemporal regulation of endothelial barrier maintenance under basal and inflammatory conditions.

On the other hand, arpin depletion increases neutrophil transmigration. Given that loss of arpin increases permeability under basal and inflammatory conditions, it is possible that neutrophils take advantage of this high permeability due to open cell contacts and high actomyosin contractility and transmigrate easier and faster. There are studies supporting the relationship between vascular permeability and neutrophil transmigration, for example, neutrophils being in contact with the endothelium receive signals through G-protein coupled receptors and integrins to secrete granules containing enzymes such as elastase, neutral serin protases and lysosomal hydrolases that can digest junctional proteins including VE-Cadherin that leads to increased vascular permeability [82]. Neutrophil elastase can also induce phosphorylation of MLC, actomyosin contractility and thus increased permeability *in vitro* [97]. Neutrophils also release several cytokines and chemokines that directly modulate vascular permeability such as TNFα and CXCL8 [98]. Leaky microvessels facilitate the diffusion of interstitial

chemokines into the vascular lumen leading to increased neutrophils revers transmigration [99]. Adhesion of neutrophils on the endothelium via the adhesion molecule ICAM-1 results in actin polymerization and cytoskeletal reorganization via PKC, Rho, src family kinases and consequently increased vascular permeability [82, 100]. These are some examples in which increased permeability depend on neutrophil presence. Although neutrophil presence can induce vascular permeability, it has been clearly shown that the endothelial mechanisms governing junction opening and diapedesis are different and independent. Using cortactin-deficient mice, our group could demonstrated that vascular permeability is induced by RhoA/ROCK-dependent actomyosin contractility, but that neutrophils could not exploit open contacts for easier transmigration because also ICAM-1 clustering around adhering neutrophils was disturbed, clearly showing that both mechanisms have to work in order for neutrophils to be able to extravasate [24, 27]. Additionally, VE-Cadherin phosphorylation at Tyr685 increased vascular permeability, whereas Tyr731 phosphorylation facilitated leukocyte extravasation *in vivo,* suggesting that both processes are controlled by distinct molecular mechanisms [15]. However, the role of the Arp2/3 complex in neutrophil transmigration is controversial because it has been shown that its inhibition reduces monocyte transmigration in the blood brain barrier [26], but increases neutrophil transmigration across HUVEC monolayers [62]. It is not known whether this is a leukocyte-specific response or rather dependent on different vascular beds. Thus, more research is needed to unravel how exactly arpin contributes to the transmigration of neutrophils and other leukocytes and whether this mechanism is related to its function as Arp2/3 complex inhibitor.

In this project, we also report for the first time a total arpin knock-out mouse on C57BL/6 genetic background that was generated for us by the company Cyagen using the CRISPR/Cas method. These mice grow and develop normally as WT C57BL/6 mice at least until week 12 when the arpin-deficient mice were used for experiments, suggesting that arpin is not essential for embryonic, fetal, premature, and early adult stages, similar to what was

described for other mice deficient for ABP or Arp2/3 inhibitors, including cortactin [24], α-actinin3 [101], cononin1A [102], PICK1 [103] and gadkin [104]. Importantly, knock-out mice for ArpC4 [51] and ArpC3 [50], subunits of the Arp2/3 complex and the NPF N-WASP [105] and WAVE2 [106] are not viable, demonstrating the vital importance of Arp2/3 and their activators for embryonic development, in contrast to Arp2/3-inhibitors and non-essential ABP. Remarkably, the results of the vascular permeability experiments and histological analyses showed a clear vascular phenotype in the lung, including edema, microhemorrhage and congestion, suggesting that arpin is important for stabilizing the endothelial barrier in this organ, similar to our observations in arpin-depleted HUVEC. This vascular phenotype seen in the lung can have different underlying causes, including an increase in the intravascular hydrostatic pressure, injury or dysfunction of endothelial and epithelial barriers, or lymphedema [107]. Although, the vascular phenotype in the arpin$^{-/-}$ mice is obvious, it does not compromise the life of the mice at least into early adulthood. Further characterization of older arpin$^{-/-}$ mice will reveal how this phenotype affects later life of these mice; and whether these mice are more susceptible to develop inflammatory diseases or cancer due to weakened barrier functions. It will be also interesting to analyze if arpin regulates endothelial barrier integrity in different organs such as heart and brain in which arpin is also highly expressed.

Intravital microscopy in inflamed cremaster muscles of arpin$^{-/-}$ mice revealed the importance of arpin for correct regulation of adhesion and diapedesis during neutrophil extravasation, which is in line with reduced neutrophil transmigration across arpin-depleted HUVEC. Although there are a few studies related to endothelial ABP and NPFs in the regulation of leukocyte transmigration, most have been done using *in vitro* models to exclude a potential role of neutrophil-ABP and lack of endothelial-specific KO mice. Cortactin was the first endothelial ABP identified to regulate neutrophil rolling *in vivo* in the TNF-inflamed cremaster [24]. In neutrophils, hematopoietic cell-specific lyn substrate 1 (HS1) is a cortactin-related and leukocyte-specific ABP

that also participates in the recruitment of neutrophils in vivo upon CXCL1 stimulation of cremaster muscles [108]. Neutrophil myosin1E (Myo1E) regulates adhesive interaction with the endothelium and Myo1E deficiency caused increased rolling velocity, decreased firm adhesion and reduced transmigration [109], but endothelial Myo1E was not involved in this regulation. In this project, we did not study the expression and functions of arpin in neutrophils, and we do not discard the possibility that *in vivo* arpin-deficiency in neutrophils could also contribute to the observed effects on neutrophil adhesion and diapedesis. Future experiments using chimeric mice will show how the different steps of the extravasation cascade are regulated by arpin in the endothelium, the neutrophil or both.

9. CONCLUSIONS

The results shown in this project suggest that arpin, besides being an Arp2/3 complex inhibitor, participates in organizing the molecular machinery that regulates actomyosin contractility and endothelial barrier functions. In this respect, arpin seems to be involved in the expression and activation regulation of ZIPK and ROCK1 to induce stress fiber formation, increased permeability, and leukocyte transmigration. Thus, we propose a model in which arpin is normally expressed in basal conditions and enriched at the cell-cell contacts to maintain endothelial barrier integrity. During inflammation, arpin is downregulated to induce the formation of actomyosin stress fibers and open the intercellular junctions leading to increased permeability and transmigration of leukocytes (Figure 9.1). We hope that this first arpin study in endothelial cells will initiate further research to better understand the role of arpin in vascular diseases and acute inflammatory responses.

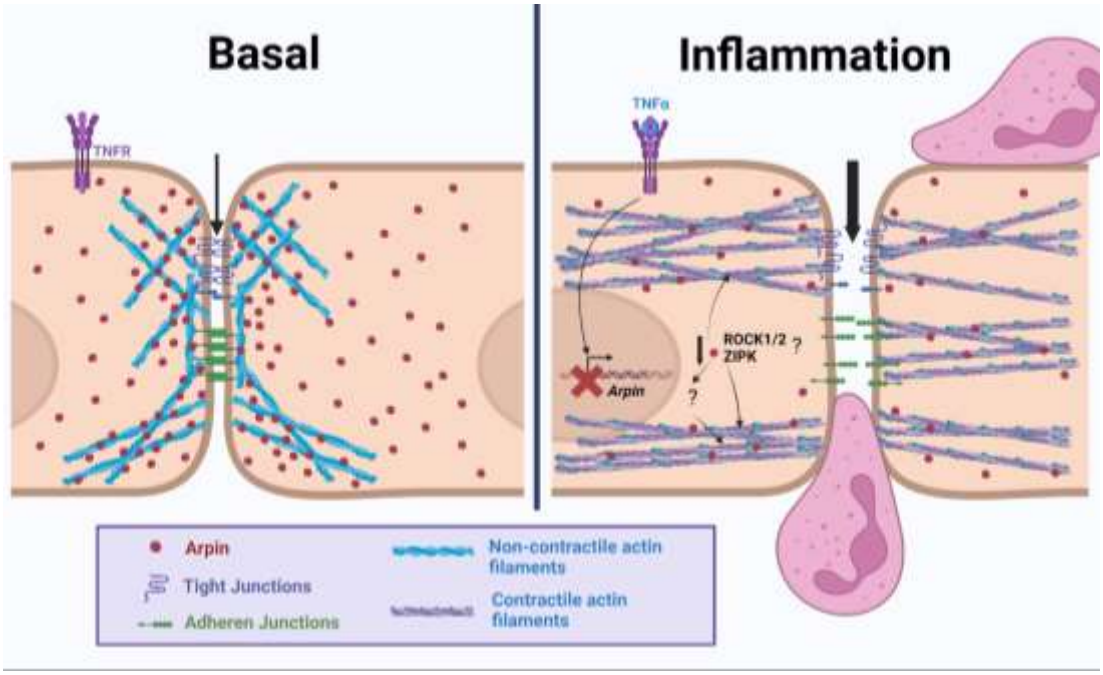

Figure 9.1. Proposed model for the functions of arpin in EC. In basal conditions (left), arpin is located throughout the cytoplasm with enrichment at cell-cell junction and low vascular permeability. During inflammation (right), arpin is downregulated leading to the formation of contractile actin stress fibers, junction architecture disruption and increased vascular permeability. Opening of the cell contacts then facilitates neutrophil transendothelial migration and extravasation. Question marks indicate the hitherto unknown mechanisms of how arpin regulates the activity of ROCK1/2 and ZIPK to induce the formation of actomyosin stress fibers.

10. PERSPECTIVES

- To characterize the arpin promoter region
- To unravel the mechanism through which arpin regulates ROCK1/2 and ZIPK expression and activity.
- To analyze the role of arpin in other functions of EC including angiogenesis and would healing.
- To characterize whether the functions of highly vascularized organs including brain, heart, and kidney are affected in arpin$^{-/-}$ mice.
- To investigate arpin expression in neutrophils and its role in neutrophil migration and effector functions.
- To unravel neutrophil recruitment in different organs including lungs and brain of arpin$^{-/-}$ mice.

11. REFERENCES

1. Feletou, M. (2011) in *The Endothelium: Part 1: Multiple Functions of the Endothelial Cells-Focus on Endothelium-Derived Vasoactive Mediators*, San Rafael (CA).

2. Cerutti, C. & Ridley, A. J. (2017) Endothelial cell-cell adhesion and signaling, *Exp Cell Res.* **358**, 31-38.

3. Dejana, E. (2004) Endothelial cell-cell junctions: happy together, *Nat Rev Mol Cell Biol.* **5**, 261-70.

4. Nitta, T., Hata, M., Gotoh, S., Seo, Y., Sasaki, H., Hashimoto, N., Furuse, M. & Tsukita, S. (2003) Size-selective loosening of the blood-brain barrier in claudin-5-deficient mice, *J Cell Biol.* **161**, 653-60.

5. Bazzoni, G. & Dejana, E. (2004) Endothelial cell-to-cell junctions: molecular organization and role in vascular homeostasis, *Physiol Rev.* **84**, 869-901.

6. Prasain, N. & Stevens, T. (2009) The actin cytoskeleton in endothelial cell phenotypes, *Microvasc Res.* **77**, 53-63.

7. Cao, G., O'Brien, C. D., Zhou, Z., Sanders, S. M., Greenbaum, J. N., Makrigiannakis, A. & DeLisser, H. M. (2002) Involvement of human PECAM-1 in angiogenesis and in vitro endothelial cell migration, *Am J Physiol Cell Physiol.* **282**, C1181-90.

8. O'Brien, C. D., Lim, P., Sun, J. & Albelda, S. M. (2003) PECAM-1-dependent neutrophil transmigration is independent of monolayer PECAM-1 signaling or localization, *Blood.* **101**, 2816-25.

9. Aghajanian, A., Wittchen, E. S., Allingham, M. J., Garrett, T. A. & Burridge, K. (2008) Endothelial cell junctions and the regulation of vascular permeability and leukocyte transmigration, *J Thromb Haemost.* **6**, 1453-60.

10. Reglero-Real, N., Colom, B., Bodkin, J. V. & Nourshargh, S. (2016) Endothelial Cell Junctional Adhesion Molecules: Role and Regulation of Expression in Inflammation, *Arterioscler Thromb Vasc Biol.* **36**, 2048-2057.

11. Gavard, J. (2009) Breaking the VE-cadherin bonds, *FEBS Lett.* **583**, 1-6.

12. Rho, S. S., Ando, K. & Fukuhara, S. (2017) Dynamic Regulation of Vascular Permeability by Vascular Endothelial Cadherin-Mediated Endothelial Cell-Cell Junctions, *J Nippon Med Sch.* **84**, 148-159.

13. Gardner, T. W., Lesher, T., Khin, S., Vu, C., Barber, A. J. & Brennan, W. A., Jr. (1996) Histamine reduces ZO-1 tight-junction protein expression in cultured retinal microvascular endothelial cells, *Biochem J.* **320 (Pt 3)**, 717-21.

14. Wang, W., Dentler, W. L. & Borchardt, R. T. (2001) VEGF increases BMEC monolayer permeability by affecting occludin expression and tight junction assembly, *Am J Physiol Heart Circ Physiol.* **280**, H434-40.

15. Wessel, F., Winderlich, M., Holm, M., Frye, M., Rivera-Galdos, R., Vockel, M., Linnepe, R., Ipe, U., Stadtmann, A., Zarbock, A., Nottebaum, A. F. & Vestweber, D. (2014) Leukocyte extravasation and vascular permeability are each controlled in vivo by different tyrosine residues of VE-cadherin, *Nat Immunol.* **15**, 223-30.

16. Orlova, V. V., Economopoulou, M., Lupu, F., Santoso, S. & Chavakis, T. (2006) Junctional adhesion molecule-C regulates vascular endothelial permeability by modulating VE-cadherin-mediated cell-cell contacts, *J Exp Med.* **203**, 2703-14.

17. Li, X., Stankovic, M., Lee, B. P., Aurrand-Lions, M., Hahn, C. N., Lu, Y., Imhof, B. A., Vadas, M. A. & Gamble, J. R. (2009) JAM-C induces endothelial cell permeability through its association and regulation of {beta}3 integrins, *Arterioscler Thromb Vasc Biol.* **29**, 1200-6.

18. Shaw, S. K., Perkins, B. N., Lim, Y. C., Liu, Y., Nusrat, A., Schnell, F. J., Parkos, C. A. & Luscinskas, F. W. (2001) Reduced expression of junctional adhesion molecule and platelet/endothelial cell adhesion molecule-1 (CD31) at human vascular endothelial junctions by cytokines tumor necrosis factor-alpha plus interferon-gamma Does not reduce leukocyte transmigration under flow, *Am J Pathol.* **159**, 2281-91.

19. Schnoor, M. (2015) Endothelial actin-binding proteins and actin dynamics in leukocyte transendothelial migration, *J Immunol.* **194**, 3535-41.

20. Vestweber, D. (2015) How leukocytes cross the vascular endothelium, *Nat Rev Immunol.* **15**, 692-704.

21. Kolaczkowska, E. & Kubes, P. (2013) Neutrophil recruitment and function in health and inflammation, *Nat Rev Immunol.* **13**, 159-75.

22. Barreiro, O., Yanez-Mo, M., Serrador, J. M., Montoya, M. C., Vicente-Manzanares, M., Tejedor, R., Furthmayr, H. & Sanchez-Madrid, F. (2002) Dynamic interaction of VCAM-1 and ICAM-1 with moesin and ezrin in a novel endothelial docking structure for adherent leukocytes, *J Cell Biol.* **157**, 1233-45.

23. Carman, C. V. & Springer, T. A. (2004) A transmigratory cup in leukocyte diapedesis both through individual vascular endothelial cells and between them, *J Cell Biol.* **167**, 377-88.

24. Schnoor, M., Lai, F. P., Zarbock, A., Klaver, R., Polaschegg, C., Schulte, D., Weich, H. A., Oelkers, J. M., Rottner, K. & Vestweber, D. (2011) Cortactin deficiency is associated with reduced neutrophil recruitment but increased vascular permeability in vivo, *J Exp Med.* **208**, 1721-35.

25. Sidibe, A. & Imhof, B. A. (2014) VE-cadherin phosphorylation decides: vascular permeability or diapedesis, *Nat Immunol.* **15**, 215-7.

26. Park, M., Kim, H. J., Lim, B., Wylegala, A. & Toborek, M. (2013) Methamphetamine-induced occludin endocytosis is mediated by the Arp2/3 complex-regulated actin rearrangement, *J Biol Chem.* **288**, 33324-34.

27. Garcia-Ponce, A., Citalan-Madrid, A. F., Velazquez-Avila, M., Vargas-Robles, H. & Schnoor, M. (2015) The role of actin-binding proteins in the control of endothelial barrier integrity, *Thromb Haemost.* **113**, 20-36.

28. Patterson, C. E. & Lum, H. (2001) Update on pulmonary edema: the role and regulation of endothelial barrier function, *Endothelium.* **8**, 75-105.

29. Stossel, T. P., Chaponnier, C., Ezzell, R. M., Hartwig, J. H., Janmey, P. A., Kwiatkowski, D. J., Lind, S. E., Smith, D. B., Southwick, F. S., Yin, H. L. & et al. (1985) Nonmuscle actin-binding proteins, *Annu Rev Cell Biol.* **1**, 353-402.

30. Stossel, T. P. (1993) On the crawling of animal cells, *Science.* **260**, 1086-94.

31. Dominguez, R. (2009) Actin filament nucleation and elongation factors--structure-function relationships, *Crit Rev Biochem Mol Biol.* **44**, 351-66.

32. Firat-Karalar, E. N. & Welch, M. D. (2011) New mechanisms and functions of actin nucleation, *Curr Opin Cell Biol.* **23**, 4-13.

33. Pollard, T. D. (2016) Actin and Actin-Binding Proteins, *Cold Spring Harb Perspect Biol.* **8**.

34. Spindler, V., Schlegel, N. & Waschke, J. (2010) Role of GTPases in control of microvascular permeability, *Cardiovasc Res.* **87**, 243-53.

35. Rottner, K. & Stradal, T. E. (2011) Actin dynamics and turnover in cell motility, *Curr Opin Cell Biol.* **23**, 569-78.

36. Goley, E. D. & Welch, M. D. (2006) The ARP2/3 complex: an actin nucleator comes of age, *Nat Rev Mol Cell Biol.* **7**, 713-26.

37. Goley, E. D., Rammohan, A., Znameroski, E. A., Firat-Karalar, E. N., Sept, D. & Welch, M. D. (2010) An actin-filament-binding interface on the Arp2/3 complex is critical for nucleation and branch stability, *Proc Natl Acad Sci U S A.* **107**, 8159-64.

38. Quinlan, M. E., Heuser, J. E., Kerkhoff, E. & Mullins, R. D. (2005) Drosophila Spire is an actin nucleation factor, *Nature.* **433**, 382-8.

39. Kovar, D. R. (2006) Molecular details of formin-mediated actin assembly, *Curr Opin Cell Biol.* **18**, 11-7.

40. Breitsprecher, D. & Goode, B. L. (2013) Formins at a glance, *J Cell Sci.* **126**, 1-7.

41. Cao, J. & Schnittler, H. (2019) Putting VE-cadherin into JAIL for junction remodeling, *J Cell Sci.* **132**.

42. Tojkander, S., Gateva, G. & Lappalainen, P. (2012) Actin stress fibers--assembly, dynamics and biological roles, *J Cell Sci.* **125**, 1855-64.

43. Vinzenz, M., Nemethova, M., Schur, F., Mueller, J., Narita, A., Urban, E., Winkler, C., Schmeiser, C., Koestler, S. A., Rottner, K., Resch, G. P., Maeda, Y. & Small, J. V. (2012) Actin branching in the initiation and maintenance of lamellipodia, *J Cell Sci.* **125**, 2775-85.

44. Abu Taha, A., Taha, M., Seebach, J. & Schnittler, H. J. (2014) ARP2/3-mediated junction-associated lamellipodia control VE-cadherin-based cell junction dynamics and maintain monolayer integrity, *Mol Biol Cell.* **25**, 245-56.
45. Rotty, J. D., Wu, C. & Bear, J. E. (2013) New insights into the regulation and cellular functions of the ARP2/3 complex, *Nat Rev Mol Cell Biol.* **14**, 7-12.
46. Campellone, K. G. & Welch, M. D. (2010) A nucleator arms race: cellular control of actin assembly, *Nat Rev Mol Cell Biol.* **11**, 237-51.
47. Molinie, N. & Gautreau, A. (2018) The Arp2/3 Regulatory System and Its Deregulation in Cancer, *Physiol Rev.* **98**, 215-238.
48. Robinson, R. C., Turbedsky, K., Kaiser, D. A., Marchand, J. B., Higgs, H. N., Choe, S. & Pollard, T. D. (2001) Crystal structure of Arp2/3 complex, *Science.* **294**, 1679-84.
49. Schwob, E. & Martin, R. P. (1992) New yeast actin-like gene required late in the cell cycle, *Nature.* **355**, 179-82.
50. Yae, K., Keng, V. W., Koike, M., Yusa, K., Kouno, M., Uno, Y., Kondoh, G., Gotow, T., Uchiyama, Y., Horie, K. & Takeda, J. (2006) Sleeping beauty transposon-based phenotypic analysis of mice: lack of Arpc3 results in defective trophoblast outgrowth, *Mol Cell Biol.* **26**, 6185-96.
51. van der Kammen, R., Song, J. Y., de Rink, I., Janssen, H., Madonna, S., Scarponi, C., Albanesi, C., Brugman, W. & Innocenti, M. (2017) Knockout of the Arp2/3 complex in epidermis causes a psoriasis-like disease hallmarked by hyperactivation of transcription factor Nrf2, *Development.* **144**, 4588-4603.
52. Dimchev, V., Lahmann, I., Koestler, S. A., Kage, F., Dimchev, G., Steffen, A., Stradal, T. E. B., Vauti, F., Arnold, H. H. & Rottner, K. (2021) Induced Arp2/3 Complex Depletion Increases FMNL2/3 Formin Expression and Filopodia Formation, *Front Cell Dev Biol.* **9**, 634708.
53. Espinoza-Sanchez, S., Metskas, L. A., Chou, S. Z., Rhoades, E. & Pollard, T. D. (2018) Conformational changes in Arp2/3 complex induced by ATP, WASp-VCA, and actin filaments, *Proc Natl Acad Sci U S A.* **115**, E8642-E8651.

54. Abu Taha, A. & Schnittler, H. J. (2014) Dynamics between actin and the VE-cadherin/catenin complex: novel aspects of the ARP2/3 complex in regulation of endothelial junctions, *Cell Adh Migr.* **8**, 125-35.

55. Pollard, T. D. (2007) Regulation of actin filament assembly by Arp2/3 complex and formins, *Annu Rev Biophys Biomol Struct.* **36**, 451-77.

56. Kurisu, S. & Takenawa, T. (2009) The WASP and WAVE family proteins, *Genome Biol.* **10**, 226.

57. Linardopoulou, E. V., Parghi, S. S., Friedman, C., Osborn, G. E., Parkhurst, S. M. & Trask, B. J. (2007) Human subtelomeric WASH genes encode a new subclass of the WASP family, *PLoS Genet.* **3**, e237.

58. Molinie, N., Rubtsova, S. N., Fokin, A., Visweshwaran, S. P., Rocques, N., Polesskaya, A., Schnitzler, A., Vacher, S., Denisov, E. V., Tashireva, L. A., Perelmuter, V. M., Cherdyntseva, N. V., Bieche, I. & Gautreau, A. M. (2019) Cortical branched actin determines cell cycle progression, *Cell Res.* **29**, 432-445.

59. Mooren, O. L., Li, J., Nawas, J. & Cooper, J. A. (2014) Endothelial cells use dynamic actin to facilitate lymphocyte transendothelial migration and maintain the monolayer barrier, *Mol Biol Cell.* **25**, 4115-29.

60. Rosa, A., Giese, W., Meier, K., Alt, S., Klaus-Bergmann, A., Edgar, L. T., Bartels-Klein, E., Collins, R. T., Szymborska, A., Coxam, B., Bernabeu, M. O. & Gerhardt, H. (2022) WASp controls oriented migration of endothelial cells to achieve functional vascular patterning, *Development.* **149**.

61. Mooren, O. L., Kim, J., Li, J. & Cooper, J. A. (2015) Role of N-WASP in Endothelial Monolayer Formation and Integrity, *J Biol Chem.* **290**, 18796-805.

62. Huang, D., Ding, Q., Chen, S., Lu, S., Zhang, Y. & Long, M. (2021) E-selectin negatively regulates polymorphonuclear neutrophil transmigration through altered endothelial junction integrity, *FASEB J.* **35**, e21521.

63. Chanez-Paredes, S., Montoya-Garcia, A. & Schnoor, M. (2019) Cellular and pathophysiological consequences of Arp2/3 complex inhibition: role of inhibitory proteins and pharmacological compounds, *Cell Mol Life Sci*.

64. Maritzen, T., Zech, T., Schmidt, M. R., Krause, E., Machesky, L. M. & Haucke, V. (2012) Gadkin negatively regulates cell spreading and motility via sequestration of the actin-nucleating ARP2/3 complex, *Proc Natl Acad Sci U S A.* **109**, 10382-7.

65. Madasu, Y., Yang, C., Boczkowska, M., Bethoney, K. A., Zwolak, A., Rebowski, G., Svitkina, T. & Dominguez, R. (2015) PICK1 is implicated in organelle motility in an Arp2/3 complex-independent manner, *Mol Biol Cell.* **26**, 1308-22.

66. Rocca, D. L., Martin, S., Jenkins, E. L. & Hanley, J. G. (2008) Inhibition of Arp2/3-mediated actin polymerization by PICK1 regulates neuronal morphology and AMPA receptor endocytosis, *Nat Cell Biol.* **10**, 259-71.

67. Rocca, D. L., Amici, M., Antoniou, A., Blanco Suarez, E., Halemani, N., Murk, K., McGarvey, J., Jaafari, N., Mellor, J. R., Collingridge, G. L. & Hanley, J. G. (2013) The small GTPase Arf1 modulates Arp2/3-mediated actin polymerization via PICK1 to regulate synaptic plasticity, *Neuron.* **79**, 293-307.

68. Dang, I., Gorelik, R., Sousa-Blin, C., Derivery, E., Guerin, C., Linkner, J., Nemethova, M., Dumortier, J. G., Giger, F. A., Chipysheva, T. A., Ermilova, V. D., Vacher, S., Campanacci, V., Herrada, I., Planson, A. G., Fetics, S., Henriot, V., David, V., Oguievetskaia, K., Lakisic, G., Pierre, F., Steffen, A., Boyreau, A., Peyrieras, N., Rottner, K., Zinn-Justin, S., Cherfils, J., Bieche, I., Alexandrova, A. Y., David, N. B., Small, J. V., Faix, J., Blanchoin, L. & Gautreau, A. (2013) Inhibitory signalling to the Arp2/3 complex steers cell migration, *Nature.* **503**, 281-4.

69. Sokolova, O. S., Chemeris, A., Guo, S., Alioto, S. L., Gandhi, M., Padrick, S., Pechnikova, E., David, V., Gautreau, A. & Goode, B. L. (2017) Structural Basis of Arp2/3 Complex Inhibition by GMF, Coronin, and Arpin, *J Mol Biol.* **429**, 237-248.

70. Dang, I., Linkner, J., Yan, J., Irimia, D., Faix, J. & Gautreau, A. (2017) The Arp2/3 inhibitory protein Arpin is dispensable for chemotaxis, *Biol Cell.* **109**, 162-166.

71. Chanez-Paredes, S., Montoya-Garcia, A., Castro-Ochoa, K. F., Garcia-Cordero, J., Cedillo-Barron, L., Shibayama, M., Nava, P., Flemming, S., Schlegel, N., Gautreau, A. M., Vargas-Robles, H., Mondragon-Flores, R. & Schnoor, M. (2021) The Arp2/3 Inhibitory Protein Arpin Is Required for Intestinal Epithelial Barrier Integrity, *Front Cell Dev Biol.* **9**, 625719.

72. Galiveti, C. R., Rozhdestvensky, T. S., Brosius, J., Lehrach, H. & Konthur, Z. (2010) Application of housekeeping npcRNAs for quantitative expression analysis of human transcriptome by real-time PCR, *RNA.* **16**, 450-61.

73. Livak, K. J. & Schmittgen, T. D. (2001) Analysis of relative gene expression data using real-time quantitative PCR and the 2(-Delta Delta C(T)) Method, *Methods.* **25**, 402-8.

74. Lartey, N. L., Vargas-Robles, H., Guerrero-Fonseca, I. M., Garcia-Ponce, A., Salinas-Lara, C., Rottner, K. & Schnoor, M. (2022) The Actin-Binding Protein Cortactin Promotes Sepsis Severity by Supporting Excessive Neutrophil Infiltration into the Lung, *Biomedicines.* **10**.

75. Lartey, N. L., Valle-Reyes, S., Vargas-Robles, H., Jimenez-Camacho, K. E., Guerrero-Fonseca, I. M., Castellanos-Martinez, R., Montoya-Garcia, A., Garcia-Cordero, J., Cedillo-Barron, L., Nava, P., Filisola-Villasenor, J. G., Roa-Velazquez, D., Zavala-Vargas, D. I., Morales-Rios, E., Salinas-Lara, C., Vadillo, E. & Schnoor, M. (2022) ADAM17/MMP inhibition prevents neutrophilia and lung injury in a mouse model of COVID-19, *J Leukoc Biol.* **111**, 1147-1158.

76. Gavins, F. N. & Chatterjee, B. E. (2004) Intravital microscopy for the study of mouse microcirculation in anti-inflammatory drug research: focus on the mesentery and cremaster preparations, *J Pharmacol Toxicol Methods.* **49**, 1-14.

77. Mako, V., Czucz, J., Weiszhar, Z., Herczenik, E., Matko, J., Prohaszka, Z. & Cervenak, L. (2010) Proinflammatory activation pattern of human umbilical vein endothelial cells induced by IL-1beta, TNF-alpha, and LPS, *Cytometry A.* **77**, 962-70.

78. Chen, Y., Li, R., Shang, S., Yang, X., Li, L., Wang, W. & Wang, Y. (2021) Therapeutic Potential of TNFalpha and IL1beta Blockade for CRS/ICANS in

CAR-T Therapy via Ameliorating Endothelial Activation, *Front Immunol.* **12**, 623610.

79. Garcia Ponce, A., Citalan Madrid, A. F., Vargas Robles, H., Chanez Paredes, S., Nava, P., Betanzos, A., Zarbock, A., Rottner, K., Vestweber, D. & Schnoor, M. (2016) Loss of cortactin causes endothelial barrier dysfunction via disturbed adrenomedullin secretion and actomyosin contractility, *Sci Rep.* **6**, 29003.

80. Waschke, J., Curry, F. E., Adamson, R. H. & Drenckhahn, D. (2005) Regulation of actin dynamics is critical for endothelial barrier functions, *Am J Physiol Heart Circ Physiol.* **288**, H1296-305.

81. Khromov, A., Choudhury, N., Stevenson, A. S., Somlyo, A. V. & Eto, M. (2009) Phosphorylation-dependent autoinhibition of myosin light chain phosphatase accounts for Ca2+ sensitization force of smooth muscle contraction, *J Biol Chem.* **284**, 21569-79.

82. DiStasi, M. R. & Ley, K. (2009) Opening the flood-gates: how neutrophil-endothelial interactions regulate permeability, *Trends Immunol.* **30**, 547-56.

83. Hoganson, D. M., Pryor, H. I., 2nd & Vacanti, J. P. (2008) Tissue engineering and organ structure: a vascularized approach to liver and lung, *Pediatr Res.* **63**, 520-6.

84. Werner, A. C., Weckbach, L. T., Salvermoser, M., Pitter, B., Cao, J., Maier-Begandt, D., Forne, I., Schnittler, H. J., Walzog, B. & Montanez, E. (2020) Coronin 1B Controls Endothelial Actin Dynamics at Cell-Cell Junctions and Is Required for Endothelial Network Assembly, *Front Cell Dev Biol.* **8**, 708.

85. Moztarzadeh, S., Radeva, M. Y., Sepic, S., Schuster, K., Hamad, I., Waschke, J. & Garcia-Ponce, A. (2022) Lack of adducin impairs the stability of endothelial adherens and tight junctions and may be required for cAMP-Rac1-mediated endothelial barrier stabilization, *Sci Rep.* **12**, 14940.

86. Jubrail, J., Africano-Gomez, K., Herit, F., Mularski, A., Bourdoncle, P., Oberg, L., Israelsson, E., Burgel, P. R., Mayer, G., Cunoosamy, D. M., Kurian, N. & Niedergang, F. (2020) Arpin is critical for phagocytosis in macrophages and is targeted by human rhinovirus, *EMBO Rep.* **21**, e47963.

87. Li, Y., Qiu, J., Pang, T., Guo, Z., Su, Y., Zeng, Q. & Zhang, X. (2017) Restoration of Arpin suppresses aggressive phenotype of breast cancer cells, *Biomed Pharmacother.* **92**, 116-121.

88. Belvitch, P., Brown, M. E., Brinley, B. N., Letsiou, E., Rizzo, A. N., Garcia, J. G. N. & Dudek, S. M. (2017) The ARP 2/3 complex mediates endothelial barrier function and recovery, *Pulm Circ.* **7**, 200-210.

89. Mong, P. Y. & Wang, Q. (2009) Activation of Rho kinase isoforms in lung endothelial cells during inflammation, *J Immunol.* **182**, 2385-94.

90. Zeng, W., Sun, Z., Ma, T., Song, X., Li, S., Zhang, Q., Yuan, W., Li, J., Liu, L., Zhu, M. & Chen, H. (2021) Elevated ZIPK is required for TNF-alpha-induced cell adhesion molecule expression and leucocyte adhesion in endothelial cells, *Acta Biochim Biophys Sin (Shanghai).* **53**, 567-574.

91. Millan, J., Cain, R. J., Reglero-Real, N., Bigarella, C., Marcos-Ramiro, B., Fernandez-Martin, L., Correas, I. & Ridley, A. J. (2010) Adherens junctions connect stress fibres between adjacent endothelial cells, *BMC Biol.* **8**, 11.

92. Angulo-Urarte, A., Casado, P., Castillo, S. D., Kobialka, P., Kotini, M. P., Figueiredo, A. M., Castel, P., Rajeeve, V., Mila-Guasch, M., Millan, J., Wiesner, C., Serra, H., Muixi, L., Casanovas, O., Vinals, F., Affolter, M., Gerhardt, H., Huveneers, S., Belting, H. G., Cutillas, P. R. & Graupera, M. (2018) Endothelial cell rearrangements during vascular patterning require PI3-kinase-mediated inhibition of actomyosin contractility, *Nat Commun.* **9**, 4826.

93. Citalan-Madrid, A. F., Vargas-Robles, H., Garcia-Ponce, A., Shibayama, M., Betanzos, A., Nava, P., Salinas-Lara, C., Rottner, K., Mennigen, R. & Schnoor, M. (2017) Cortactin deficiency causes increased RhoA/ROCK1-dependent actomyosin contractility, intestinal epithelial barrier dysfunction, and disproportionately severe DSS-induced colitis, *Mucosal Immunol.* **10**, 1237-1247.

94. Zhang, Y., Zhang, C., Zhang, H., Zeng, W., Li, S., Chen, C., Song, X., Sun, J., Sun, Z., Cui, C., Cao, X., Zheng, L., Wang, P., Zhao, W., Zhang, Z., Xu, Y., Zhu, M. & Chen, H. (2019) ZIPK mediates endothelial cell contraction through

myosin light chain phosphorylation and is required for ischemic-reperfusion injury, *FASEB J.* **33**, 9062-9074.

95. Viita, T., Kyheroinen, S., Prajapati, B., Virtanen, J., Frilander, M. J., Varjosalo, M. & Vartiainen, M. K. (2019) Nuclear actin interactome analysis links actin to KAT14 histone acetyl transferase and mRNA splicing, *J Cell Sci.* **132**.

96. Figueiredo, A. M., Barbacena, P., Russo, A., Vaccaro, S., Ramalho, D., Pena, A., Lima, A. P., Ferreira, R. R., Fidalgo, M. A., El-Marjou, F., Carvalho, Y., Vasconcelos, F. F., Lennon-Dumenil, A. M., Vignjevic, D. M. & Franco, C. A. (2021) Endothelial cell invasion is controlled by dactylopodia, *Proc Natl Acad Sci U S A.* **118**.

97. Ushakumari, C. J., Zhou, Q. L., Wang, Y. H., Na, S., Rigor, M. C., Zhou, C. Y., Kroll, M. K., Lin, B. D. & Jiang, Z. Y. (2022) Neutrophil Elastase Increases Vascular Permeability and Leukocyte Transmigration in Cultured Endothelial Cells and Obese Mice, *Cells.* **11**.

98. McColl, S. R., St-Onge, M., Dussault, A. A., Laflamme, C., Bouchard, L., Boulanger, J. & Pouliot, M. (2006) Immunomodulatory impact of the A2A adenosine receptor on the profile of chemokines produced by neutrophils, *FASEB J.* **20**, 187-9.

99. Owen-Woods, C., Joulia, R., Barkaway, A., Rolas, L., Ma, B., Nottebaum, A. F., Arkill, K. P., Stein, M., Girbl, T., Golding, M., Bates, D. O., Vestweber, D., Voisin, M. B. & Nourshargh, S. (2020) Local microvascular leakage promotes trafficking of activated neutrophils to remote organs, *J Clin Invest.* **130**, 2301-2318.

100. Wang, Q. & Doerschuk, C. M. (2002) The signaling pathways induced by neutrophil-endothelial cell adhesion, *Antioxid Redox Signal.* **4**, 39-47.

101. MacArthur, D. G., Seto, J. T., Chan, S., Quinlan, K. G., Raftery, J. M., Turner, N., Nicholson, M. D., Kee, A. J., Hardeman, E. C., Gunning, P. W., Cooney, G. J., Head, S. I., Yang, N. & North, K. N. (2008) An Actn3 knockout mouse provides mechanistic insights into the association between alpha-

actinin-3 deficiency and human athletic performance, *Hum Mol Genet.* **17**, 1076-86.

102. Punwani, D., Pelz, B., Yu, J., Arva, N. C., Schafernak, K., Kondratowicz, K., Makhija, M. & Puck, J. M. (2015) Coronin-1A: immune deficiency in humans and mice, *J Clin Immunol.* **35**, 100-7.

103. Steinberg, J. P., Takamiya, K., Shen, Y., Xia, J., Rubio, M. E., Yu, S., Jin, W., Thomas, G. M., Linden, D. J. & Huganir, R. L. (2006) Targeted in vivo mutations of the AMPA receptor subunit GluR2 and its interacting protein PICK1 eliminate cerebellar long-term depression, *Neuron.* **49**, 845-60.

104. Schachtner, H., Weimershaus, M., Stache, V., Plewa, N., Legler, D. F., Hopken, U. E. & Maritzen, T. (2015) Loss of Gadkin Affects Dendritic Cell Migration In Vitro, *PLoS One.* **10**, e0143883.

105. Snapper, S. B., Takeshima, F., Anton, I., Liu, C. H., Thomas, S. M., Nguyen, D., Dudley, D., Fraser, H., Purich, D., Lopez-Ilasaca, M., Klein, C., Davidson, L., Bronson, R., Mulligan, R. C., Southwick, F., Geha, R., Goldberg, M. B., Rosen, F. S., Hartwig, J. H. & Alt, F. W. (2001) N-WASP deficiency reveals distinct pathways for cell surface projections and microbial actin-based motility, *Nat Cell Biol.* **3**, 897-904.

106. Dahl, J. P., Wang-Dunlop, J., Gonzales, C., Goad, M. E., Mark, R. J. & Kwak, S. P. (2003) Characterization of the WAVE1 knock-out mouse: implications for CNS development, *J Neurosci.* **23**, 3343-52.

107. Malek, R. & Soufi, S. (2023) Pulmonary Edema in *StatPearls*, Treasure Island (FL).

108. Latasiewicz, J., Artz, A., Jing, D., Blanco, M. P., Currie, S. M., Avila, M. V., Schnoor, M. & Vestweber, D. (2017) HS1 deficiency impairs neutrophil recruitment in vivo and activation of the small GTPases Rac1 and Rap1, *J Leukoc Biol.* **101**, 1133-1142.

109. Vadillo, E., Chanez-Paredes, S., Vargas-Robles, H., Guerrero-Fonseca, I. M., Castellanos-Martinez, R., Garcia-Ponce, A., Nava, P., Giron-Perez, D. A., Santos-Argumedo, L. & Schnoor, M. (2019) Intermittent rolling is a defect

of the extravasation cascade caused by Myosin1e-deficiency in neutrophils, *Proc Natl Acad Sci U S A.* **116**, 26752-26758.